THE DURABILITY OF ADHESIVE JOINTS: AN ENGINEERING STUDY.

by

Didier R. Lefebvre

Dissertation submitted to the Faculty of the

Virginia Polytechnic Institute and State University

in partial fulfillment of the requirements for the degree of

DOCTORATE OF PHILOSOPHY

in

Materials Engineering Science

APPROVED:

H. F. Brinson, Chairman

D. A. Dillard, Chairman

T. C. Ward

J. P. Wightman

K. L. Reifsnider

W. Grant

June 17, 1988

Blacksburg, Virginia

THE DURABILITY OF ADHESIVE JOINTS: AN ENGINEERING STUDY.

by

Didier R. Lefebvre

H. F. Brinson, Chairman

D. A. Dillard, Chairman

Materials Engineering Science

(ABSTRACT)

Water diffusion through the adhesive is the rate controlling factor for the durability of many metal-to-polymer bonds exposed to moist environments. A methodology is proposed, to relate the diffusion coefficient of water in polymers to temperature, strain and penetrant concentration. The approach used is based on well known free volume theories. In the rubbery state, it is assumed that the transport kinetics is governed by the constant redistribution of the free volume, caused by the segmental motions of the polymeric chains. An expression for the diffusion coefficient is inferred from the temperature, strain and penetrant concentration of the free volume. It is shown that the free volume treatment can be extended to the glassy range by introducing a few additional features in the model. The stress dependence of solubility as well as the non-fickian driving forces contributing to mass transport are predicted from the Flory-Huggins theory. Experimental validation of the concentration dependence and temperature dependence of the diffusion coefficient is shown. The effect of mechanical strain on diffusivity and solubility in the glassy state is also investigated experimentally, using both the permeation and sorption techniques. Good agreement with theory is generally found. The coupling mechanisms between the diffusion process and the viscoelastic response of the adhesive are explained. A numerical scheme for fully coupled solutions is implemented in a two- dimensional finite element code. A few numerical solutions are shown. In the case of bonds undergoing unusually harsh environmental exposure however, alternate methods must be sought for durability characterization and prediction. This is illustrated with the case of rubber-to-steel joints exposed to a cathodic potential in seawater. The mechanical analysis of a durability specimen is presented and a procedure for debond prediction is suggested.

Acknowledgements

The author acknowledges with gratitude the source of funding as well as the academic advisors who made this work possible. The financial support was provided by the Office of Naval Research (ONR) N00014-82-K-0185 and N00014-85-K-0145, Arlington, VA 22217; the project monitor was Dr. L. H. Peebles. The advisors were Dr. D. A. Dillard and Dr. H. F. Brinson.

Gratitude is extended to the Faculty involved in both the Center For Adhesion Science and the Materials Engineering Science program, for encouraging the kind of interdisciplinary thinking which is so essential in the field of Adhesion Science.

Thanks are given to Dr. S. Weinhold, to Dr. S. Matsuoka, to Dr. T. C. Ward and to Dr. J. P. Wightman, for their helpful comments and suggestions. Finally, the author is indebted to Mr. Reed for his assistance in the fabrication of the various specimens, and to S. Roy for his decisive collaboration in the numerical analysis of the diffusion problem.

Table of Contents

List of Illustrations

List of Tables

OBJECTIVES:

Adhesively bonded joints have potential for wide usage in a variety of structural applications. In many present day applications, conventional fasteners such as bolts, rivets, welds etc., are found to be unsuitable, particularly when the components are made of polymeric or composite material. Penetration methods (i.e. drilling holes, etc.) give rise to high stress concentrations and, in the case of composites, sever the fiber reinforcement, causing a reduction in joint strength. These problems can be overcome in a simple and inexpensive way by replacing conventional fasteners with adhesive bonds. Unfortunately, the promise of adhesive bonding has existed for over a decade, with slow progress being made towards their use in engineering designs. While adhesive bonds are being used, they are largely confined to low-stress applications. They have yet to find their place in highly stressed primary structural applications in aerospace, automobile, composites or similar industries wherein lie their huge potential.

Why has industry not fully exploited the potential of adhesive bonding? One reason is that their integrity over the lifetime of a structure - say 5 to 20 years of service - cannot yet be predicted in a satisfactory manner. This problem can be traced to the fact that adhesive bonds have properties that are time dependent. Adhesives are known to creep in service and hostile environmental parameters, such as temperature and moisture, tend to accelerate the degradation process, making it rather difficult to predict the structural integrity in a design lifetime.

Moisture induced failure of polymer-to-metal interfaces is a severe problem in applications involving coatings, sealants and adhesives. Such effects are particularly pronounced when the adherend and/or the adhesive are subject to moisture-induced degradation, and when the displacement of the bond-line by water is energetically favorable. Thermodynamics of surface energies and work of adhesion has proved quite successful for predicting the ultimate stability or lack of stability of a joint. Unfortunately, these approaches have not been able to incorporate kinetics to provide predictions for the time to failure. A significant challenge is to develop a rational basis to combine thermodynamics, mechanics and transport kinetics into a tool for an understanding of bond durability. Since the problem of durability is strongly interdisciplinary in nature, a scheme is needed in which ideas from all the key disciplines involved are combined in an integrated computational tool. Such a scheme would provide a predictive capability by which the results of small scale tests could be used to determine the lifetime of a given joint. A need therefore exists for improved experimental characterization techniques and for advanced computational procedures. The successful conclusion of such a research program would give the designer and manufacturers: a better characterization of their products, the possibility of enlarging markets by developing better user confidence in structural adhesives, and lowered costs through reduction in unrealistic safety factors.

The following generic research objectives are proposed:

(1) Develop or improve phenomenological descriptions of the mechanical response of adhesives, and of moisture diffusion in adhesives.

(2) Develop adequate characterization techniques for the mechanical behavior of the adhesive, for moisture diffusion along the bond line and for environmentally-induced failure.

(3) Incorporate the resulting predictive capabilities into a well documented computational tool.

This dissertation addresses, in varying degrees of depth, the three suggested research avenues. As we enter more detailed theoretical discussions, an effort will be made not to lose sight of the final goal, viz: providing an **engineering solution** to the durability problem. This means that although an effort will be made to understand mechanisms at the molecular level, a lack of complete understanding of a fundamental question will not deter us from describing the material response in a mathematical manner. Following, is a brief outline of the proposed study of the durability problem:

We first observe that moisture plays a central role in the degradation process of adhesive joints. Obviously, there are two main rate limiting parameters: the transport rate of moisture and the rate of environmental degradation. For this reason, a durability study should naturally proceed along two different directions: (1) the study of moisture diffusion and (2) the determination of a failure criterion. While a general theoretical approach can be developed for the former, no general method exists for the latter because failure mechanisms are too specific to a given adherend-interphase-adhesive system. Therefore, a general theoretical approach will be proposed for the diffusion problem, while an empirical approach will be favored for the failure study.

The underlying idea for modelling diffusion will be based on the free volume concept, i.e., that the motion of diffusing molecules depends on the space available to them in the form of vacancies between polymer chains. Since this free volume is also known to control the rate of creep or relaxation, a unified mechanical-diffusional theory can be used. While our reasoning initially will occur at the molecular level, the proposed model will be entirely phenomenological, mainly to reduce material characterization to an engineering level. The problem of the transport rate will be addressed by adapting and enhancing existing diffusion and viscoelasticity theories based on free volume concepts.

The second stage in the study of durability, involves the loss of mechanical strength. It has been established that there are two main failure modes in adhesive joints: cohesive (inside the adhesive) and interfacial (along the boundary between the adhesive and the adherend). Whereas criteria for cohesive failure are already available, much work remains to be done on the problem of interfacial failure. The difficulty arises from the fact that interfacial failures usually occur in moist environment as a result of a chemical or physical attack on the interphase. Since these degradation phenomena are difficult to represent analytically, empirical methods are often used. One such method, based on the critical concentration concept will be reviewed and tested experimentally.

The limit of the general methodology proposed above, is found in the case of joints exposed to unusually harsh conditions. This will be illustrated with the case of rubber-to-steel bonds undergoing cathodic debonding in seawater. An alternate methodology will be proposed and a description of a durability specimen will be given.

1. A MODEL FOR DIFFUSION IN POLYMERS. GOVERNING EQUATIONS:

Introduction:

Moisture may enter a bond by diffusion through the adhesive, through the adherends or by moving along an interphase region. If one assumes that water molecules have the same degradation effect on the adhesive and interphase region, regardless of their migration path, then it becomes of ultimate concern to be able to understand and predict the kinetics of moisture ingression via the different paths. This chapter investigates an important mode of moisture intrusion in a joint: bulk diffusion through the adhesive.

Earlier work has demonstrated that the diffusion rate in a polymer can be increased by a number of factors such as temperature, stress and damage. In particular, "non-Fickian" kinetics often associated with a sharp diffusion front, has been attributed to a strong dependence of the

diffusion coefficient on concentration and/or moisture induced damage. Externally applied stresses, residual stresses, and swelling stresses are known to affect diffusion rate. These various features (with the exception of damage) are reviewed in light of their usefulness to the specific problem of moisture diffusion in adhesive joints. Although damage can significantly enhance moisture ingression, it is reasonable to exclude it from this preliminary investigation because joints in service in moist environments are normally loaded to a small fraction of their ultimate breaking strength (dry), thereby minimizing damage arising solely from the applied load.

In Chapter 1, the theoretical background leading to the diffusion governing equations, will be reviewed in detail. Although the key concepts underlying the proposed theoretical treatment have been studied by several other workers, some novelty is introduced in the mathematical formulation of the constitutive relations. One of the major objectives of this study is to offer a treatment unifying both the diffusion behavior and mechanical behavior into a single phenomenological model. It will be shown that the unified approach not only facilitates the description of the coupling between diffusion and stress relaxation, but also leads to a common material characterization. Many workers have recognized the importance, in the case of polymers, of the interdependence between the diffusion process and stress relaxation. Unfortunately, the solutions proposed to date have either dealt with specific boundary value problems, or have failed to include in one single treatment, all the known forms of coupling. It follows that the solutions offered were often severely restricted in their conditions of applicability. By contrast, this treatment is meant to be as general as possible, and to be implemented in a finite element code. Unlike closed form solutions, the Finite Element Method can deal with almost any kind of boundary value problem of interest to designers. In the field of adhesion engineering, our goal is to provide designers with a general computational method to predict moisture intrusion into adhesive bond lines or into composite matrices, when they are subjected to a combination of external loading and internal swelling.

Chapter 1 is introductory and thus should be appraised only in the context of the entire work. In particular, Chapter 1 is not sufficient to fully understand the effect of stress and stress relaxation on diffusion. The constitutive relations for the mechanical behavior and swelling behavior are discussed in Chapter 3.

General Form of the Diffusion Governing Equation:

Let us consider a binary mixture consisting of a penetrant of small size (e.g.: water) permeating a polymer. The polymer is isotropic, amorphous and can be in either the glassy, leathery or rubbery state. It is natural to assume that the small penetrant molecules are much more mobile than the polymeric macromolecules. It follows that mass transport in this system can be described in terms of one flux only, namely that of the penetrant, because the polymer can be considered as a fixed reference. In general, the mass flux of penetrant can be separated in four components, each corresponding to a class of thermodynamic driving force[1] . Each driving force gives rise to small perturbations in the random walk of the diffusing species. Assuming the driving forces are uncoupled, and the departure from randomness small, the resulting macroscopic fluxes are additive:

$$\mathbf{J} = \mathbf{J}^C + \mathbf{J}^T + \mathbf{J}^\sigma + \mathbf{J}^\phi \tag{1}$$

where:
- $\mathbf{J}^C$ = Fickian mass flux (entropy driven)
- $\mathbf{J}^T$ = thermally driven mass flux
- $\mathbf{J}^\sigma$ = stress induced mass flux
- $\mathbf{J}^\phi$ = forced mass flux (driven by an external force)

(Bold characters will represent vectorial quantities throughout this dissertation)

The Fickian flux arises as a result of concentration gradients and is given by:

$$\mathbf{J}^C = -D\nabla C \tag{2}$$

where:
- D = diffusion coefficient
- C = penetrant concentration
- ∇ = gradient operator

Expression (2) is known as Fick's First Law as long as D is a constant or a function of C only. It will be shown later that the diffusion coefficient is a function of temperature and stress (or strain) as well:

$$D = D(C, T, \sigma) \tag{3}$$

where: T = temperature

σ = stress.

The thermal flux is driven by temperature gradients and is known as the Soret Effect[1]:

$$\mathbf{J}^T = -\frac{D^T C}{RT} \nabla LnT \tag{4}$$

where: D^T = thermal diffusion coefficient

Thermal diffusion becomes a significant component of the overall flux when an adhesive undergoes frequent temperature fluctuations. Sudden variations in external temperature give rise to temperature gradients internally which may persist for a long time, especially when the structure has a low thermal conductivity.

The stress induced flux is produced by a non-uniform stress field[2] and is given by:

$$\mathbf{J}^\sigma = -\frac{DC}{RT} \nabla W_p \tag{5}$$

where: R = gas constant

W_p = potential energy function

There is no general form for W_p. It is a function of the local entropy change of the penetrant when the polymer is subject to a stress (strain) field. Since the stress distribution within a joint is rarely uniform, proper attention should be given to this effect a priori. Furthermore, if the adhesive tends to swell by a large amount in the presence of the penetrant, $\mathbf{J}^\sigma$ could conceivably become quite large because differential swelling across the adhesive is generally constrained by stiff

adherends, leading to large pressure gradients internally, under either sorption or desorption processes. A possible form for W_p will be suggested in this chapter.

The forced diffusion flux is of importance in cases when the penetrant molecules are subject to an external force field (e.g., electrical or inertial). In an adhesive joint such a field may exist locally in the region known as the interphase. Close to a hydrophilic oxide layer, the intermolecular field experienced by a water molecule can be more intense than in the bulk polymer. This disparity is expected to cause local perturbations in the diffusive flux. It should be noted that, in this article, $\mathbf{J}^{\phi}$ refers to a component of the flux arising from any external force field, with the exception of stress fields. The effect of stress fields is already incorporated in the $\mathbf{J}^{\sigma}$ component of the flux.

Let us now consider the total flux J. Since conservation of mass must be satisfied, we must have:

$$\frac{\partial C}{\partial t} = -\nabla \cdot \mathbf{J} \tag{6}$$

where t is time, leading to the final governing equation:

$$\frac{\partial C}{\partial t} = \nabla \cdot \left\{ D(C, T, \sigma)\left[\nabla C + \frac{C}{RT} \nabla W_p \right] + \mathbf{J}^T + \mathbf{J}^{\phi} \right\} \tag{7}$$

In the remaining discussion, the problem will be reduced to that of the diffusion in a medium of uniform temperature and in the absence of an external force field ($\mathbf{J}^T = \mathbf{J}^{\phi} = 0$). Expression (7) shows that the effect of stress is twofold: (1) stress field gradients give rise to a thermodynamic force ∇W_p and (2) stress also affects the mobility of the penetrant, quantified here by the diffusion coefficient. The effect of stress on mobility does not disappear in a uniform stress field, although the stress induced driving force does vanish.

At this point, it is useful to recall that polymeric adhesives are viscoelastic in nature. Thus, our governing equation is valid instantaneously only. Stress and stress gradients need to be updated constantly in order to properly account for the rheology of the material. The problem of the coupling between the diffusion boundary value problem and the viscoelasticity boundary value problem

will be addressed in more detail in Chapter 3. For the time being, we just need to keep in mind that the governing equation is implicitly time dependent on the right hand side of the equation.

A thorough literature review[2-7] led us to conclude that expression (7) contains many of the known features necessary for modelling non-Fickian transport in the absence of damage. These features are:

1. the history dependence of the diffusion coefficient, in this case, through the coupling with the viscoelastic response,

2. the effect of a non-uniform stress distribution, and

3. the concentration dependence of the diffusion coefficient. (Although listed as a source of anomalous behavior, this concentration dependence does not in fact violate Fick's Second Law in its most general form).

Note that the proposed governing equation is by no means the only possible theoretical model. It just contains provision for important features often found in separate theories, but not in a unified approach.

The stress dependence of the solubility (accompanied here by an implicit time dependence) has also been identified as a source of non-Fickian behavior[7-9]. This difficulty can be addressed in the framework of a numerical analysis, by normalizing the concentration with respect to the saturation level at the current time step, and by providing an adequate model for the stress dependence of solubility. Such a model will be discussed later in this chapter.

A Model for the Diffusion Coefficient Based on the Cohen-Turnbull Theory:

The purpose of this section is to establish a general theory for predicting the diffusion coefficient of small molecules in polymeric materials. Particular attention will be devoted to the temperature dependence, stress dependence and penetrant concentration dependence of D .

The Cohen-Turnbull Model:

The Cohen-Turnbull model[10,11] was originally developed to describe self-diffusion in an ideal liquid made of hard spheres, but it has been extended to concentrated solutions and undiluted polymers. The model is based on the idea that molecular transport occurs by the movement of molecules into voids, with a size greater than some critical value. Voids are formed by the statistical redistribution of the free volume. Free volume is defined as:

$$V_f = V - V_o \tag{8}$$

where: V = specific volume

V_o = occupied volume

Furthermore, it is assumed that:

1. Free volume is continually redistributed with time, and that no local free energy is required for redistribution. As a result, distribution is random.
2. Molecular transport occurs by the movement of diffusing molecules into voids of at least their molecular size, which are formed as a result of the random redistribution of free volume.

In the case of the self diffusion (or viscous flow) of a polymer, the molecular jump representation must be replaced by the concept of segmental rearrangements which can occur whenever the surrounding free volume reaches some critical value V_c. In other words, in order for a portion of the polymeric chain to take a new conformation, the "cage" formed by nearest neighbors must reach a critical size.

The probability that n increments of free volume of average size V_f would accumulate into a void of size V_c is proportional to $\exp(-\theta \frac{V_c}{V_f})$, where θ is an overlap factor arising from the fact that the same void is available to more than one molecule. In the case of viscous flow, critical volume V_c must be large enough to allow a local rearrangement of the chain conformation, whereas in the case of the diffusion of a small penetrant, V_c must be large enough to allow a local molecular jump of the penetrant. Thus V_c is a characteristic of the polymer only in the case of self diffusion (or viscous processes) and V_c is a characteristic of a given polymer-penetrant pair in the case of the diffusion of a small penetrant molecule. From the form of the probability distribution, it follows that the diffusion coefficient contains an activation volume term:

$$D = D_o \exp(-\theta \frac{V_c}{V_f}) \tag{9}$$

Equation (9) implies that free volume is the only parameter involved in describing transport phenomena. This theory is not sufficient however, at temperatures too low relative to the glass transition temperature T_g, when motions of the chains within the free volume are too slow. Nor does it apply at very high temperatures where activation energy barriers must be overcome[13] . Note that in the framework of the Cohen-Turnbull theory the free volume is not the true free volume in the geometric sense, but only that portion of the total free volume which can be redistributed with no local change in free energy. It follows that the occupied volume V_o defined here is not the hard shell volume, but a larger quantity which can be changed by a stress field (i.e. the occupied volume is compressible).

The Macedo-Litovitz and Vrentas-Duda Theories:

Macedo and Litovitz[12] introduced an expression for the self-diffusion coefficient very similar to that of Cohen and Turnbull, except that it contains an activation energy factor:

$$D = D_o \exp\left(-\frac{E}{RT}\right) \exp\left(-\theta \frac{V_c}{V_f}\right) \tag{10}$$

It was postulated that in addition to the minimum hole-size requirement, an energy barrier must be surmounted. When inverted, expression (10) describes a viscosity. The obtained form is virtually identical to a known extension of the WLF equation including an Arrhenius-like temperature dependence[13]. In the glassy state (non-equilibrium), the temperature dependence predicted by the elementary WLF equation is known to be incorrect and an Arrhenius temperature dependence has been widely reported. This finding is consistent with expression (10) and will be the object of further discussion later.

Vrentas et *al.*[14] developed a constitutive behavior for the self diffusion in polymers based on equation (10). Their treatment of the free volume is more complex than the one used in this work. In addition to the free volume treatment of Cohen and Turnbull, the Flory-Huggins polymer solution theory and some aspects of the entanglement theory of Bueche are employed. An average free volume $\overline{V}_f$ as well as an average critical volume $\overline{V}_c$ are defined for the binary mixture sorbent (subscript 1) - polymer (subscript 2):

$$\overline{V}_f = k_{11}\omega_1(k_{21} + T - T_{g1}) + k_{12}\omega_2(k_{22} + T - T_{g2}) \tag{11}$$

$$\overline{V}_c = \omega_1 \hat{V}_1^* + \omega_2 \xi \hat{V}_2^* \tag{12}$$

where:

ω_i	=	mass fraction of component i;
T_{gi}	=	glass transition temperature of component i;
k_{11}, k_{21}	=	free volume parameters for the solvent;
k_{12}, k_{22}	=	free volume parameters for the polymer.

ξ = ratio of the critical molar volume of the penetrant jumping unit to the critical molar volume of the polymer jumping unit

$\hat{V}_i^*$ = specific critical hole free volume of component i.

In the limit, when the mass fraction of penetrant is small, $\overline{V}_f$ and $\overline{V}_e$ become mainly polymer dependent and the above approach becomes equivalent to the one shown herein. Our simpler approach, in which the free volume of the mixture is dominated by that of the polymer is very reasonable because polymers with a large moisture solubility are not suitable for the structural adhesive applications we are concerned with.

Extension of the Doolittle Theory to the Problem of Diffusion of Small Molecules:

Doolittle proposed an empirical equation relating polymer viscosity to the free volume, which was found to apply to polymers in their rubbery range[13]. Fluidity F, the inverse of viscosity is given by:

$$F = A^{-1} \exp(-B\frac{V - V_f}{V_f}) \tag{13}$$

where A and B are empirical constants. The parallelism between equations (9) and (13) is striking. This was explained earlier by the fact that the elementary process for viscous flow and the elementary process for sorbent diffusion are identical. In order to prove that equations (9) and (13) are identical mathematically, one can use Einstein's equation for the diffusion coefficient and Stokes' equation for the friction constant. According to Einstein's equation for the diffusion coefficient[15]:

$$D = \frac{kT}{f_n} \tag{14}$$

where: D = diffusion coefficient

k = Boltzman constant

T = temperature

f_n = friction constant

Equation (14) holds for any thermally driven process governed by the three-dimensional random walk of diffusing species. Stokes' equation states that the friction constant is proportional to viscosity[15] :

$$f_n = \lambda\eta \tag{15}$$

As reviewed by Ferry[13], the work of Rouse and Bueche demonstrated that equation (15) holds for polymers and that the proportionality coefficient λ is a function of density, molecular weight, and molecular geometry[13] . In this case, f_n is a measure of segmental frictional resistance. Combining (14) and (15) yields:

$$D = \lambda^{-1}\ kT\ F \tag{16}$$

And we find a diffusion coefficient of the form:

$$D = \mu T\ \exp\left(-\theta\frac{V - V_f}{V_f}\right) \tag{17}$$

where μ is a material constant. Let η and η_o be the viscosities of the polymer; f and f_o the fractional free volumes at a given temperature T and a reference temperature T_o, respectively. (The fractional free volume is defined as the ratio V_f/V). Doolittle, in his work on the viscous flow of polymers showed that[13]:

$$Ln\frac{\eta}{\eta_o} = B(\frac{1}{f} - \frac{1}{f_o}) \tag{18}$$

where B is the empirical constant mentioned earlier. Assuming that f changes linearly with temperature,

$$f = f_o + \alpha_o(T - T_o) \tag{19}$$

and combining with expression (18) leads to the well known WLF equation for the shift factor a:

$$Ln\ a = -\frac{\frac{B}{f_o}(T - T_o)}{\frac{f_o}{\alpha} + T - T_o} \tag{20}$$

The WLF equation concerns itself with the viscoelastic response. It was noted earlier that in general, the critical hole size V_e for the local rearrangement of a polymer segment is not the same as the critical hole size for penetrant jump. It can be seen in expression (9) that a change in V_e can be expressed mathematically by varying θ, with V_e remaining constant. Noting that θ and B are inversely related, it is now possible to conveniently extend the above results to the diffusion of a penetrant of small size, simply by replacing B by B^D, a numerical parameter inversely related to the minimum hole size for the jump of a small penetrant molecule.

By combining expressions (14) (15) and (18) a diffusion counterpart of the Doolittle equation is found:

$$D = \frac{D_o}{T_o}\ T\ \exp\left\{-B^D(\frac{1}{f} - \frac{1}{f_o})\right\} \tag{21}$$

Derivation of the Constitutive Equation for the Diffusion of a Penetrant of Small Size:

Several investigations in the field of rheology have suggested that free volume is a good unifying parameter to describe changes in the time scale of material response. In the WLF equation, the effect of temperature was incorporated by stating that the fractional free volume was a linear function of temperature in the rubbery range. Likewise, the effect of stress and solvent concentration can be introduced by stating as a first approximation that the fractional free volume is a linear function of the dilatational stress component and the solvent concentration. Knauss and Emri[16] used this concept to develop a nonlinear viscoelastic constitutive behavior centered on free volume effects. They postulated that the change in fractional free volume due to each variable was additive:

$$f = f_0 + \alpha \Delta T + \varepsilon^f_{kk} + \gamma C \tag{22}$$

where:
- α = coefficient (volumetric) of thermal expansion of the free volume
- γ = coefficient (volumetric) of swelling
- ε^f_{kk} = volume dilatation of the free volume due to external loads

However, as pointed out by Knauss and Emri it is more appropriate to state that the free volume depends on the temperature history, strain history and swelling history if we are to extend this concept to the glassy range. Thus f should be written in the form of a sum of convolution integrals:

$$f = f_o + \alpha(t) * dT + \varepsilon^f_{kk}(t) + \gamma(t) * dC \tag{23}$$

At first, we will limit ourselves to the simpler case where α, M and γ are time independent and equation (23) reduces to (22). These assumptions are known to be correct above T_g where the system is always close to thermodynamic equilibrium. The linearity in concentration is unlikely to

be obeyed when strong diluents are used and high concentrations are approached. For this reason, it will be assumed that the change in free volume due to the solvent is better described by:

$$\Delta f = \gamma C^N \tag{24}$$

And (22) then becomes:

$$f = f_o + \alpha \Delta T + \varepsilon_{kk}^f + \gamma C^N \tag{25}$$

The exponent N must be considered as an adjustable parameter relating to the occurrence of non-zero volume change on mixing. Substituting (25) in (21) yields an expression for the diffusion coefficient:

$$D = \frac{D_o}{T_o} T \exp\left\{ \frac{B^D}{f_o} \frac{\alpha(T - T_o) + \varepsilon_{kk}^f + \gamma C^N}{f_o + \alpha(T - T_o) + \varepsilon_{kk}^f + \gamma C^N} \right\} \tag{26}$$

Although there are eight parameters in this theory, each has a precise physical significance. Subscript o, on any variable refers to a reference temperature T_o. In order to use B^D, f, and α from the WLF theory, it is convenient to use $T_o = T_g$. The domain of validity of equation (26) is the same as that of the WLF equation, that is, roughly: $\{T_g, T_g + 100\}$.

As pointed out previously, an activation energy must be introduced if one wishes to extend (26) above $T_g + 100$. This temperature range however, is not considered in the current discussion.

Extension to the Glassy State, Physical Aging:

Expression (26) was originally derived for small penetrant molecules and for temperatures corresponding to the rubbery range of the material. Local motions of the main chains or of the side groups, as well as brownian motions of the penetrant molecules, are known to persist in the glassy state as well. A list of possible local chain motions is given in Reference 13. Since such local segmental rearrangements can drive the diffusion of small penetrant molecules, the phenomenological

model derived earlier still applies in principle below the glass transition temperature, except for the temperature dependence. The reason the temperature term is not valid any more is that α describes the dilatation of the free volume above T_g only. (α is equal to the difference between the volume thermal expansion coefficient of the specific volume and that of the occupied volume). Below T_g, the fractional free volume is much less temperature dependent (although it is still time dependent due to aging). It has been shown by Matsuoka et *al.* that the abrupt change in the temperature dependence at the Glass Transition can be explained by using Adam-Gibbs' formula for the relaxation behavior[17]. Adam-Gibbs' formula expresses the shift factor in terms of the configurational entropy of the polymer, rather than in terms of the free volume. The configurational entropy is used as a measure of the size of the cooperatively rearranging region and seems to be a better description of the state of the polymer below T_g than the free volume. This entropy based approach leads to an Arrhenius-like equation if the entropy is frozen at some value, as in the rapidly quenched glassy state, or leads to a Vogel-Fulcher-like equation (same as WLF) above T_g. In order to remain consistent with the above results as well as with expression (10), the following form is proposed for the diffusion coefficient below T_g:

$$D = D_g \exp(-\frac{\Delta H}{RT}) \exp\left\{ \frac{B^D}{f_g} \quad \frac{\varepsilon^f_{kk} + \gamma C^N}{f_g + \varepsilon^f_{kk} + \gamma C^N} \right\} \tag{27}$$

where: ΔH = activation energy

R = the gas constant

Expression (27) states that the free volume continues to govern the effect of stress and swelling below the glass transition temperature, implying that these forces act primarily on very local volumetric properties such as the critical void size. By contrast temperature appears to affect chain motions over larger volumes encompassing cooperative segmental motions. The Arrhenius temperature dependence shown in expression (27) has been observed experimentally on numerous penetrant-polymer systems below the Glass Transition Temperature[7]. Often, the Arrhenius form is also used above T_g, with an activation energy differing from that below T_g. This is simply due to

the fact that the WLF equation can be mathematically fitted as an Arrhenius equation by using an apparent activation energy.

Of course, f is not the same at, and below the glass transition temperature. Thus expression (27) by itself gives an incomplete description of the material behavior. This apparent inconsistency is dealt with by introducing physical aging into the model. We will see that the use of a shift factor (acceleration factor) is phenomenologically equivalent to having a reduced v_{kk}^f.

In the rubbery state, equilibrium is reached very rapidly in response to variations in temperature, stress, and penetrant concentration. This is due to the fact that the free volume response is quasi-instantaneous under these conditions. By contrast, a material in the glassy state is not in thermodynamic equilibrium, and the response of the free volume to changes in external conditions is delayed. For this reason, a time dependent diffusion coefficient containing hereditary integrals is more promising for the glassy range. Expression (27) is still valid instantaneously however, and can be used in an iterative numerical scheme. Glassy polymers have a volume enthalpy and entropy which are larger that they would be in the equilibrium state. This metastable (or supercooled) state causes the free volume to slowly collapse with time until equilibrium is reached. The phenomenon is known as physical aging [18] . Successful diffusion modelling in the glassy range must incorporate this important effect.

Struik[18] proposed a simple method to incorporate aging in existing constitutive equations. The time dependent reduction of the free intermolecular space causes relaxation processes to take place over a longer time. Thus, an acceleration factor was defined in order to relate actual time to effective time:

$$d\lambda = a(t)dt \tag{28}$$

where: λ = effective time

t = actual time

$a(t)$ = acceleration factor

The acceleration factor may also be defined in terms of molecular mobility M(t):

$$a(t) = \frac{M(t_e + t)}{M(t_e)} \tag{29}$$

where: t_e = aging time at the start of service life or testing

t = service life or test time

Struik proposed the following power law for the acceleration factor:

$$a(t) = \left(\frac{t_e}{t_e + t} \right)^{\mu} \tag{30}$$

where μ is a constant and: $0 \leq \mu \leq 1$. Expression (30) was derived theoretically and confirmed by long term experiments[18] . We conclude that expression (23) can be readily modified to incorporate aging, by replacing actual time t by effective time λ in the integral symbols. Moreover, we have established from the above discussion that λ is related to t by:

$$\lambda = \int_0^t \left(\frac{t_e}{t_e + \xi} \right)^{\mu} d\xi \tag{31}$$

At this stage, it must be noted that there exists a secondary transition temperature T_ω in the glassy range, below which physical aging ceases, due to extremely low molecular mobility. It follows that the above treatment no longer applies below T_ω. Adamson[19] has proposed both a conceptual model and an experimental method to estimate the free volume in the entire glassy region, including the truly glassy region below T_ω. Further, his data confirm that the Free Volume Theory of molecular mobility -with some minor revisions- still explains observed sorption behavior in the glassy domain. It is true that the physics of free volume is basically incorrect in a non-equilibrium state such as the glassy state. It all remains that the basic concepts of the theory are still extremely helpful in deriving correct predictive models for the behavior under stress. As demonstrated by Knauss[16] , in the field of Viscoelasticity, these models can be valuable tools for life prediction, in spite of their inherent imperfection.

A Potential Field Function for the Stress-Induced Diffusion Flux:

It was shown earlier that stress (strain) can affect the diffusion rate in two ways: (1) by altering the mobility of the penetrant and (2) by producing an extra driving force. By relating the diffusion coefficient to strain, we addressed the mobility effect. We now must establish a theoretical background to estimate the magnitude of the stress-induced driving force. A primary cause for this driving force in a joint is uneven swelling in the direction of the moisture flux. Uneven swelling gives rise to pressure gradients along constrained bond lines. In contrast to fluids where pressure energy is dissipated, viscoelastic solids (eg: adhesives) will store some elastic energy, causing the chemical potential of the penetrant to be changed. The potential energy function introduced in expression (5) is a measure of this free energy change.

Various forms have been suggested for potential field function W_p by workers interested in the diffusion of interstitials in stressed metals[20,21], in the stress-induced diffusion of macromolecules[2,22], and in the stress assisted diffusion of small penetrants in polymers[9]. In each case, the method consisted of finding the entropic potential of the diffusing species under the stress conditions of interest. For the problem of transport of small penetrant molecules in polymers, we will take the free energy of mixing of a sorbent (subscript 1) with a polymer (subscript 2), for our entropic potential function. From the Flory-Huggins theory[23], we know that the chemical potential of the sorbent is given by:

$$\mu_1 = \mu_1^o + RT\ [\chi_1\ v_2^2 + Ln\ v_1 + v_2] \tag{32}$$

where: v_1 = volume fraction of penetrant

v_2 = volume fraction of polymer

χ_1 = Flory-Huggins interaction parameter

Let V_1 and V_2 be the volume of penetrant and polymer respectively, in the binary mixture. The fractional free volume may then be defined as:

$$f = \frac{V_f}{V_2} \tag{33}$$

Using the same notation as in the section dealing with diffusivity, and assuming that the penetrant tends to fill the available free volume, the volume of penetrant may be approximated by:

$$V_1 = V_2 \, f \tag{34}$$

The volume fraction of polymer under stress may be approximated by:

$$v_{2\varepsilon} = \frac{1}{1 + f_o + \varepsilon_{kk}^f + \gamma C^N} \tag{35}$$

Likewise, the volume fraction of penetrant under stress (before the system has recovered an equilibrium state) may approximated by:

$$v_{1\varepsilon} = \frac{f_o + \gamma C^N}{1 + f_o + \varepsilon_{kk}^f + \gamma C^N} \tag{36}$$

Since the formation of extra "holes" in the presence of mechanical deformation does not affect the sum of all pair-wise interaction energies between the polymer and the penetrant molecules, the enthalpy term in expression (32) is unchanged under stress. Thus the chemical potential μ_1^ε of the penetrant in a strained polymer is given by:

$$\mu_1^\varepsilon = \mu_1^o + RT \left[\chi \left(\frac{1}{1 + f_o + \gamma C^N} \right)^2 + Ln \left(\frac{f_o + \gamma C^N}{1 + f_o + \varepsilon_{kk}^f + \gamma C^N} \right) + \frac{1}{1 + f_o + \varepsilon_{kk}^f + \gamma C^N} \right] \tag{37}$$

The excess chemical potential of the penetrant with respect to the unperturbed state is given by:

$$\delta\mu_1^\varepsilon = RT \left[Ln \left(\frac{1 + f_o + \gamma C^N}{1 + f_o + \varepsilon_{kk}^f + \gamma C^N} \right) + \frac{1}{1 + f_o + \varepsilon_{kk}^f + \gamma C^N} - \frac{1}{1 + f_o + \gamma C^N} \right] \tag{38}$$

$\delta\mu_i$ is the excess entropic potential of the diffusing species under stress, and can be taken as our potential field function W_p.

Rearranging expression (38) and noting that $f_o \ll 1$, $\varepsilon'_{kk} \ll 1$ and $\gamma C^N \ll 1$ in all polymer-penetrant systems of interest in this study (small strains, minimal swelling), it immediately follows that:

$$\nabla W_p \simeq - RT \ \nabla \varepsilon'_{kk} \tag{39}$$

and the stress-induced flux is:

$$J^\sigma \simeq + DC \ \nabla \varepsilon'_{kk} \tag{40}$$

Note that ε'_{kk} is related to the trace of the stress tensor by an instantaneous compressibility. Thus, to some extent, $\nabla \varepsilon'_{kk}$ is analogous to a pressure gradient. However, in contrast to pressure, which can only be positive, strain or stress may be positive or negative, leading to an increase or decrease of the chemical potential. Therefore, the excess chemical potential defined earlier is an algebraic quantity.

Consider a polymer constrained between two rigid adherends held at a fixed distance. If the polymer tends to swell in the presence of moisture, ε'_{kk}, which is the mechanical component of free volume dilatation, becomes negative and more so as the concentration of penetrant increases (See chapter 3 for the constitutive relations describing the hygro-mechanical behavior). Thus ∇C and $\nabla \varepsilon'_{kk}$ have opposite signs and the two corresponding fluxes are of the same sign, leading to accelerated moisture penetration. This prediction is consistent with a number of results reported in Reference 7.

The Stress and Temperature Dependence of Solubility:

The stress (strain) dependence of solubility must be addressed if one wishes to obtain correct concentration predictions. In this section, Peterlin's approach[24] will be used to evaluate the solubility S in relation to temperature and stress. It will be shown that the predicted sensitivity of S to stress, is an order of magnitude lower than the sensitivity of the diffusion coefficient to stress and that an Arrhenius-type of relation is obeyed for temperature. Once again, the free volume concept will prove to be extremely helpful in deriving the constitutive equations.

Peterlin[24] used the Hildelbrand treatment of the thermodynamics of polymer-solvent mixtures, in which the entropy of mixing appears as a function of the fractional free volumes of the polymer (f_2) and of the penetrant (f_1). The mixture is treated as a two-component Van der Waal liquid whose entropy is proportional to the logarithm of the volume available for kinetic movement, which is assumed to be equal to the free volume of the mixture[23]. Assuming that the resultant free volume fraction of the two-component system can be obtained by a linear rule of mixture,

$$f = v_1 f_1 + v_2 f_2 \tag{41}$$

the following expression for the chemical potential of the penetrant was obtained:

$$\mu_1 = \mu_1^o + RT\left[\chi_1 v_2^2 + v_2^\varepsilon + Ln(1 - v_2^\varepsilon)\right] \tag{42}$$

where:

$$v_2^\varepsilon = \frac{f_2 v_2}{f_1 + (f_2 - f_1)v_2} \tag{43}$$

Expression (42) is another form of the Flory-Huggins equation shown in the previous section. (the same notation is used). Note that f_2, the free volume fraction of the polymer is equal to the f_o pa-

rameter introduced earlier and that the free volume fraction f_1 of a low molecular penetrant is generally larger than f_2. The chemical potential of the sorbent in the vapor phase is given by:

$$\mu_1 = \mu_1^o + RT\ Ln\ \frac{P}{P_T} \tag{44}$$

where P/P_T is the activity of the vapor in terms of partial pressure. At equilibrium, the chemical potential of the sorbent in the vapor phase must be equal to the chemical potential of the sorbent dispersed in the polymer. Expressing this equality and assuming small sorption (v_2 close to 1), gives:

$$v_1 = \frac{f_2 P}{f_1 P_T} \exp[-(1+\chi_1)] \tag{45}$$

By definition, solubility in weight fraction can be expressed as:

$$S = \frac{\rho_1 v_1}{P\ \rho_2\ v_2} \tag{46}$$

where: ρ_1 = density of the sorbent

ρ_2 = density of the polymer

It follows that solubility is related to the polymer free volume fraction by:

$$S = \frac{f_2 \rho_1}{f_1 \rho_2 P_T} \exp[-(1+\chi_1)] \tag{47}$$

The fractional free volume appears as an entropic quantity measuring the probability for the creation of a sorption site. Thus, by changing the free volume of the polymer component, stress acts predominantly on the entropy of the system (see expressions (42) and (43)). According to our notation, the free volume fraction of the polymer under strain is given by:

$$f_2 = f_2^o(1 + \frac{\epsilon_{kk}}{f_2^o}) \tag{48}$$

where: $f_2^* = f_o$.

Substituting expression (48) into (47) yields our final result for the strain dependence of solubility:

$$S = \frac{f_o \rho_1}{f_1 \rho_2 P_T} \exp[-(1+\chi_1)] (1 + \frac{\varepsilon_{kk}^f}{f_o}) \tag{49}$$

Now, from the Flory-Huggins theory, we know that the interaction parameter is related to the heat of mixing ΔH_1 by:

$$\chi_1 = \frac{\Delta H_1}{R T v_2^2} \tag{50}$$

Substituting (50) in (49) and noting that v_2 is close to 1, yields an Arrhenius type of temperature dependence:

$$S = S_A \exp(-\frac{\Delta H_1}{RT}) [1 + \frac{\varepsilon_{kk}^f}{f_o}] \tag{51}$$

where: S_A = constant.

ΔH_1 = activation energy for solubility (enthalpy of mixing).

Note that in the case of a vapor in contact with the polymer, the activation energy for solubility also contains the heat of condensation of the vapor. This is due to the fact that in the Hidelbrand theory, the reference state of the two unmixed components is the liquid state.

Thus, according to this treatment, the relative change in solubility due to stress is equal to the mechanical dilatation of the free volume normalized to the initial free volume fraction:

$$\frac{\delta S}{S_o} = \frac{\varepsilon_{kk}^f}{f_o} \tag{52}$$

where: S_o = solubility under zero strain for a fixed temperature.

An alternate and more direct treatment of the strain dependence of solubility is to immediately assume that the solubility is proportional to the total fractional free volume of the polymer. This model is based on the assumptions that (1) once equilibrium sorption is achieved sorbent molecules fill all the available free volume, including the strain-induced free volume, and that (2) swelling is negligible:

$$S = \frac{S_o}{f_o} \; (f_o + \varepsilon_{kk}^f) \tag{53}$$

which is obviously equivalent to expression (52). It will be shown in Chapter 2 that the above result agrees quite well with data collected on the carbon dioxide-low density PE system, but that lack of agreement is found in the case of water in Ultem 1000.

The relative change of the diffusion coefficient due to a small strain will be determined in Chapter 2. It will be shown that:

$$\frac{\delta D}{D_o} = \frac{B^D}{f_o^2} \; \varepsilon_{kk}^f \tag{54}$$

Recalling that B^D is close to 1 and that f_o is quite small (0.03), we conclude that diffusivity should be more sensitive to strain than solubility, by one order of magnitude or two. Also, note that diffusivity is much less affected by strain in the rubbery range than in the glassy range. This property may be attributed to the larger free volume and to the virtual incompressibility of rubbers.

Conclusion:

A comprehensive model for the diffusion of gases and vapors in polymers in a uniform temperature field and in the absence of a non-mechanical driving force has been discussed. In the isothermal case, all our results can be summarized in a system of three governing equations:

$$\frac{\partial \overline{C}}{\partial t} = \nabla \cdot \left\{ D\ (\varepsilon_{kk}^{f} C)\ \left[\nabla \overline{C} - \overline{C} \nabla \varepsilon_{kk}^{f} \right] \right\} \tag{55}$$

$$\overline{C} = \frac{C}{S_o [1 + \beta_S \varepsilon_{kk}^{f}]\, P} \tag{56}$$

$$D(\varepsilon_{kk}^{f} C) = D_o \ \exp\left\{ \frac{B^D}{f_o} \ \frac{\varepsilon_{kk}^{f} + \gamma C^N}{f_o + \varepsilon_{kk}^{f} + \gamma C^N} \right\} \tag{57}$$

where:

- $\overline{C}$ = normalized concentration
- S_o = solubility in the reference state
- β_S = experimentally or theoretically determined coefficient
- P = vapor pressure
- D_o = diffusion coefficient in the reference state
- ε_{kk}^{f} = dilatation of the free volume
- γ = coefficient of swelling expansion
- f_o = reference fractional free volume of the polymer
- B^D = parameter inversely related to the critical void size

It is now firmly established that the diffusion boundary value problem of interest in joint durability studies is highly non-linear and is coupled with the mechanical response of the polymer. The fully coupled solution for a number of boundary value problems will be given in Chapter 3, using finite element analysis. Note that equations (55) to (57) are implicitely time dependent. It

follows that the above closed form representations are incorrect when not properly coupled, in some iterative scheme, with the equations describing the viscoelastic response. (Convolution notations, as in expression (23), could be used, but would only add confusion, with no real gain in rigor)

In Chapter 2, experimental diffusion data on a number of polymer-penetrant systems will be used to validate the diffusivity and solubility models developed in this section. Particular emphasis will be placed on the effect of stress (strain) on the transport rate.

2. A MODEL FOR DIFFUSION IN POLYMERS. EXPERIMENTAL:

Introduction:

Governing equations for the diffusion of moisture in adhesives and more generally, for the diffusion of small molecules in polymers, have been derived in Chapter 1. A theory for the diffusion coefficient, based on free volume, and a theory for solubility, based on the thermodynamics of mixtures, have been proposed. In Chapter 2, the diffusivity and solubility models are validated, using selected experimental data from the literature as well as data collected by the author. Since the primary goal of this section is to verify transport theories, the polymers studied need not be good adhesives. For the same reason, other penetrants than moisture can be used. The polymer-sorbent systems studied are: ethylbenzene-polystyrene, toluene-polystyrene, toluene-

polyvinylacetate, PET-oxygen, PET-carbon dioxide, PET-water, Ultem polyimide-water, and low density PE-carbon dioxide. Only the polyimide was selected specifically for this study.

The new contributions are found mainly in the area of stress effects. Two general methods are available for measuring transport properties in mechanically loaded polymers: permeation and sorption. Data obtained with both techniques will be presented. Most of the literature data featuring stress effects seem to have been obtained by permeation techniques. Permeation techniques however, are limited to tensile stress states because the permeation membranes cannot be loaded in compression or in shear. (The small membrane thickness results in buckling under those conditions). For this reason, a new modified sorption technique was designed, which permits the study of compressive and shear stress states.

The Temperature and Concentration Dependence of Diffusivity in Polystyrene and in Polyvinylacetate in the Rubbery Range:

An expression for the temperature, concentration and strain dependence of diffusivity above T_g was derived in Chapter 1. In the absence of any mechanical volumetric strain, as expected in the rubbery state, we found that one should have:

$$D = \frac{D_o}{T_o} T \exp\left\{ \frac{B^D}{f_o} \frac{\alpha(T - T_o) + \gamma C^N}{f_o + \alpha(T - T_o) + \gamma C^N} \right\} \qquad (26')$$

Expression (26′) was fitted with diffusion coefficients from experimental data obtained by Vrentas et *al.*[14,27] for the temperature and concentration dependence in the rubbery range. The data were extracted from step-change sorption experiments following a complex procedure discussed in Reference 27. The solute-polymer systems investigated were: ethylbenzene-polystyrene, toluene-polystyrene, and toluene-polyvinylacetate. Each set of data provides diffusion coefficients for a number of concentrations and temperatures.

Expression (26′) was fitted to each of the three data sets using a nonlinear least squares routine. D was expressed in m^2/sec in order to compare the fitting parameters with the known WLF constants. The resulting parametric curves with the corresponding experimental data for the ethylbenzene-polystyrene, the toluene-polystyrene, and the toluene-polyvinylacetate systems, are shown in Figures 1,2 and 3 respectively. By itself, the excellent correlation obtained only shows that the mathematical form of Expression (26′) is correct. In order to demonstrate the predictive capability of the model, the fitting parameters were compared with the expected constants as given by the free volume theory of Williams, Landel and Ferry. The results are summarized in table 1 and 2. Within a small error, the obtained values for B^D/f_g, D_g and T_g were correct and were independent of the nature of the solvent. In addition, the obtained T_g values for the two polymers were quite close to the actual T_g's.

Since the amount of swelling is so large in the three polymer-solvent systems investigated, our model was in fact pushed beyond its expected solvent mass fraction range. In principle, the Vrentas-Duda model would be more appropriate when such high solvent concentrations are found in the polymer. In practice, however, the number of fitting parameters is so large in the Vrentas-Duda model (14 parameters, versus 7 in Expression (26′), that from a purely mathematical point of view, its curve fitting capability is not improved significantly over that of Expression (26′). We conclude that Expression (26′) is an excellent phenomenological representation of the temperature and concentration dependence of the diffusion coefficient in the rubbery range. Since moisture concentrations in adhesives are relatively low compared to the concentrations encountered in the three systems above, we a-fortiori expect excellent results in a study of moisture diffusion in adhesives, in a comparable temperature range.

The Stress Dependence of Diffusivity in Amorphous PET and in Semicrystalline PET:

The predictive capability of the Free Volume Theory for stress dependence in a glassy polymer was verified using experimental data collected by the authors of Reference 28. The diffusion of 0_2, $C0_2$ and H_20 through strained PolyEthylene Terephtalate films and through pressurized PET containers was studied. The measured parameter was permeability P, which is related to the diffusion coefficient (D) and solubility (S) by:

$$P = DS \tag{56}$$

Experimental Procedure:

A standard permeation apparatus manufactured by Modern Controls was used. A schematic of the permeation cell is given in Figure 4. The sorbent and carrier gas were both maintained at one atmosphere. Thus, the driving force for permeation was a partial pressure differential; not an absolute pressure differential. The films were loaded externally and sandwiched between the two elements of the permeation cell. Due to the absence of internal pressure, a barrier of silicon grease at the film-cell interface was sufficient to prevent any leakage. The PET films were mounted in the permeation cell under zero stress and oxygen was allowed to reach a steady state flux through the membrane. The films were then progressively stressed to higher levels; steady state permeation was re-established at each level. Two types of PET films were studied: extruded and biaxially oriented. The stretched films were produced at 100 C on a long film stretcher. Orientation was 4X by 2.8X.

In another experiment, two-liter PET bottles (oriented 4X by 2.8X upon blowing) were pressurized with carbon dioxide. The bottles were capped with a gage/valve assembly and pressurized. The sorbents studied were carbon dioxide and water, ie: not necessarily the pressurizing gas. A permeability value was calculated from the sorbent flux, the internal pressure and the average bottle thickness. The bottles were assumed to be cylindrical and stresses were calculated using thin wall vessel theory. All the data reported in this section were collected at room temperature, by the authors of Reference 28.

Results and Discussion:

Evaluation of Parameters B, f_g, β_f and γ in the case of amorphous PET:

Since our constitutive equations have been derived in terms of the volumetric expansion of the free volume, we need a stress-strain relationship in order to use the available permeability data reported as a function of the stress state. For a fully amorphous material, ε_{kk}^f is related to the hydrostatic stress σ_{kk} by:

$$\varepsilon_{kk}^f = \frac{\beta_f}{3}\ \sigma_{kk} \tag{57}$$

where: β_f = compressibility of the free volume. (As explained earlier, the occupied volume in the sense of Turnbull is compressible). From References 13 and 30, we find that: $f_g \simeq 0.033$ and we learn that for amorphous PET:

$$\frac{\beta_f}{\alpha_f} \simeq 0.36\ cm^2/kg$$

From Reference 30: $\alpha_f \simeq 1.6510^{-4}\ °C^{-1}$. The above value for α_f was given for a semi-crystalline PET. Assuming α_f is unchanged for amorphous PET we have:

$$\beta_f = 0.6\ 10^{-5}\ \text{cm}^2/kg\ \ (4.17\ 10^{-7}\ \text{in}^2/\text{lb})$$

B can be evaluated from α_f and the WLF parameters C_1 and C_2 of the shift factor:

$$B = 2.303\,\alpha_f C_1 C_2 \tag{58}$$

Using the standard values for an amorphous polymer ($C_1 = 17.44$ and $C_2 = 51.6$) we find:

$$B = 0.34 \tag{59}$$

Since the penetrant molecules of interest are small, we will further make the assumption $B^D \simeq B$. The value of γ does not need to be calculated with accuracy in this analysis. It will be sufficient to know that it can be neglected for low activity penetrants. (For the penetrants considered in this section, γ is probably of the order of 10^{-6}).

The stress dependence of D and P in the glassy state:

Equation (27) can be rewritten as follows:

$$D = D_0\ \exp\left[\frac{B^D}{f_g}\ \frac{\gamma C^N}{f_g + \varepsilon_{kk}^f + \gamma C^N}\right]\ \exp\left[\frac{B^D}{f_g}\ \frac{\varepsilon_{kk}^f}{f_g + \varepsilon_{kk}^f + \gamma C^N}\right] \tag{60}$$

Since the penetrants of interest (0_2, $C0_2$ and H_20) have a low activity in PET, swelling is minimal and the following approximation is valid:

$$\gamma C^N \ll f_g \tag{61}$$

Furthermore, for low strain levels, we also have:

$$\varepsilon_{kk}^f \ll f_g \tag{62}$$

Therefore expression (60) may be rewritten as:

$$D \simeq D_0 \exp\left(\frac{B^D}{f_g^2}\ \varepsilon_{kk}^f\right) \tag{63}$$

At low strain levels, then:

$$D \simeq D_0\left(1+\frac{B^D}{f_g^2}\ \varepsilon_{kk}^f\right) \tag{64}$$

Combining expressions (57) and (64) gives the relative change in diffusivity due to an externally applied load:

$$\frac{\Delta D}{D}=\frac{B^D}{f_g^2}\ \frac{\beta_f}{3}\ \sigma_{kk} \tag{65}$$

If the Hildelbrand-Peterlin theory is obeyed, S is a much weaker function of σ_{kk} than D (See the section on solubility in Chapter 1) and we can rewrite equation (65) in terms of a relative change in permeability:

$$\frac{\Delta P}{P}=\frac{B^D}{f_g^2}\ \frac{\beta_f}{3}\ \sigma_{kk} \tag{66}$$

Expressions (65) and (66) are valid for small stresses only. They predict the **initial** variation of P and D due to an externally applied load.

Correction For Crystallinity:

As a first approximation the following correction can be used for semi-crystalline polymers[25]:

$$D = D_a\ (1 - X_c) \tag{67}$$

or:

$$P = P_a\ (1 - 2X_c + X_c^2) \tag{68}$$

where: P_a and D_a are the permeability and diffusivity for the amorphous phase and X_c is the degree of crystallinity. The above correction accounts for the fact that the amorphous phase dominates transport properties. Note that this correction does not appear in the relative changes $\frac{\Delta D}{D}$ or $\frac{\Delta P}{P}$. A more important correction must be made however: In a semi-crystalline polymer, the stress experienced by the amorphous phase is smaller than that experienced by the material as a whole. This is due to the fact that (1) the amorphous regions have a higher compressibility than the crystalline regions and (2) displacement continuity at the interface between the amorphous phase and crystalline phase must be satisfied[25] . Therefore (66) must be modified slightly by introducing the ratio ϕ of the effective stress (experienced by the amorphous region) to the externally applied stress:

$$\frac{\Delta P}{P} = \phi\ \frac{B^D}{f_g^2}\ \frac{\beta_f}{3}\ \sigma_{kk} \tag{69}$$

The morphology of a semi-crystalline polymer depends on the circumstances of crystallization and subsequent thermal and mechanical treatment[13]. As a result, ϕ is expected to be a strong function of the specimen thermal and mechanical history, making predictions of ϕ nearly impossible. We will now check the agreement of expression (69) with experimental data borrowed from Reference 28. These data show the dependence on stress of the permeability of PET to 0_2, $C0_2$ and H_20.

The Case of Extruded PET:

The extruded PET studied was slightly crystalline: 4%. This will allow us to verify expression (69) for quasi-amorphous PET i.e.: $\phi \simeq 1$.

The experimental data are summarized in Figure 5. Two cases were studied: a balanced biaxial stress state and a uniaxial stress state. Permeability was found to be independent of the direction of the applied stress, indicating that the extruded films were isotropic.

$\sigma_{kk} = 2\sigma$ and $\sigma_{kk} = \sigma$ for a biaxial and uniaxial stress state respectively. For a balanced biaxial stress state, the initial permeability changes for amorphous PET can then be predicted by:

$$\frac{\Delta P}{P} = 2 \frac{B^D}{f_g^2} \frac{\beta_f}{3} \sigma \tag{70}$$

and similarly, for a uniaxial stress state:

$$\frac{\Delta P}{P} = \frac{B^D}{f_g^2} \frac{\beta_f}{3} \sigma \tag{71}$$

Expression (70) gives: $\frac{\Delta P}{P\sigma} = 12.6\ Gpa^{-1}$ ($8.7\ 10^{-5}psi^{-1}$) and expression (71) gives: $\frac{\Delta P}{P\sigma} = 6.3\ Gpa^{-1}$ ($4.4\ 10^{-5}psi^{-1}$). Figure 5 shows that the agreement with experimental data is remarkable. The doubling of the initial slope from uniaxial to biaxial stress states is a good check of the proposed free volume-based model. Examination of (60) suggests that the permeability should increase more slowly at higher stresses. This is not borne out of Figure 5 and is perhaps indicative of damage formation or morphology changes.

The Case of Oriented PET:

As indicated earlier, permeability tests were also conducted on biaxially oriented PET. The main differences in transport properties with extruded PET are related to the higher degree of crystallinity, resulting in a lower value of ϕ (A degree of crystallinity of 28% was reported for the oriented PET studied in this section). ϕ was evaluated on semicrystalline PET by the authors of Reference 30. A value of .694 was reported but unfortunately cannot be reused for specimens having undergone a different thermal and mechanical history. Since the available data points for oriented PET were obtained from pressurized cylinders, we have: $\sigma_{kk} = 1.5\ \sigma_h$, where: σ_h is the hoop stress.

It is found that, in order to obtain a good fit with experiment, ϕ must be close to 0.46. Results pertaining to oriented PET are summarized in Figure 6. Our value of ϕ suggests a different crystalline morphology than in the sample studied by the authors of Reference 30.

Summary:

Our findings on the stress dependence of D and P can be summarized as follows:

1. The free volume approach can predict the initial stress-induced variation of the permeability of an amorphous, glassy polymer. The slope prediction for amorphous PET is excellent.
2. The doubling of the slope from a uniaxial stress state to a biaxial stress state constitutes a good check of the free volume concept.
3. A correction can be made to account for the degree of crystallinity. This is due to the fact that the volumetric stress level experienced by the amorphous phase (dominating transport properties) is smaller than that experienced by the material as a whole. Unfortunately ϕ is difficult to predict, due to a complex dependence on the sample thermal and mechanical history.
4. Expression (65) reveals an interesting property of polymers:
   Materials with a low diffusivity (i.e. a low f_i) will be more sensitive to stress because $\frac{\Delta D}{D}$ is inversely proportional to f_i^2

The Strain Dependence of Diffusivity in a Thermoplastic Polyimide:

Experimental Procedure:

The polymer selected for this study was an amorphous thermoplastic Polyetherimide with the commercial name of Ultem[31] 1000 (T_g = 217 C). The measurement method used was sorption. The classical sorption experiment features a plane sorbate sheet of known thickness, suspended in an atmosphere maintained at constant temperature and at constant pressure. Mass uptake is plotted as a function of square root of time, and D is extracted from the initial slope. In our study, sample geometries were designed, to permit deformation of the polymer in tension, compression, or shear; while monitoring small weight changes simultaneously. This was accomplished by using a plastically deformable substrate as a light-weight loading fixture. The arrangement for the sorption cell was an adaptation of the Mc-Bain apparatus[6] . In order to avoid periodic removal of the sample from the sorption cell, the sample was suspended directly from a digital balance by a Nylon wire. Relative humidity was controlled by circulating moist air originating from a vapor exchanger containing a saturated salt solution. For optimal temperature control, the sorption cell and vapor exchanger were both kept immmersed in a thermostated water bath. The digital balance was a Sartorius 1800 with a precision of 0.1 mg and with a serial I/O port which was used for real time data acquisition. A schematic of the set-up is given in Figure 7. The tests were conducted at 60 C and at a relative humidity of 87%, generated by a sodium chloride solution. (Early tests of the apparatus showed that a 100% RH produces condensation on the specimen during small temperature fluctuations)

Specimen Preparation:

Ultem 1000 was selected for four main reasons: (1) its excellent adhesion to aluminum made it attractive for the kind of specimen geometry used, (2) its thermoplastic nature facilitates the interpretation of the results in light of the Free Volume Theory, (3) the relatively high diffusion coefficient of water in Ultem permits rapid data collection (D in Ultem is roughly 10 times higher than in an epoxy), and (4) stress relaxation is not a concern within the time frame of the tests, due to the large temperature gap between the test temperature (60 C) and T_g (217 C). In order to obtain tensile or compressive strains, Ultem films were bonded to the surface of a rectangular aluminum beams (Al 6061), and the beams were then plastically deformed to the desired residual curvature with a four point bending fixture (The beam substrate concept was originally proposed by Putter[32]). Beam curvature was uniform between the two central loading points and could yield residual longitudinal strain values on the outer skin, as high as 3.5%, in either a tensile or compressive mode. At this point, it is important to note that although the largest residual strains obtained in this study were well below the 7-8% tensile elongation yield limit of Ultem[31], our calculations indicate that the yield strain of Ultem 1000 could have been exceeded during the deformation operation in some cases. This is simply due to the fact that the recoverable elastic component of the beam deformation typically is four times larger that the plastic component. Thus the lowest residual strain which may have been associated with prior plastic yield was estimated to be around 1.5%. Following the bending procedure, the extremities of the beam with non-uniform curvatures were cut off. The specimen dimensions were the product of a compromise between the following requirements: (1) an upper limit on specimen weight was imposed by the capacity of the balance used (100g in our case), (2) the largest possible beam thickness was desirable in order to minimize beam deflections and lower the experimental error on strain, (3) the film thickness had to be small compared to the beam thickness, in order to produce a uniform through-the-thickness strain distribution and in order to limit test duration, and (4) the weight of the film had to be large enough so that the mass gain would not too small compared to the weight range of the balance.

The beam thickness and film thickness were 12.7 mm and 0.38 mm respectively. The specimen width was 25.4 mm. The aluminum substrate was vapor degreased, grit blasted, FPL etched, and primed with a solution of Ultem in methylene chloride (5g of Ultem per 100 ml). The film was bonded by compression molding at 250 C and 14 Mpa (2000 psi) in a hot press. This bonding procedure produced a polymer-to-metal bond of sufficient quality to withstand large deformations as well as environmental attack for the duration of the test. Note that for small strains, an elastic deformation was produced in the film. This can be explained by the fact that stress relaxation was minimal in the time frame of the sorption tests (one day for a thickness of .38mm). Finally, all the specimens were conditioned in a vacuum oven at 60 C, for three days, prior to plastic deformation and testing.

In order to obtain a shear strain state, samples were made consisting of a solid aluminum cylinder coated with a thin polyimide film of uniform thickness. This was accomplished by molding a square block of of Ultem around the cylinder, which was then machined down with a lathe with a tolerance of +/-25 microns. The cylinders were then plastically deformed in a torsional jig, thereby producing a quasi-uniform shear strain in the film bonded to their outer skin. The design requirements, surface treatments and bonding technique were the same as with the beam specimens. The cylinder diameter and film thickness were 12.6 mm and 0.5 mm respectively. Shear strains as large as 4% could be obtained. All the torsional specimens were conditioned in a vacuum oven at 60 C for five days, prior to plastic deformation and testing.

Results and Discussion:

A typical sorption curve obtained from our tests is shown in figure 8. The initial mass gain was not linear when plotted against time, but became linear when plotted against square root of time. Figure 9 illustrates this result by showing a plot of the fractional weight increase (multiplied by a factor of two), against the square root of time normalized to the film thickness. The straight line up to 70% of the saturation level is indicative of Fickian behavior with a constant diffusion

coefficient. The factor of two on the ordinate axis originates from the fact that only one side of the film is exposed to water vapor. Since initial moisture penetrations proceeds as in a semi-infinite medium, the initial rate of mass uptake was half of what it would have been in a free film. The correction factor simply enabled us to extract the diffusion coefficient by measuring the initial slope according to the classical procedure.

Further examination of Figure 8 reveals that, as the maximum mass is approached, a departure from ideal Fickian behavior occurs, in the form of a sudden excess sorption. The excess mass was consistently observed on most specimens. Since this effect is also observed on neat films, it must be related to some kind of bulk viscoelastic response of Ultem. The exact nature of the mechanism involved is still unknown at this stage. It is fortunate that this relaxation phenomenon did not come into play at an earlier stage of sorption, when it would have most likely given rise to a non-Fickian kinetics. The dashed line in Figure 8 represents the extrapolated Fickian sorption. Since the anomalous behavior is transient and short, the extrapolated asymptote, and not the actual maximum, was used for the determination of the solubility of water vapor in Ultem.

Figure 10 shows the diffusion coefficient of water in Ultem, normalized to its value at zero strain, versus the longitudinal component of the strain (on the outer skin of a plastically bent beam). Positive, as well as negative strain values are plotted. For small strains, a linear response, consistent with our theoretical predictions for an amorphous polymer in the elastic range can be seen. Note that the compressive strain state lowers diffusivity, whereas the tensile stress state increases diffusivity, as expected. Further, whenever the longitudinal strain exceeds 1 % in absolute value, a slope reversal occurs. A very large decrease in D at high tensile elongations, similar to what we encountered in our study, has been reported in polyethylene drawn at 60 C and tested at 25 C. The sharp drop was attributed to orientation-induced crystallization[25] . Because of the lack of symmetry in Ultem's molecular chains however, this mechanism is unlikely to have occured here. As for the increase of D at large compressive strains, damage growth appears to be a plausible explanation, since defects are known to enhance the transport rate in polymers[7]. However, no damage could be detected visually in any of the specimens. At this point, it is instructive to recall that plastic deformation is likely to have developed in the specimens featuring a residual surface longi-

tudinal strain as low as 1.5%, which is precisely the strain level at which we see our theoretical predictions fail. The precise molecular events which could lead to such an abrupt change in diffusion behavior under plastic deformation are not known at this time.

Recalling that the compressibility of the free volume is roughly one half of that of the specific volume, the initial slope in Figure 10 can be related to a slope with respect to the dilatational strain of the free volume, by the following approximation:

$$\frac{\Delta D}{D_o \, \varepsilon_{kk}} = \frac{\Delta D}{D_o \, \varepsilon_{xx}} \quad \frac{2}{(1 - \nu_1 - \nu_2)} \tag{72}$$

with: ν_1 = lateral Poisson's Ratio (Plastic deformation of the beam)

ν_2 = Poisson's ratio of the polymer

Poisson' s ratio ν_1 was approximated by the value 0.5 because the residual deformation in the beam (after unloading the bending fixture) is dominated by the plastic component of strain, and plastic flow is known to occur with no volume change. Poisson's ratio ν_2 was reported[33] to be 0.435. Once multiplied by the correction factor introduced in expression (72), the experimentally measured slope for small strains (in Figure 10), was found to be equal to 1230 (dimensionless). According to the Free Volume Theory, this value must be equal to $\frac{B^D}{f_g^2}$. If B^D is assumed to be equal to 0.4, a f_g equal to 0.018 is found. If B^D is assumed to be equal to 1.0, a f_g equal to 0.029 is found. (.4 to 1 is the range for B suggested in the literature[13]) Noting that these two values are close to the lower and upper limits quoted for f_g in the literature[13], we conclude that expression (64) is obeyed at low strain levels and that the assumption that the stress dependence of D below T_g is free volume governed, is verified.

Figure 11 shows the diffusion coefficient of water vapor in Ultem, normalized to its value at zero strain, versus shear strain (on the skin of a plastically twisted cylinder). The Lagrangian definition of strain is used. Diffusivity is found to be independent of the level of shear strain. Since a pure shear strain state does not alter the specific volume of the material, the above result constitutes a crucial verification of the Free Volume Theory.

Summary:

Our findings on the strain dependence of D can be summarized as follows:

1. Expression (64) can predict the initial strain-induced variation of diffusivity in the water-Ultem system, both under a tensile stress state and a compressive stress state.
2. The initial reduction of D under a compressive stress state, constitutes an excellent check of the free volume concept.
3. Shear strain does not affect D.

The Strain Dependence of Solubility in Low Density Polyethylene and in a Thermoplastic Polyimide:

The Case of Carbon Dioxide in Low Density Polyethylene:

A behavior consistent with the theories proposed in Chapter 1 has been reported in Reference 25, where the authors studied the permeation of CO_2 in low density polyethylene films under strain (see Figure 12). For small strains, expression (51) is able to describe the behavior correctly **within the experimental error**. The main result is the confirmation that solubility is fairly insensitive to low

strains. Practically, this means that if a polymer-penetrant system exhibiting similar behavior was encountered in a durability study, the solubility could easily be assumed to be stress independent. For large strains, expression (51) also leads to correct predictions[25] (see Figure 12), but it is difficult to lend any significance to this result in view of the fact that crystallinity appears, leading to properties which cannot be adequately described by an unmodified free volume theory. It was also shown in Chapter 1 that diffusivity is much more sensitive to strain than solubility, roughly by an order of magnitude; this is also quite evident in the experimental data presented in Figure 12. We conclude that the solubility models based on the thermodynamics of mixtures approach and the free volume occupation approach seem to work reasonably well at low strains for the Polyethylene carbon dioxide system. The fact that one finds agreement below T_g, where thermodynamic equilibrium is not achieved, is not too surprising when one considers that the derivation were based primarily on geometric considerations (either lattice theory or free volume occupancy).

The Case of Water Vapor in Ultem Polyimide:

The solubility data discussed in this section were collected along with the diffusivity data presented in Figures 10 and 11. The same specimens and the same conditions were used. Figure 13 shows the relative change of the solubility of water in Ultem films subjected to varying levels of longitudinal strains. Re-using expression (72) and replacing D by S yields a slope with respect to the dilatation of the free volume, equal to 1077 (dimensionless), which is roughly the slope we found for the diffusion coefficient. According to expression (51), this slope should be close to 40. The reason behind this sharp departure from the theory could be related to the fact that the hydrogen bond network of the polyimide is gradually broken up under strain, thereby releasing an increasing number of hydrogen bond sites for water. Unfortunately, this explanation is not consistent with our data for D under a shear strain. Figure 14 shows the relative change of the solubility of water in Ultem films subjected to varying levels of shear strains. As in the case of

diffusivity, solubility is found to be independent of the level of shear strain. This result was expected, since a pure shear strain state does not change the specific volume of the material; but it is not consistent with the hydrogen bond argument developed above because hydrogen bonds would also be broken up under shear.

Summary:

1. Expression (51) can predict the initial variation of solubility under a uniaxial strain, in the carbon dioxide-low density PE system, but not in the water-Ultem system.
2. A shear strain state does not affect solubility in the water-Ultem system, as expected.

Conclusion:

With the exception of the strain dependence of solubility in Ultem, good agreement has been found between the theory and experiment. This leads us to conclude that the models presented in Chapter 1 hold very promising predictive capabilities for joint durability studies. The lack of agreement with the solubility model for certain materials can be easily remedied, simply by replacing expression (51) by an equation determined empirically. Such a procedure is perfectly legitimate in the framework of an engineering solution of the durability problem.

Thus far, the data were mainly a description of the short term response of the polymer. Our level of confidence is now sufficient to embark in more complex simulations, including the viscoelastic behavior of the polymer over longer times. Chapter 3 will include a validation problem

featuring a time dependent diffusion coefficient, as well as numerical simulations of moisture penetration in a butt joint.

Table 1. Self Diffusion Data for Polystyrene.

SOURCE:	$\log D_g$	B^*/f_g	α_g (deg-1)	f_g	T_g (C)	γ	N
PS FERRY'S WLF theory	-	30.30	.00069	0.033	97.	-	-
ETHYLBENZENE - POLYSTYR DIFF DATA BEST FIT	-24.3	17.9	.00255	0.074	80.	0.48	0.61
TOLUENE - POLYSTYR DIFF DATA BEST FIT	-24.6	16.4	.00099	0.014	88.	0.51	0.90

Table 2. Self Diffusion Data for Polyvinylacetate.

SOURCE:	$\log D_g$	B^*/f_g	α_g (deg-1)	f_g	T_g (C)	γ	N
PVac FERRY'S WLF theory	-	35.71	.00044	0.028	32.	-	-
TOLUENE - PVac DIFF DATA BEST FIT	-15.5	8.8	.00450	0.319	50.3	2.1	0.91

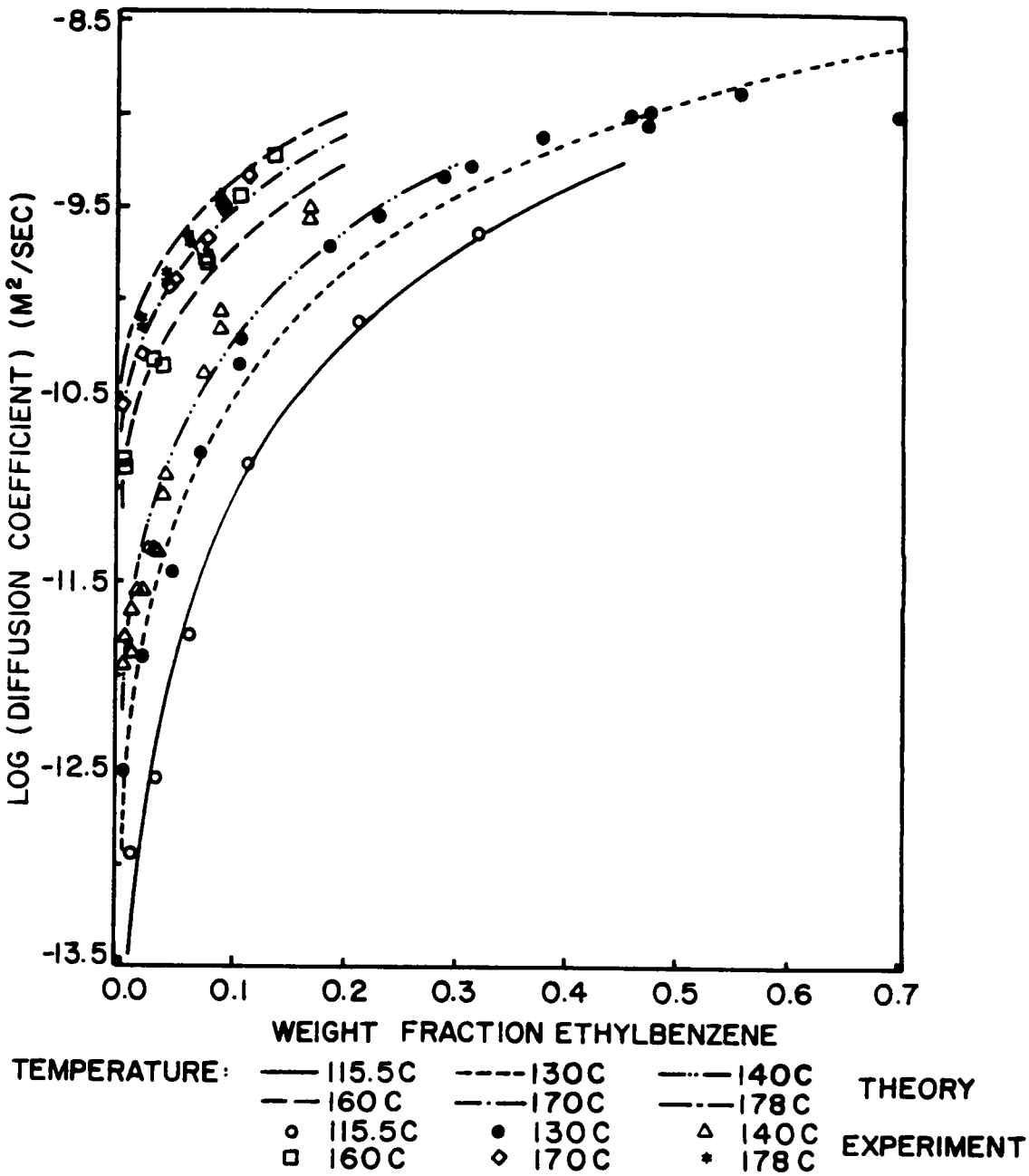

Figure 1. Validation for Temperature and Concentration Dependence: Ethylbenzene-Polystyrene System. Data from Vrentas & Duda [27].

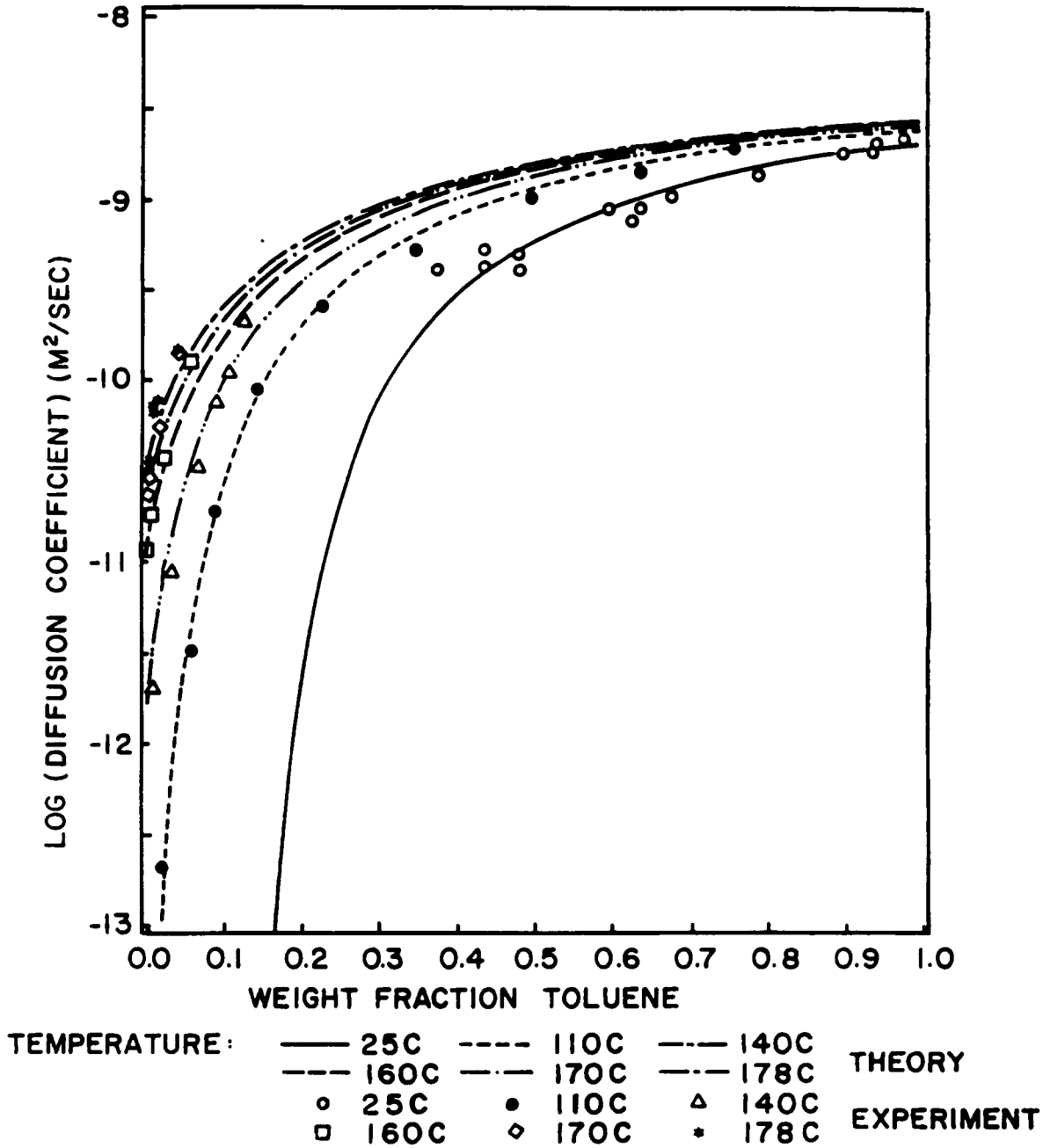

Figure 2. Validation for Temperature and Concentration Dependence: Toluene-Polystyrene System. Data from Vrentas & Duda [27].

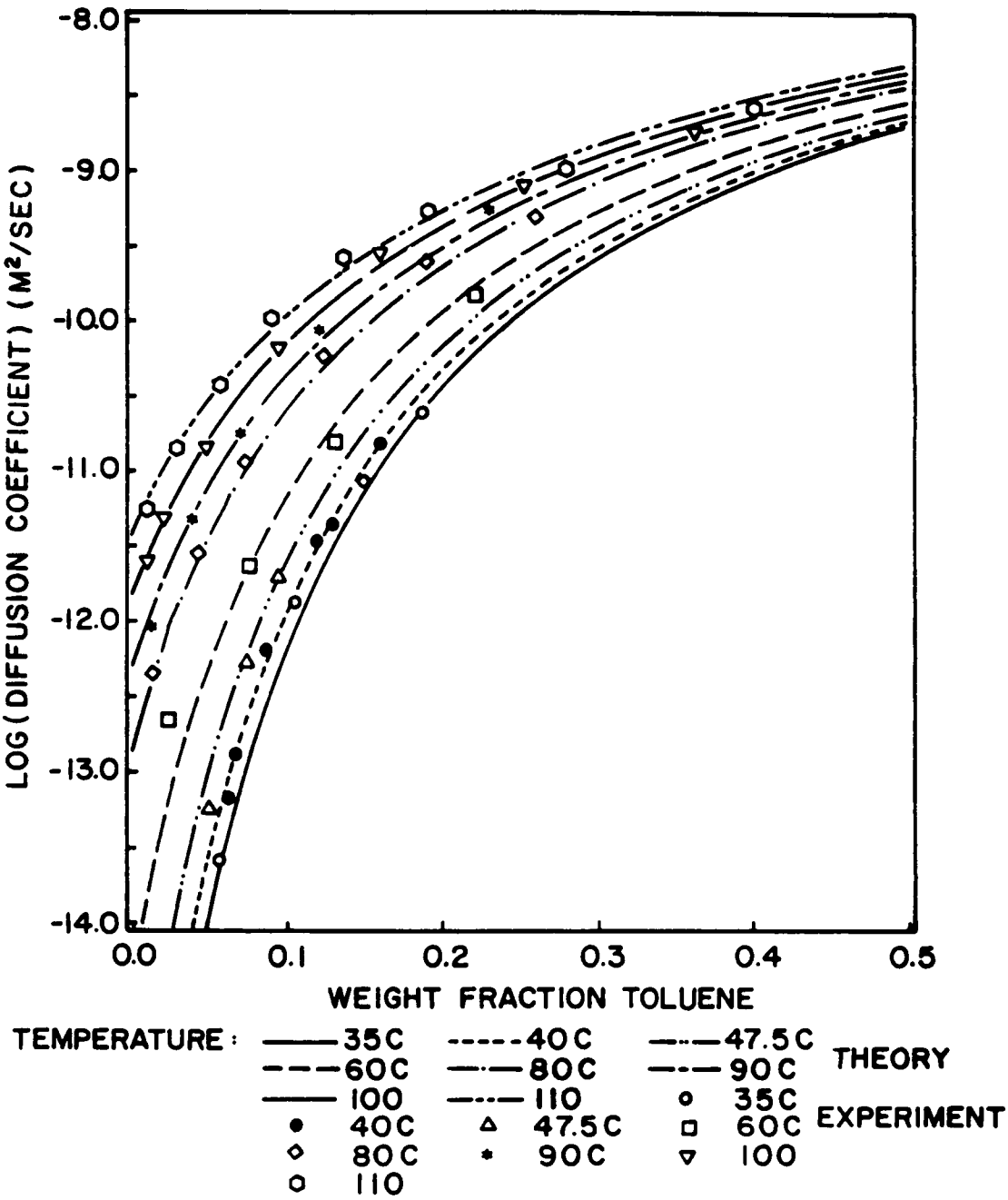

Figure 3. Validation for Temperature and Concentration Dependence: Toluene-Polyvinylacetate System. Data from Vrentas & Duda [27].

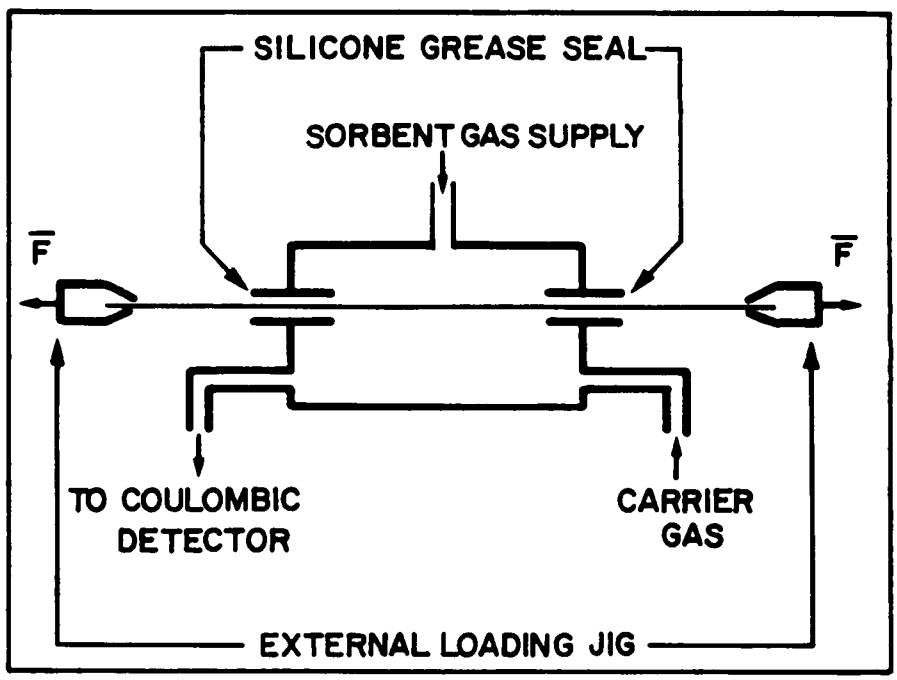

Figure 4. Cell for Permeation Studies on Mechanically Loaded PET Films.

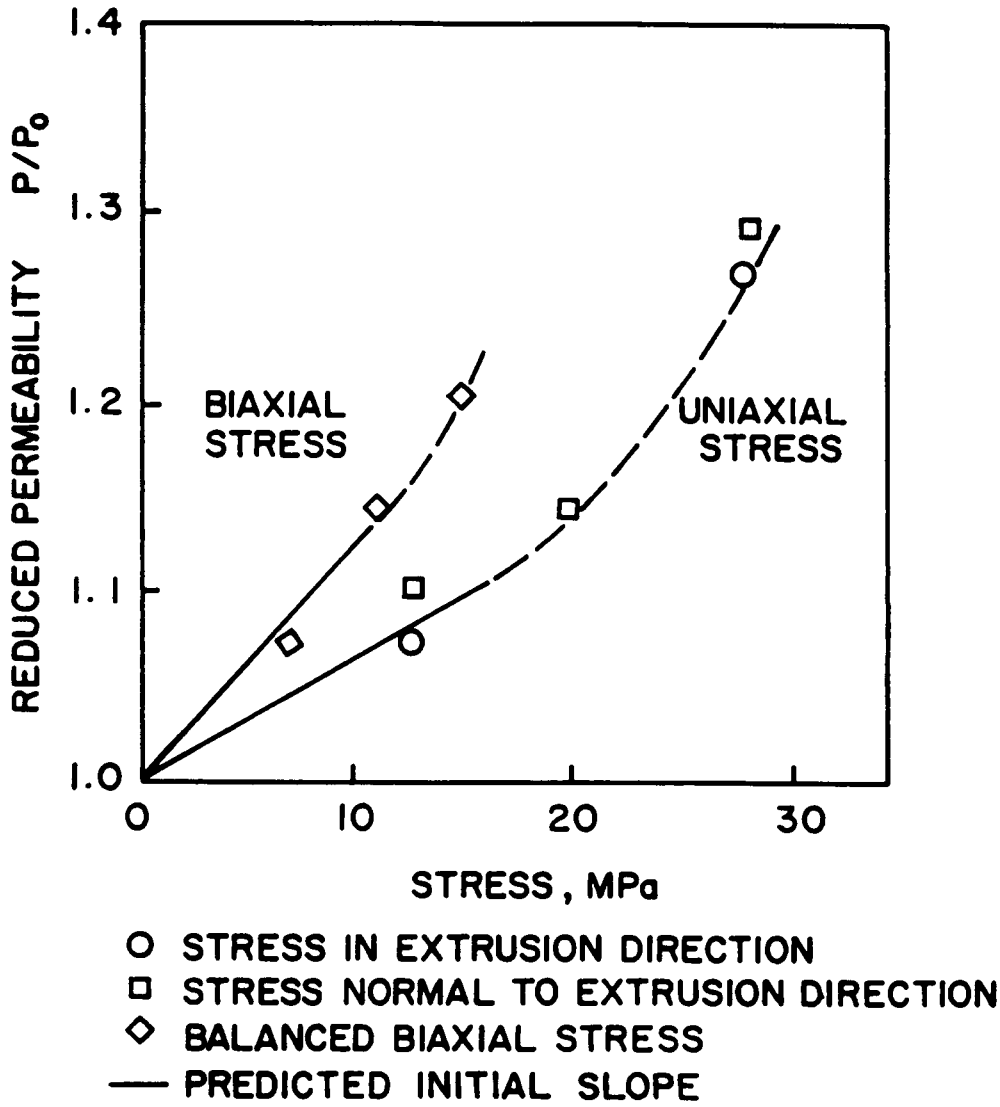

Figure 5. Stress Dependence of Permeability: Oxygen in Extruded PET [28].

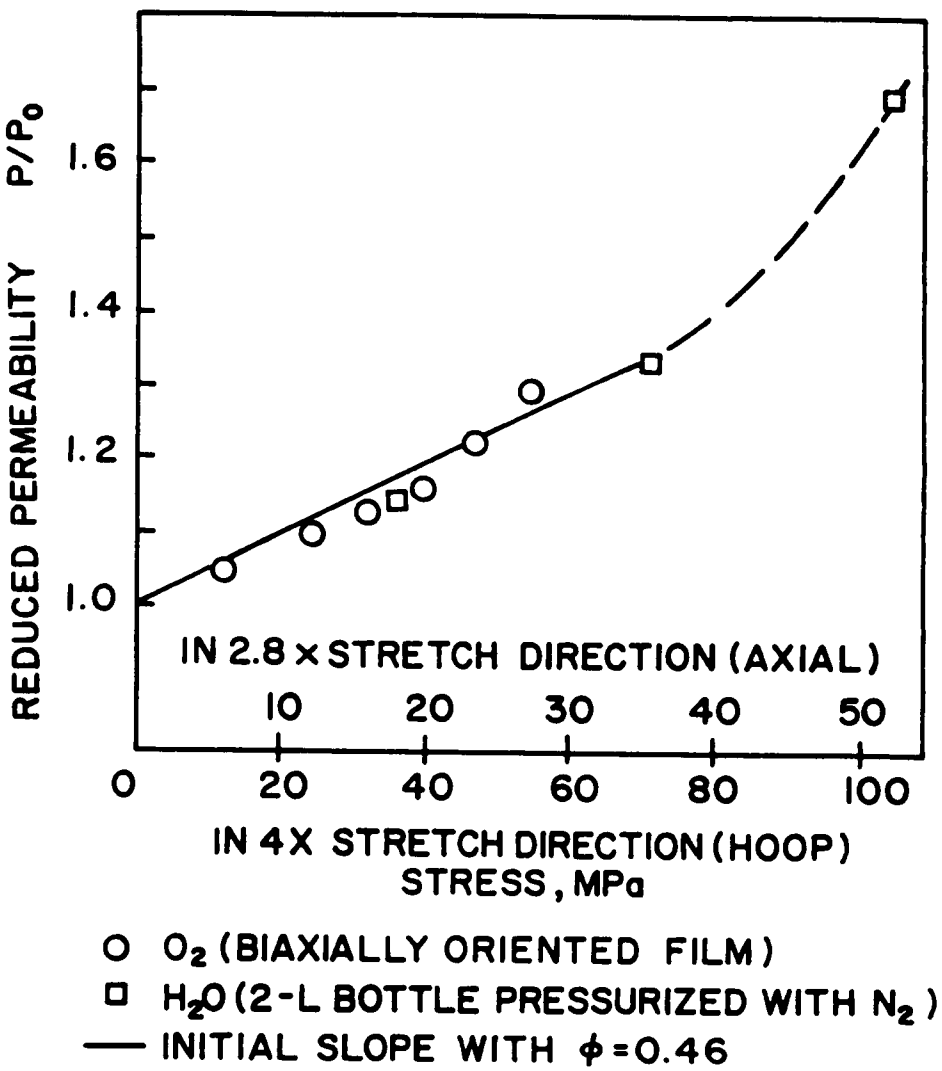

Figure 6. Effect of a Biaxial Stress on Permeability: Oxygen, Carbon Dioxide and Water in Oriented PET [28].

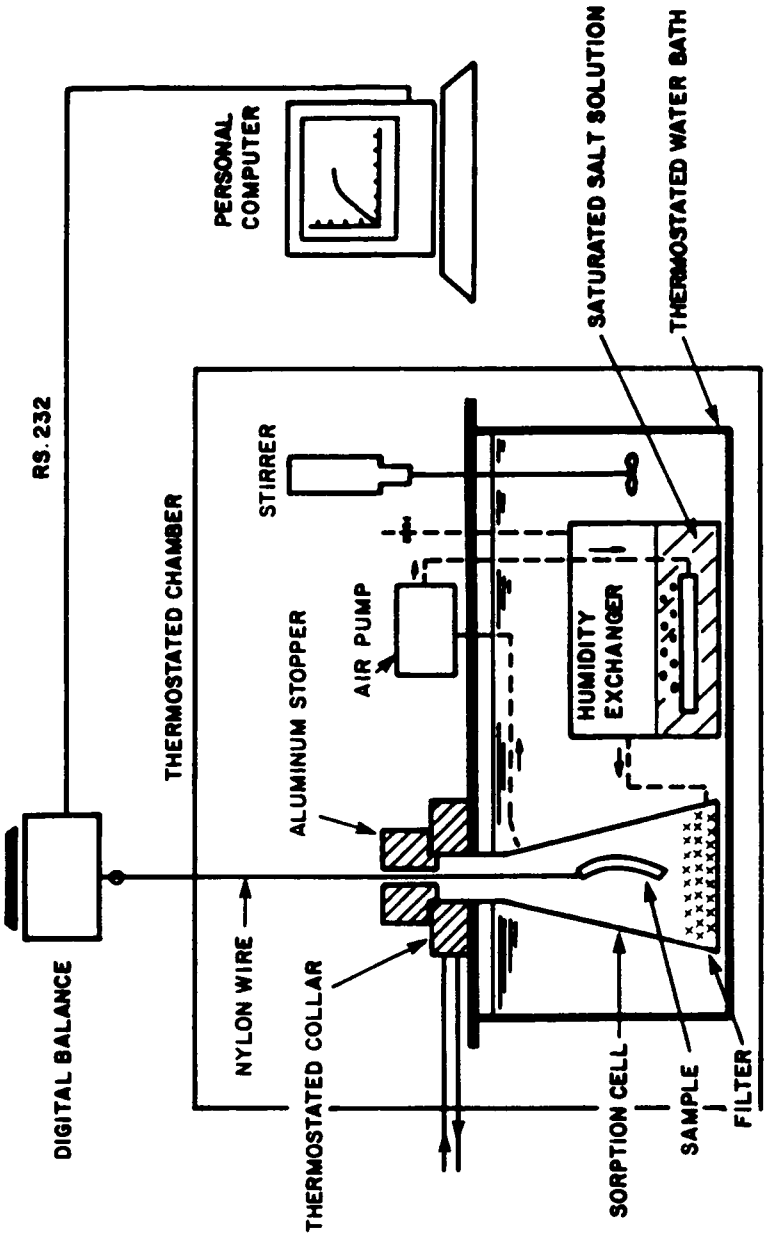

Figure 7. Modified Sorption Apparatus: Note the Beam Specimen inside the Sorption Cell.

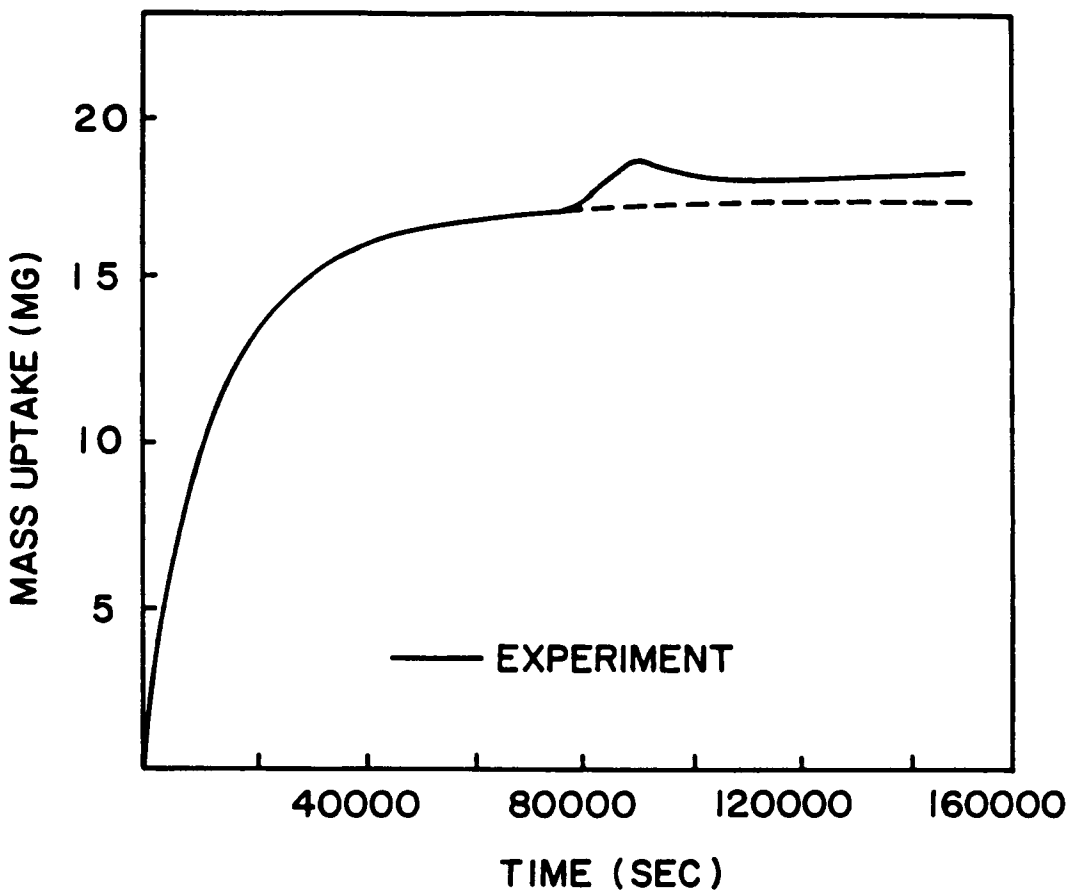

Figure 8. Sorption Curve for a Torsional Specimen: The Ultem Film is Subjected to a Shear Strain Level of .83%. (60 C).

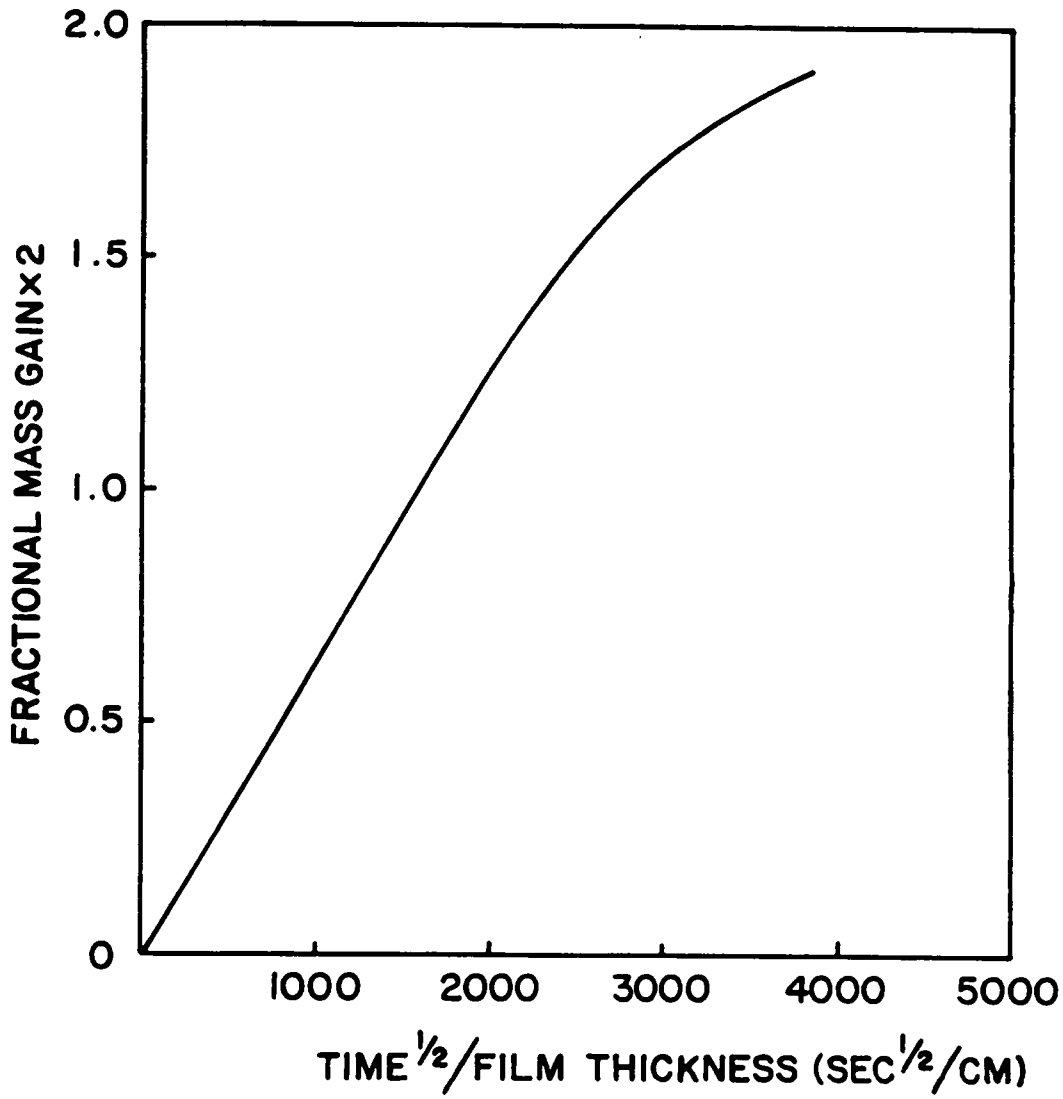

Figure 9. Normalized Sorption Curve: Same Specimen and Same Conditions as in Figure 8.

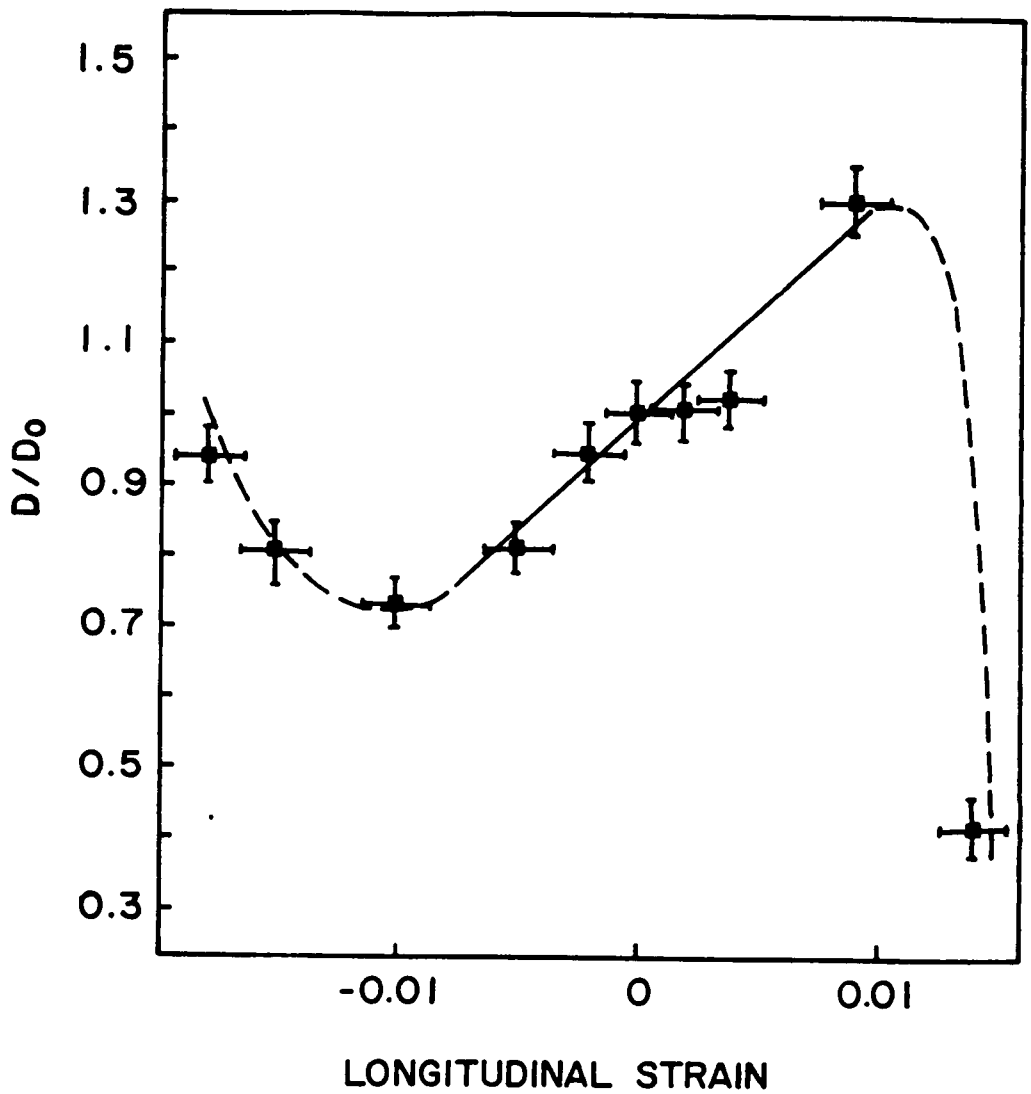

Figure 10. Effect of Strain in the Water Vapor-Ultem System: Normalized Diffusivity in a Film Subjected to a Uniaxial Strain (Beam Specimens, 60 C).

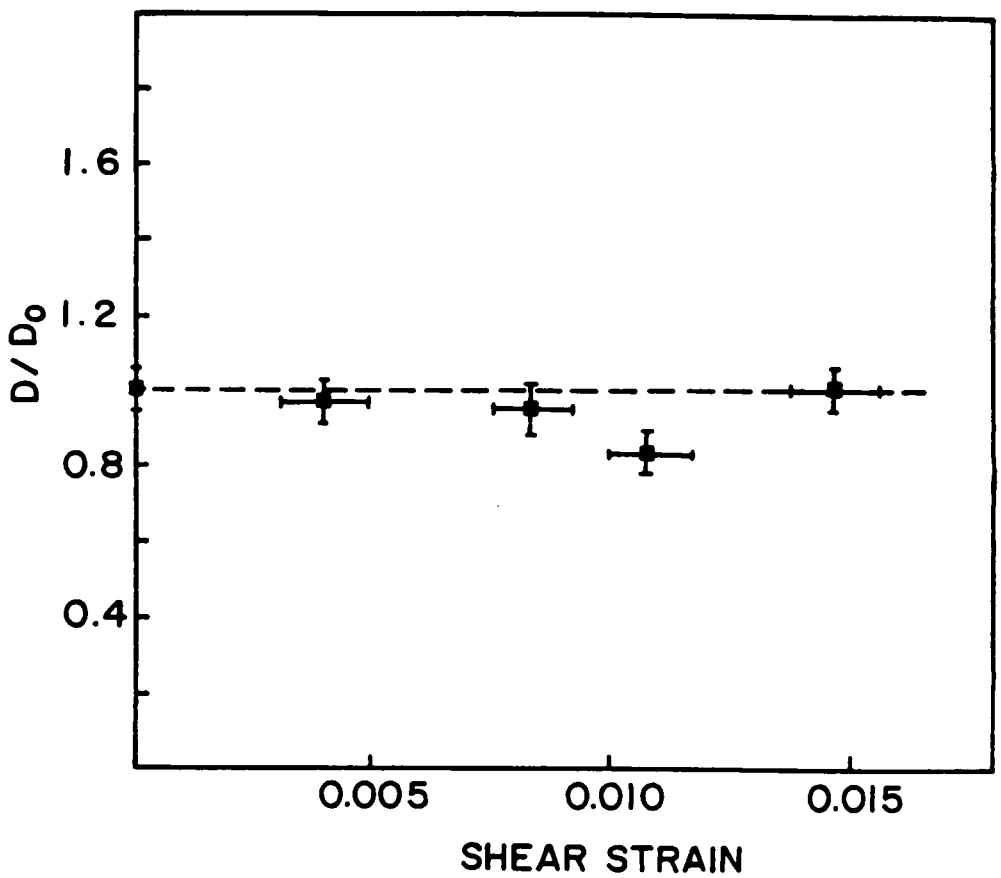

Figure 11. Effect of Strain in the Vapor-Ultem System: Normalized Diffusivity in a Film Subjected to a Shear Strain. (Torsional Specimens, 60 C).

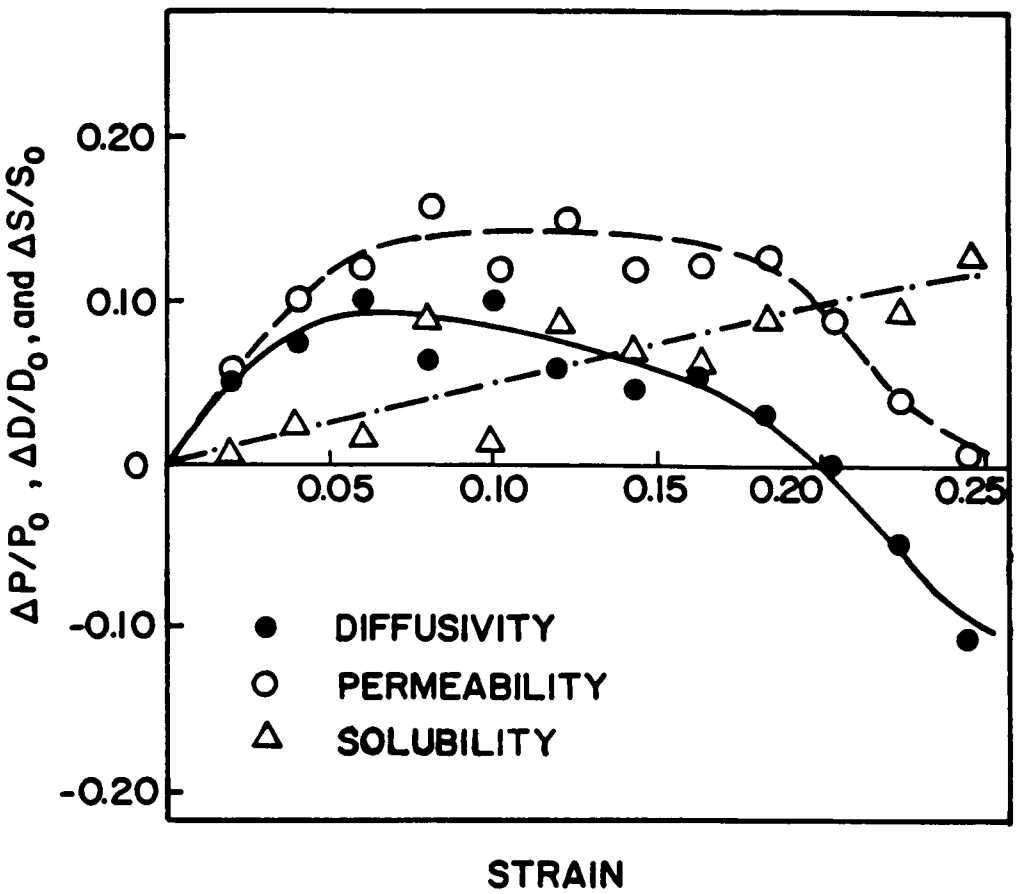

Figure 12. Effect of Strain in the Carbon Dioxide-Low Density PE system: Normalized D, S, and P vs. Unidirectional Strain. [25]

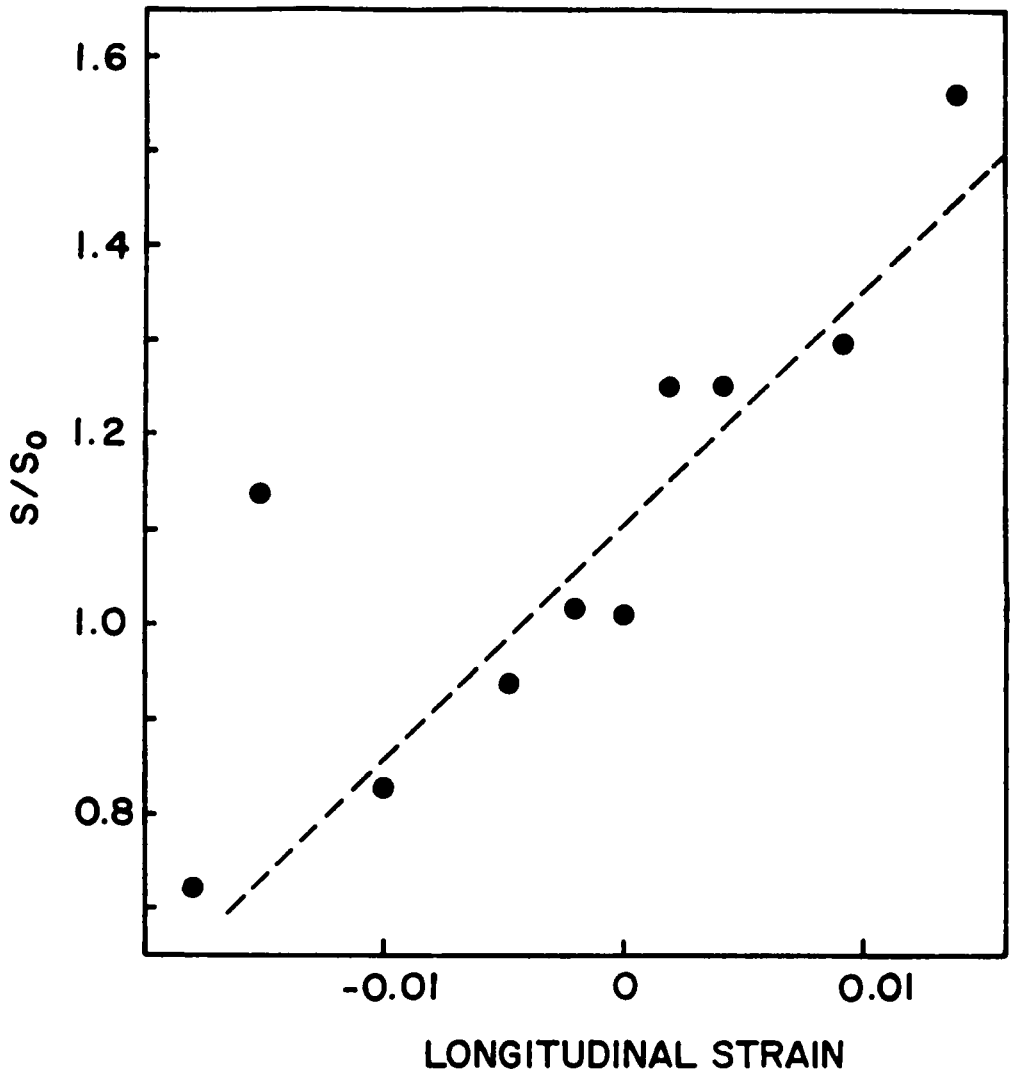

Figure 13. Effect of Strain in the Water Vapor-Ultem System: Normalized Solubility in a Film Subjected to a Biaxial Strain. (Beam Specimens, 60 C).

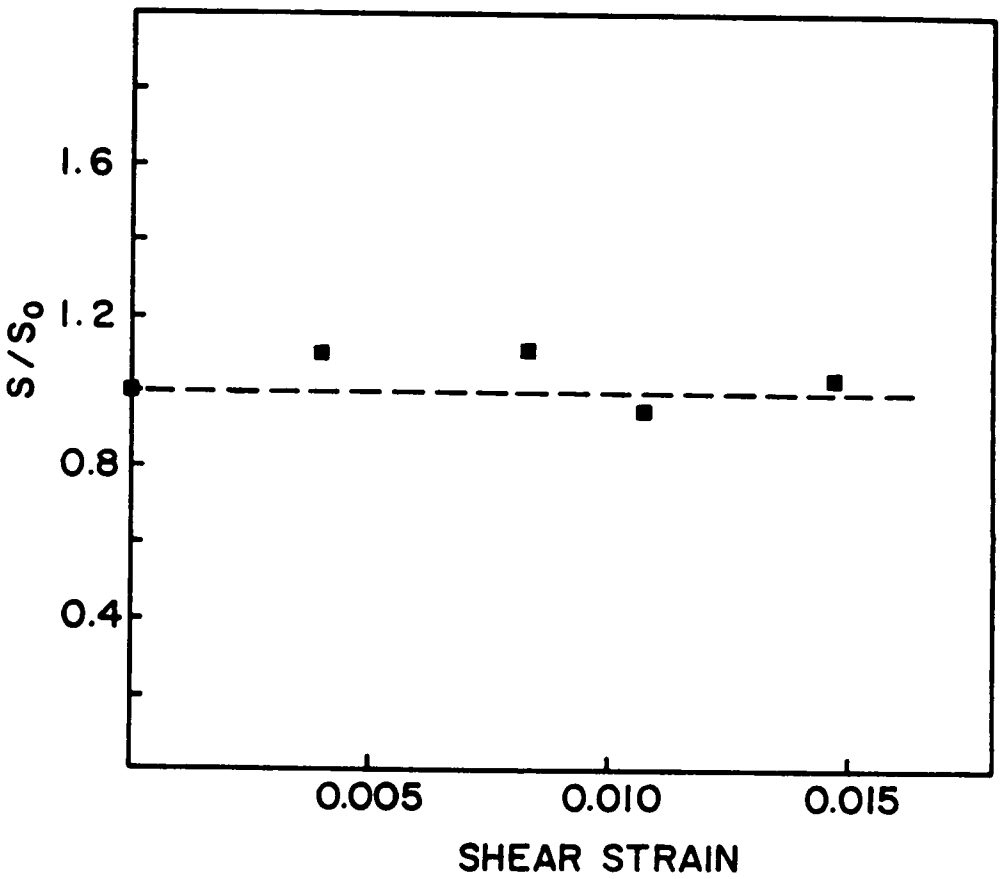

Figure 14. Effect of Strain in the Water Vapor-Ultem System: Normalized Solubility in a Film Subjected to a Shear Strain. (Torsional Specimens, 60 C).

3. A MODEL FOR THE DIFFUSION OF MOISTURE IN ADHESIVE JOINTS. NUMERICAL SIMULATIONS:

Introduction:

Governing equations for the diffusion of moisture in adhesive joints have been derived in Chapter 1 and validated experimentally in Chapter 2. In these preceding sections, the coupling of diffusion kinetics with the mechanical behavior was established. It was shown that the highly nonlinear nature of the governing equations, as well as their implicit time dependence made the use of an iterative numerical solution necessary.

In Chapter 3, a two-dimensional solution of the fully coupled diffusion problem is obtained using the finite element code NOVA. NOVA has been under continuous development at Virginia

Tech by Dr. Reddy and S. Roy for the past two years. The objective is to provide a more accurate analysis of adhesively bonded joints[34–36] . In NOVA, the mechanical response of the adhesive layer can be modelled using Schapery's or Knauss' nonlinear single integral constitutive laws for multi-axial states of stress. Penetrant permeation is modelled using the diffusion equations derived in Chapter 1 (An extensive validation study of the various original features of the code is presented in References 34 to 36). In this section, one of the most interesting capabilities of NOVA will be demonstrated by a numerical simulation reproducing experimental results featuring a **time-dependent** diffusion coefficient in a Polystyrene film strained uniaxially. Further, the effect of the various forms of strain coupling on diffusion kinetics will be studied by simulating a butt joint undergoing moisture intake from the edges. The accompanying evolution of the stress and strain fields in the adhesive layer will also be presented. Chapter 3 is the fruit of a team effort with S. Roy.

Knauss' Nonlinear Viscoelastic Theory:

Since the diffusion-governing equations are coupled with the mechanical response via volumetric strain, constitutive equations for the viscoelastic behavior of the adhesive are also needed in order to solve the fully coupled diffusion problem. Knauss' nonlinear viscoelasticity theory is the most natural choice for the present study because it employs the same phenomenological description as the diffusion constitutive behavior proposed in Chapter 1. Free volume in the sense of Turnbull, is used as a unifying parameter to describe changes in the time scale of the viscoelastic response. Specifically, the theory states that mechanical dilatational strain, temperature and sorbent, simultaneously act as a time accelerating parameter by dilating the free volume.

In the Knauss approach, the basic single integral formulation of linear viscoelasticity is used. The stress and strain tensors are related by the Stieltjes convolution integrals and the material is assumed to undergo small deformations[16]. Consider an isotropic polymer. Let $J(t)$ and $B(t)$ be the shear compliance and bulk compliance respectively. The constitutive equations in the framework of linear viscoelasticity are given by:

$$e_{ij} = \frac{1}{2} \int_{-\infty}^{t} J(t-\xi) \frac{\partial S_{ij}}{\partial \xi} \, d\xi \tag{73}$$

$$\varepsilon_{kk} = \frac{1}{3} \int_{-\infty}^{t} B(t-\xi) \frac{\partial \sigma_{kk}}{\partial \xi} \, d\xi \tag{74}$$

where:
- e_{ij} = deviatoric strain
- ε_{kk} = volumetric strain (Mechanical component)
- S_{ij} = deviatoric stress
- σ_{kk} = volumetric stress

and the indicial summation convention is assumed. The equation numbers are continued from Chapters 1 and 2.

Knauss introduced the nonlinearity by expressing that the time scale of viscoelastic response as described by $J(t)$ and $B(t)$ is a strong function of free volume dilatation Δf. The total free volume dilatation Δf is expressed as the sum of a mechanical strain contribution, a thermal expansion contribution and a sorbent expansion contribution:

$$\Delta f = \varepsilon^{f}_{kk} + \alpha \, \Delta T + \gamma C \tag{75}$$

where:
- α = coefficient of thermal expansion of the free volume
- γ = coefficient of swelling
- ε^{f}_{kk} = volume dilatation of the free volume due to external loads

This approach has been used in our derivation of an expression for the diffusion coefficient in Chapter 1. Furthermore, Knauss assumed that: (1) free volume changes do not change the distribution function of retardation times in $J(t)$ and $B(t)$, implying that the material is thermorheologically simple, and (2) the same shift factor can be used for both shear and bulk properties. Mathematically, the time is simply shifted by using the differential expression:

$$dt' = \frac{dt}{a(\Delta f)} \tag{76}$$

where t' denotes the reduced time and the shift factor $a(\Delta f)$ is given by:

$$Ln\ \{a(\Delta f)\} = -\frac{B}{f_o}\ \frac{\Delta f(T) + \varepsilon^f_{kk} + \gamma C}{f_o + \Delta f(T) + \varepsilon^f_{kk} + \gamma C} \tag{77}$$

where $\Delta f(T)$ is a function describing thermally-induced changes in the free volume in the temperature domain of interest. For example, $\Delta f(T) = \alpha(T - T_g)$ above T_g.

Thus, Knauss' shift factor is an immediate generalization of the WLF shift factor (expression 20). Note that for $\varepsilon^f_{kk} = 0$ and $\gamma C = 0$, the standard WLF equation is recovered. Knauss' nonlinear constitutive behavior can now be summarized as follows:

$$e_{ij} = \frac{1}{2} \int_{-\infty}^{t} J(\psi - \psi')\ \frac{\partial S_{ij}}{\partial \tau}\ d\tau \tag{78}$$

$$\varepsilon_{kk} = \frac{1}{3} \int_{-\infty}^{t} B(\psi - \psi')\ \frac{\partial \sigma_{kk}}{\partial \tau}\ d\tau \tag{79}$$

with:

$$\psi(t) = \int_{-\infty}^{t} \frac{dt'}{a(\Delta f)} \tag{80}$$

$$\psi' = \psi(\tau) = \int_{-\infty}^{\tau} \frac{dt'}{a(\Delta f)} \tag{81}$$

An obvious advantage in using Knauss' constitutive model in our study is that the shift factor subroutine can be shared by both the diffusion code and the viscoelasticity code. Only void size factors B and B^D differ in principle in the two boundary-value problems.

It was noted earlier that NOVA has provision for either the Schapery or Knauss nonlinear viscoelastic theories. The basic form of the constitutive equations is similar in both theories; they only differ by the form and number of nonlinearizing functions. Fortunately, it is possible to reduce Knauss' model as a particular case of Schapery's model by changing the expression for the shift factor and setting the remaining nonlinearizing functions to 1. This scheme was used in the finite element formulation of the viscoelastic behavior in NOVA.

Numerical Scheme:

The coupling between diffusion and viscoelasticity can be easily seen by cross-examining the governing equations for the Diffusion Boundary- Value Problem (DBVP, Expressions (55) to (57)) and the Constitutive equations for the Viscoelasticity Boundary-Value Problem (VBVP, Expressions (78) to (81)). The diffusion equations are strain dependent, while the viscoelastic behavior is affected by a sorbent concentration term in the shift factor. The mechanical response is also af-

fected by sorbent concentration, in that mechanical strains can be generated due to swelling. This effect is incorporated in the governing equations by stating that the total strain contains a sorbent expansion component.

The interplay between the DBVP and the VBVP is illustrated in Figure 15. Numerically, this coupling can be implemented by solving the diffusion problem and viscoelasticity problem concurrently in order to continually update the coupling variables, namely, the volumetric strain and sorbent concentration. This scheme has been encoded in NOVA and is summarized by the flow chart shown in Figure 16. Note that the strain dependence of the solubility is not included in this study. The experimental data presented in Chapter 2 seem to justify this approximation as long as the penetrant does not show much chemical affinity with the polymer.

The numerical treatment presented herein introduces an implicit time dependence in the diffusivity and in the solubility, thereby allowing the simulation of more complex sorption behaviors known as "anomalous" or "case II". Case II sorption refers to a case where the rate of transport is entirely governed by the rate of viscoelastic relaxation[7]. Anomalous diffusion refers to an intermediate case between Fickian and Case II diffusion.

Finite Element Formulation of the Problem:

Viscoelasticity Formulation:

The total strain and stress components in a material can be written as the sum of deviatoric and volumetric components:

$$\varepsilon_{ij} = e_{ij} + \frac{1}{3}\ \varepsilon_{kk}\ \delta_{ij} \tag{82}$$

$$\sigma_{ij} = S_{ij} + \frac{1}{3}\ \sigma_{kk}\ \delta_{ij} \tag{83}$$

For a viscoelastic material, the constitutive equations discussed earlier can be rewritten in the following form, if the effects due to loading history prior to t = 0 are negligible:

$$\varepsilon_{kk} = \frac{1}{3}\ B(0)\ \sigma_{kk}(t) + \frac{1}{3}\ \int_0^t \Delta B\ (\psi - \psi')\ \frac{\partial}{\partial \tau}\ \sigma_{kk}(\tau)\ .\ d\tau \tag{84a}$$

$$e_{ij} = \frac{1}{2}\ J(0)\ S_{ij}(t) + \frac{1}{2}\ \int_0^t \Delta J\ (\psi - \psi')\ \frac{\partial}{\partial \tau}\ S_{ij}(\tau)\ d\tau \tag{84b}$$

where, ψ and ψ' are given by expressions (80) and (81) respectively.

Using results from equation (84) in equations (82) and 83), one obtains for two dimensional analysis

$$\{\varepsilon\} = [C]\ *\ \{d\sigma\} \tag{85a}$$

where:

$$\{\varepsilon\} = \{\varepsilon_{11},\ \varepsilon_{22},\ \gamma_{12},\ \varepsilon_{33}\}^T \tag{85b}$$

$$[C] = \begin{bmatrix} (\frac{B}{9} + \frac{J}{3})(\frac{B}{9} - \frac{J}{6}) & 0 & (\frac{B}{9} - \frac{J}{6}) \\ & (\frac{B}{9} + \frac{J}{3}) & 0 \\ \text{symmetric} & & J \\ & & & (\frac{B}{9} + \frac{J}{3}) \end{bmatrix} \tag{85c}$$

and:

$$\{d\sigma\} = \{d\sigma_{11},\ d\sigma_{22},\ d\tau_{12}\ d\sigma_{33}\}^T \tag{85d}$$

and where the symbol (*) denotes the convolution operator.

If the transient compliances are now written in the form of a Prony series, then:

$$\Delta B(\psi) = \sum_{r=1}^{n} B_r\ (1 - \exp(-\psi/\tau_r)) \tag{86a}$$

$$\Delta J(\psi) = \sum_{r=1}^{m} J_r(1 - \exp(-\psi/\eta_r)) \tag{86b}$$

Substituting equations (86a) and (86b) in equation (85a) results in a matrix equation given by:

$$\{\varepsilon\} = [N]\ \{\sigma\} + \{H\} \tag{87}$$

where the matrix $[N]$ contains the instantaneous compliances at time t, and the vector $\{H\}$ contains the components of the hereditary strains. Pre-multiplying equation (87) by $[N]^{-1}$ and rearranging,

$$\{\sigma\} = [L]\ (\{\varepsilon\} - \{H\}) \tag{88}$$

where:

$$[L] = [N]^{-1} \tag{89}$$

The finite-element equilibrium equations may be established by invoking the principle of virtual work:

$$\{\delta u\}^T \left(\int_V [B]^T \{\sigma\}\, dV - \{F\} \right) = \{0\} \tag{90}$$

Using results from equation (88) in (90) yields,

$$\{\delta u\}^T \left(\int_V [B]^T [L] \{\varepsilon\} \, dV - \int_V [B]^T [L] \{H\} \, dV - \{F\} \right) = \{0\} \tag{91}$$

Writing the strain-displacement relations as:

$$\{\varepsilon\} = [B] \{u\} \tag{92}$$

and substituting in (91):

$$\{\delta u\}^T \left(\int_V [B]^T [L] [B] \, dV \{u\} - \int_V [B]^T [L] \{H\} dV - \{F\} \right) = \{0\} \tag{93}$$

or simply,

$$\{\delta u\}^T \{R\} = \{0\} \tag{94}$$

Noting that equation (93) contains a source of nonlinearity imbedded in the definition of the shift factor, the Newton-Raphson iteration technique is employed to solve for the displacements.

For the i^{th} iteration, the incremental displacements $\{\Delta u_i\}$ are obtained from:

$$\{\Delta u_i\} = - [K_T]^{-1} \{R_i\} \tag{95}$$

and:

$$\{u_i\} = \{u_{i-1}\} + \{\Delta u_i\} \tag{96}$$

where:

$$[K_T] = \int_V [B]^T [L] [B] \, dV \tag{97}$$

Moisture Diffusion Analysis:

The finite element formulation of Fick's Law in two dimensions is developed using the weak variational form[34–36]; the "weak" form of the variational procedure weakens the continuity requirements on the displacements, by allowing discontinuity in the displacement gradients:

$$\int_{\Omega^e} V \cdot \left[\frac{\partial C}{\partial t} - \frac{\partial}{\partial x}\left(D\,\frac{\partial C}{\partial x} + KDC\,\frac{\partial \varepsilon_{kk}}{\partial x} \right) - \frac{\partial}{\partial y}\left(D\,\frac{\partial C}{\partial y} + KDC\,\frac{\partial \varepsilon_{kk}}{\partial y} \right) \right] dxdy = 0 \quad (98)$$

For the plane strain case, the volumetric strains can be expressed as

$$\varepsilon_{kk} = \frac{\partial u}{\partial x} + \frac{\partial v}{\partial y} - \gamma C - \alpha \Delta T \quad (99)$$

Assuming that the moisture concentration may be approximated by:

$$C(x, y, t) = \sum_{j=1}^{n} \psi_j (x, y)\, C_j(t), \quad (100)$$

and the test function in expression (98) may be set to be equal to the interpolation function:

$$V = \psi_i \quad (101)$$

Substitution of Eq. (100) into the weak form of Eq. (98) (See Reddy[34]) gives

$$[M^e]\{\dot{C}\} + [K^e]\{C\} = \{F^e\} \quad (102)$$

where:

$$[M^e] = \int_{\Omega^e} \psi_i \psi_j \, dxdy \quad (103)$$

$$[K^e] = \int_{\Omega^e} D\left(\frac{\partial \psi_I}{\partial x} \cdot \frac{\partial \psi_J}{\partial x} + \frac{\partial \psi_I}{\partial y} \cdot \frac{\partial \psi_J}{\partial y} \right) dxdy \tag{104}$$

$$\{F^e\} = -\int_{\Gamma^e} \psi_I \hat{q}\, dS - K \int_{\Omega e} \left\{ D \cdot \left(\sum_{J=1}^{n} \psi_J C_J \right) \left[\left(\frac{\partial^2 u}{\partial x^2} + \frac{\partial^2 v}{\partial x \partial y} - \gamma \frac{\partial C}{\partial x} - \alpha \frac{\partial \Delta T}{\partial x} \right) \frac{\partial \psi_I}{\partial x} + \left(\frac{\partial^2 u}{\partial x \partial y} + \frac{\partial^2 v}{\partial y^2} - \gamma \frac{\partial C}{\partial y} - \alpha \frac{\partial \Delta T}{\partial y} \right) \frac{\partial \psi_I}{\partial y} \right] \right\} dxdy \tag{105}$$

and:

$$\hat{q} = -D\left\{ \left(\frac{\partial C}{\partial X} + KC \frac{\partial \varepsilon_{kk}}{\partial x} \right) n_x + \left(\frac{\partial C}{\partial y} + KC \frac{\partial \varepsilon_{kk}}{\partial y} \right) n_y \right\} \tag{106}$$

The time derivative $\{\dot{C}\}$ is approximated by using the θ - family of approximation for the n^{th} time step,

$$\theta\{\dot{C}\}_{n+1} + (1-\theta)\{\dot{C}_n\} = (\{C\}_{n+1} - \{C\}_n)/\Delta t_{n+1} \quad \text{for} \quad 0 \leq \theta \leq 1 \tag{107}$$

where θ is a weighting parameter. From equations (99) and (106), we obtain for each element,

$$[A^e]\{C\}_{n+1} - [B^e]\{C\}_n - \{P^e\}_n = \{0\} \tag{108}$$

where:

$$[A^e] = [M^e] + \theta \Delta t_{n+1} [K^e] \tag{109}$$

$$[B^e] = [M^e] - (1-\theta)\Delta t_{n+1} [K^e] \tag{110}$$

$$[P^e] = \Delta t_{n+1}(\theta \{F^e\}_{n+1} + (1-\theta)\{F^e\}_n) \tag{111}$$

Recognizing that a source of nonlinearity in the form of the diffusion coefficient D is imbedded in the matrix $[K^e]$, the Newton-Raphson technique is employed to solve for the moisture concentrations $\{C\}_{n+1}$ at each time step.

Validation Problem: Viscoelastic Diffusion Through a Polystyrene Film:

Smith et *al.*[37,38] conducted a permeation experiment to study gas transport in polystyrene and found that the diffusion coefficient for CO_2, Ar and Xe decreased with time when the polystyrene film was subjected to a constant uniaxial strain. Figures 17 and 18 reproduce experimental results from Reference 37. Figure 17 illustrates the time dependence of the diffusion coefficient for CO_2 in a Trycite film (biaxially oriented polystyrene film) at different strains at 50°C. Figure 18 illustrates the time dependence of the diffusion coefficient for CO_2 and Xe in a Trycite film at the same strain level at 50°C.

The reason these experimental data were found to be convenient for a test of NOVA is that polystyrene is adequately characterized mechanically. Reference 13 gives the viscoelastic shear compliance and the viscoelastic bulk compliance of polystyrene around the glass transition temperature (100°C). Bulk properties are rarely documented in the literature. This is due to a lack of recognition for their importance, compounded by complexities in the measurement techniques. Yet, our study demonstrates that the diffusion behavior as well as the nonlinear viscoelastic behavior are intimately related to bulk properties. In fact, the methodology developed here-in establishes that bulk characterization is an absolute necessity for improved diffusion predictions.

Although the shear compliance and bulk compliance are given for two different molecular weights (500,000 and 600,000 respectively), the properties were assumed to be usable for any high molecular weight polystyrene. This assumption is valid as long as the molecular weight is large compared to some critical value (38,000 for Polystyrene), corresponding to the onset of entanglement coupling[13].

The compliances around 100°C given in Reference 13 were curve-fitted with a Prony Series using a nonlinear least-square fitting routine. Since predictions must be compared to data at 50°C, a time-temperature shift had to be performed. It is well known that the shift factor below the glass transition temperature is governed by an activation energy instead of an activation volume, as in the case of the rubbery state. The shift factor is given by:

$$a = \exp\left[\frac{\Delta H}{R}\left(\frac{1}{T_R} - \frac{1}{T}\right)\right] \tag{112}$$

where: ΔH = activation energy

R = gas constant

T_R = reference temperature

T = temperature

Values of ΔH between 30 kcal/mole and 40 kcal/mole have been suggested by Ferry[13] and Matsuoka[17]. A value of 35 kcal/mole was taken in our study, which corresponds to a shift factor of 1500. This means that the retardation times at 50°C are 1500 larger than a 100°C, reflecting the slower mechanical response of the material at a lower temperature (time in sec). The same shift factor was used for the bulk compliance and the shear compliance[17] .

The reference temperature T_o for the diffusion problem was fixed at 50°C and the reference diffusion coefficient D_o was taken from the measured values at 50°C in Reference 37. Since all the data points in reference 37 are given at 50°C, the temperature term in the shift factor was set to zero in all the computations. The swelling coefficient of expansion γ was set to zero because the sorbents used in the permeation studies have little chemical affinity with polystyrene.

At this point, it is useful to recall that the volumetric strain e_{kk}^{f} contained in the diffusion equation corresponds to the dilatation of the free volume and not to the mechanical volumetric strain ε_{kk}, used in the governing equations for viscoelasticity. Kovac's model presented in Reference 13 postulates that the free volume dilatational strain e_{kk}^{f} is equal to the transient component of the mechanical strain ε_{kk}. Kovac's approach was used, and the free volume dilatation strain at any time was given by:

$$e_{kk}^{f} = \varepsilon_{kk} - 3B_o \sigma_{kk} \tag{113}$$

At infinite times, one finds that e_{kk}^{f} is approximately equal to one half of ε_{kk}, which is consistent with remarks made previously in Chapter 2.

Figures 19, 20 and 21 show numerical simulations produced by NOVA, of the problem studied by Smith et *al* in Reference 37. Figure 19 shows the variation of the diffusion coefficient with time for the three strain levels indicated in Figure 17. From Figure 19, it is evident that, independently of the strain level, the diffusion coefficient reaches a peak at t = 1 hour and then slowly decays back to the reference value D_o. This behavior can be attributed to an initial increase in the free volume due to the application of the uniaxial strain, followed by a continuous recovery in free volume at constant strain, as the polystyrene film undergoes shear relaxation which gradually reduces the hydrostatic stress level. A larger applied strain produces larger initial dilatation, resulting in a higher peak in the diffusion coefficient. Figure 19 also reveals that the rate of change of the diffusion coefficient (to be paralleled with the rate of change of the free volume) becomes larger as the applied strain level increases. This strain level dependence in the response rate is an excellent illustration of the nonlinear nature of the mechanical response, described here by Knauss' model. It should be noted that the initial increase in the diffusion coefficient is largely due to the fact that bulk creep occurs on a much shorter time scale than creep in shear (Our data indicate a shift of about five decades between the bulk retardation spectrum and the shear retardation spectrum). Upon examining the time scale of Figure 19, it becomes clear that the initial increase in the diffusion was not experimentally accessible to Smith et *al* . For this reason, the initial transient response

was seen as instantaneous by Smith et al. and only the relaxation part of the curve is shown in Figure 17. For the same reason, the diffusion coefficient in Figure 17 is normalized with respect to its value at a time accessible experimentally, instead of being normalized with respect to D_o, as in Figure 18. Bearing these details in mind, it becomes apparent that the right hand side of Figure 19 correlates very nicely, although not exactly, with the experimental results of Figure 17. The good agreement between the simulation and the experimental data is a strong indication that NOVA holds real promise for joint durability prediction.

The influence of penetrant molecule size on the diffusion coefficient for gases in polystyrene was qualitatively studied by varying the magnitude of void size parameter B^D. Levita and Smith[37] explained that, due to molecular shape effects, the effective critical void size of a CO_2 molecule is larger than that of Xenon. It follows, from our discussion in Chapter 1, that B^D for $C0_2$ should be smaller than that of Xenon (B^D and the critical void size V_C are inversely related). Figure 20 shows predictions obtained from NOVA for two values of B^D and a strain of 1.8% in a polystyrene film. By comparing Figure 20 with Figure 18, it can be seen that NOVA correctly predicts that a smaller penetrant molecular size leads to a faster rate of decrease in the diffusion coefficient. Since the actual B^D values for CO_2 and Xe are unknown, the above comparison is only qualitative at this point.

The effect of physical aging on the diffusion coefficient was studied by implementing equation (31) of Chapter 1 in NOVA. The penetrant was CO_2 and the values of temperature strain and t_e were set at 50°C, 1.8% and 24 hours respectively. Figure 21 shows that a faster rate of physical aging denoted by a higher value of parameter μ , causes the diffusion coefficient to decay more slowly. This behavior is expected, since a smaller free volume causes molecular relaxation processes to occur over a larger period of time. Unfortunately, no experimental data are available for comparison here.

Diffusion Kinetics in a Butt Joint.

In this section, a number of numerical simulations of moisture diffusion in the adhesive layer of a butt joint are presented. The main emphasis is on evaluating the relative importance of the various coupling effects between diffusion and mechanical strain (stress). In order to achieve this goal, a parametric study was carried out using realistic values for the adhesive properties. The adhesive mechanical properties were those of polystyrene at 50°C. The fact that polystyrene is a poor adhesive is of no concern for this kind of study. In order to study the effect of swelling, a large volume for the coefficient of swelling expansion (γ) was needed. Since γ for polystyrene is negligible, a fictitious material combining the mechanical properties of polystyrene and the coefficient of swelling expansion of a moderately hydrophilic polymer ($\gamma = 0.01$) was used.

Table 3 summarizes the four cases investigated in the parametric study. (The numbering of the cases run, should not be confused with the fundamental modes of sorption known as "Case I" and "Case II") The joint geometry and finite element discretization are given in Figure 22. Note that the mechanical boundary conditions used were a uniform axial displacement resulting in a uniform strain of 2% in the adhesive layer. The normalized moisture concentration at the free edge of the adhesive layer is unity and the initial concentration throughout the adhesive layer is zero.

Figure 23 shows the moisture concentration profiles within the adhesive layer at three different times when there is no coupling (case 1). In this case, the diffusion coefficient remains constant with time, that is, $D = D_o$. Case 1 is the classical Fickian diffusion in a plane sheet for which a closed form solution is available. For short times, as in our simulations, the sheet may be considered as a semi-infinite medium and the following approximation is convenient:

$$\overline{C}(t, y) = \mathit{erfc}\ (y/2\sqrt{D_o\, t}) \tag{114}$$

where erfc is the error function complement.

Figure 24 shows the moisture concentration profiles for the case where there is viscoelastic coupling only, that is, when both the diffusion coefficient and the shift factor are dependent on the transient component of the dilatational strain (Case 2).

Figure 25 depicts the case where there is full coupling in the diffusion coefficient and in the shift factor. This means that the diffusion coefficient and the shift factor are both a function of the dilatational strain and of the moisture concentration at any given point in the adhesive. Note the dramatic increase in penetration rate relative to the two previous cases, as well as the convex shape of the concentration profiles. The moisture profiles for the fully coupled diffusion problem (Case 4) are not shown because they are indistinguishable from those plotted in Figure 25 (Case 3). In addition to all the features of case 3, case 4 includes the contribution of the strain-induced driving force ∇W_p. This last case required the use of 135 time steps, compared to about 50 time steps for case 1.

Lastly, Figure 26 presents the results for each of the four previous cases, for comparison at time t = 60 minutes. Note that case 3 and case 4 are still indistinguishable after 60 minutes. Only strain and concentration coupling in the diffusion coefficient seem to have a significant accelerating effect. Of course, the effect of differential swelling would have appeared if a larger value of the coefficient of moisture expansion had been used. High magnitudes for γ, promoting case II kinetics, are encountered when the penetrant is a good solvent of the polymer. For structural adhesives in the presence of moisture however, γ is expected to be close to 0.01 (An estimate of γ from data in Reference 39 yields a value of 0.014 for a 3501-6 epoxy). The various types of diffusion behaviors in polymers have been graphically summarized by Hopfenberg and Frish[6] in terms of penetrant activity and temperature (see Figure 30). Examination of this chart confirms that non-Fickian driving forces are not operative below T_g as long as penetrant activity is small, and that a concentration dependent diffusion coefficient is then sufficient to describe the transport behavior.

The main findings from this study may be summarized as follows:

1. The mechanical and hygroelastic coupling terms in the diffusion coefficient must be included in a durability analysis, due to their substantial accelerating effect on penetration kinetics.

2. The effect of differential swelling can be counted as negligible for a typical structural adhesive. Polymers for which this extra driving force becomes important are not likely to be selected for adhesive applications, due to their poor performance in moist environments.

Evaluation of the Stress and Strain Fields in a Butt Joint Upon Moisture Penetration:

The results presented in this section were generated by running case 3 (see Table 3) with NOVA. The bond line discretization, mechanical boundary conditions and material properties were the same as earlier (same γ and same mechanical properties). The stress and strain fields were plotted at three different elapsed times: 0 min., 30 min. and 60 min. On each plot presented here-in, free edge OB of the butt joint is located at the right-hand side and distance along the bond line is normalized with respect to the semi-width of the joint.

Figures 27 and 28 illustrate the effect of moisture-induced swelling on the mechanical components of normal strain ε_{xx} and transverse strain ε_{yy}, respectively. In Figure 27, the absorbed moisture induces swelling strains within the adhesive, resulting in a lower value of ε_{xx} . Note that ε_{xx} refers to the **mechanical** component of strain. In the BVP considered here, three types of strains are used: the mechanical strain, the hygroscopic strain and the kinematic strain. The kinematic strain (2 % here) always remains equal to the sum of the mechanical and hygroscopic strains. Since the boundary conditions used impose a uniform positive kinematic normal strain of two percent initially, the lower values of mechanical strain ε_{xx} in the presence of moisture, remain positive. Note that in an unloaded butt joint, ε_{xx} would have become negative, reflecting the constraining effect

of the stiff adherends surrounding the adhesive. By comparing Figure 27 with Figure 25, it appears quite clearly that the region with a lowered normal strain corresponds to the domain occupied by moisture.

Figure 28 shows a negative initial transverse strain resulting from the transverse Poisson's contraction upon loading. In the absence of moisture, the algebraic value of ε_{yy} would tend to increase initially and then decrease, due to the transient bulk response of the polymer. The initial bulk creep can be seen here in the unperturbed region at time = 30 min., causing the Poisson's ratio to decrease. The subsequent bulk relaxation can be seen near the free edge as the Poisson's ratio increases again at longer times. As in the case of the normal strain, moisture-induced swelling causes an abrupt change in the distribution of ε_{yy}, and the transverse strain field in the dry region seems to be unchanged.

Figure 29 depicts the effect of moisture-induced swelling on the distribution of normal stress σ_{xx}. The comments made for ε_{xx} in Figure 27 can be repeated here. The only difference in behavior is found in the dry region ahead of the moisture front, where a stress reduction due to viscoelastic relaxation can be seen.

Conclusion:

Governing equations for the diffusion of small molecules in polymers have been derived and incorporated into a two-dimensional Finite Element code. In the case of an adhesive joint, simulations have shown that the main accelerating effects in the diffusion rate of moisture through the bond line can be traced to the strain and concentration dependence of the diffusion coefficient, the latter playing a predominant role.

Invariably, the development of powerful predictive capabilities raises the question of the adequacy of material characterization. A main finding of this study is that the bulk properties (also called volumetric properties) of the adhesive play a central role in the coupling mechanisms between the diffusion behavior and the viscoelastic response. Unfortunately, the bulk characterization of polymers has not received proper attention in experimental mechanics. This trend must be reversed if rigorous predictions of the hygromechanical behavior of adhesives are sought.

Notation

ε_{ij}	: Strain components produced due to applied mechanical stress.
e_{ij}	: Deviatoric strain components.
ε_{kk}	: Dilatational strain
ε'_{kk}	: Transient component of mechanical strain ε_{kk}
σ_{ij}	: Cauchy stress tensor
S_{ij}	: Deviatoric stress components
σ_{kk}	: Dilatational stress
$B(0)$	: Bulk compliance at time $t = 0$
$\Delta B(\psi)$	: Transient bulk compliance
$J(0)$	: Shear compliance at time $t = 0$
$\Delta J(\psi)$	: Transient shear compliance
ψ	: Reduced time
$a(\Delta f)$	: Shift factor
M_r	: Constant coefficient in Prony series
J_r	: Constant coefficient in Prony series
τ_r	: Retardation time for bulk compliance
η_r	: Retardation time for shear compliance
δ_{ij}	: Kronecker delta
$\{\delta u\}$	: First variation in displacement
$[B]$	: Strain displacement transformation matrix
$\{F\}$	: Vector of external forces
$[K_T]$	: Tangent stiffness matrix
Ω^e	: Domain of integration (area)

Γ^e : Path of integration (Line)

V : Test function

$C(x, y, t)$: Moisture concentration

D : Diffusion coefficient

K : A material constant

$\psi_j(x, y)$: Interpolation function for j^{th} node

$C_j(t)$: Moisture concentration at j^{th} node

γ : Coefficient of expansion due to moisture sorption

α : Coefficient of thermal expansion

ΔT : Temperature change

Δt_{n+1} : Step-size for the n^{th} time step

n_x : x –direction cosine for unit vector normal to the boundary

n_y : y –direction cosine for unit vector normal to the boundary

Table 3. Summary of butt joint simulations.

Case #	Strain dependence in D & *a*	Concentration dependence in D & *a*	Strain-induced driving force	Mechanical BCs (longitudinal strain)
1	No	No	No	2%
2	Yes	No	No	2%
3	Yes	Yes*	No	2%
4	Yes	Yes*	Yes	2%

(*$\gamma = 0.01$)

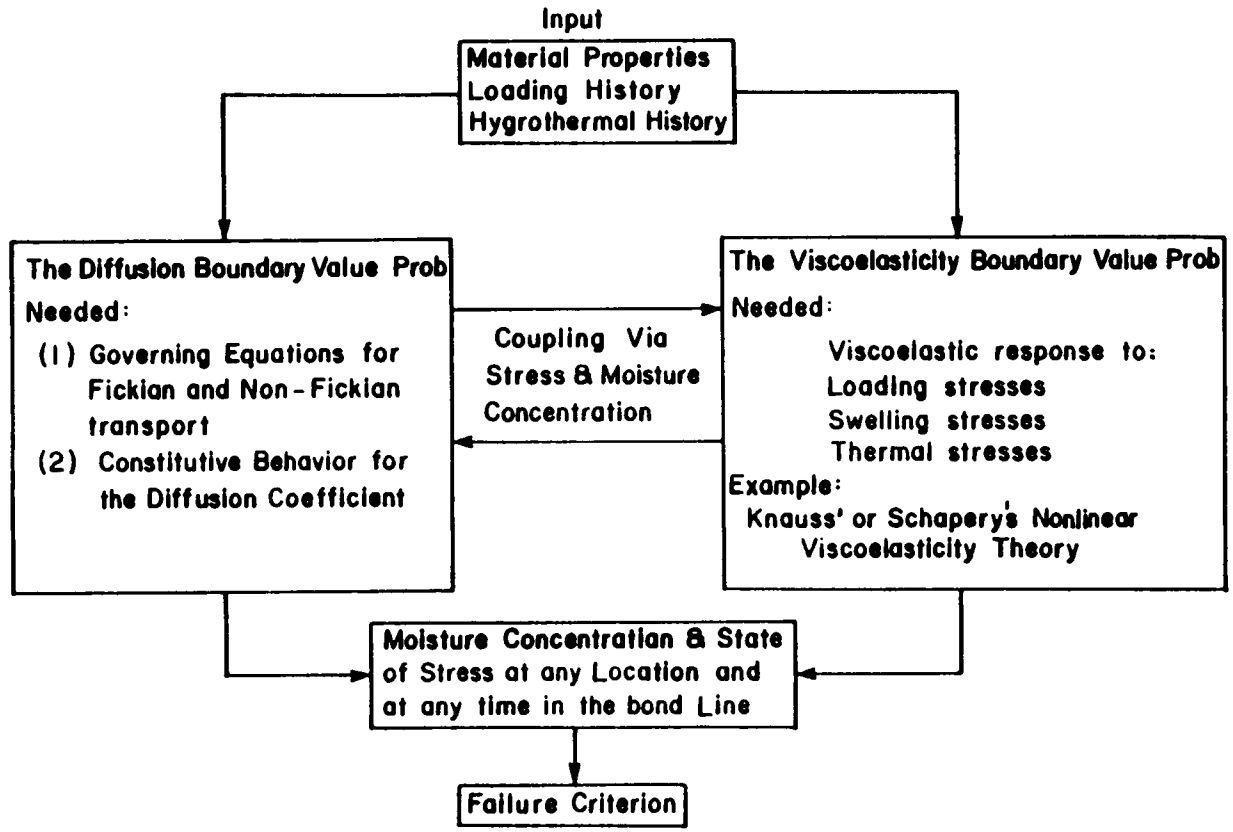

Figure 15. Coupling Between the DBVP and the VBVP.

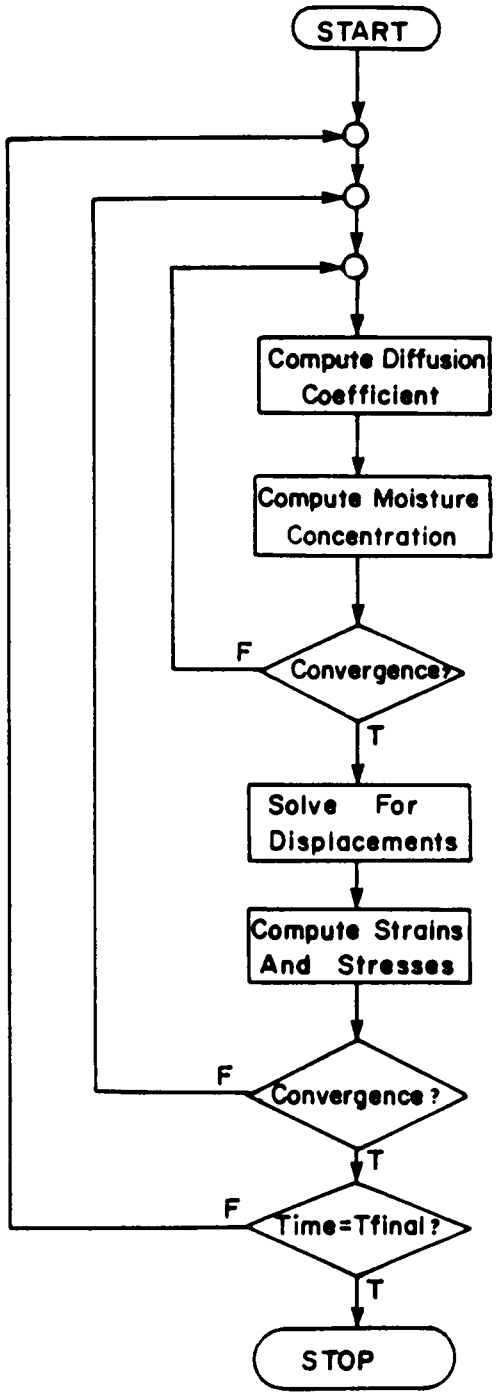

Figure 16. Algorithm for the Fully Coupled Problem.

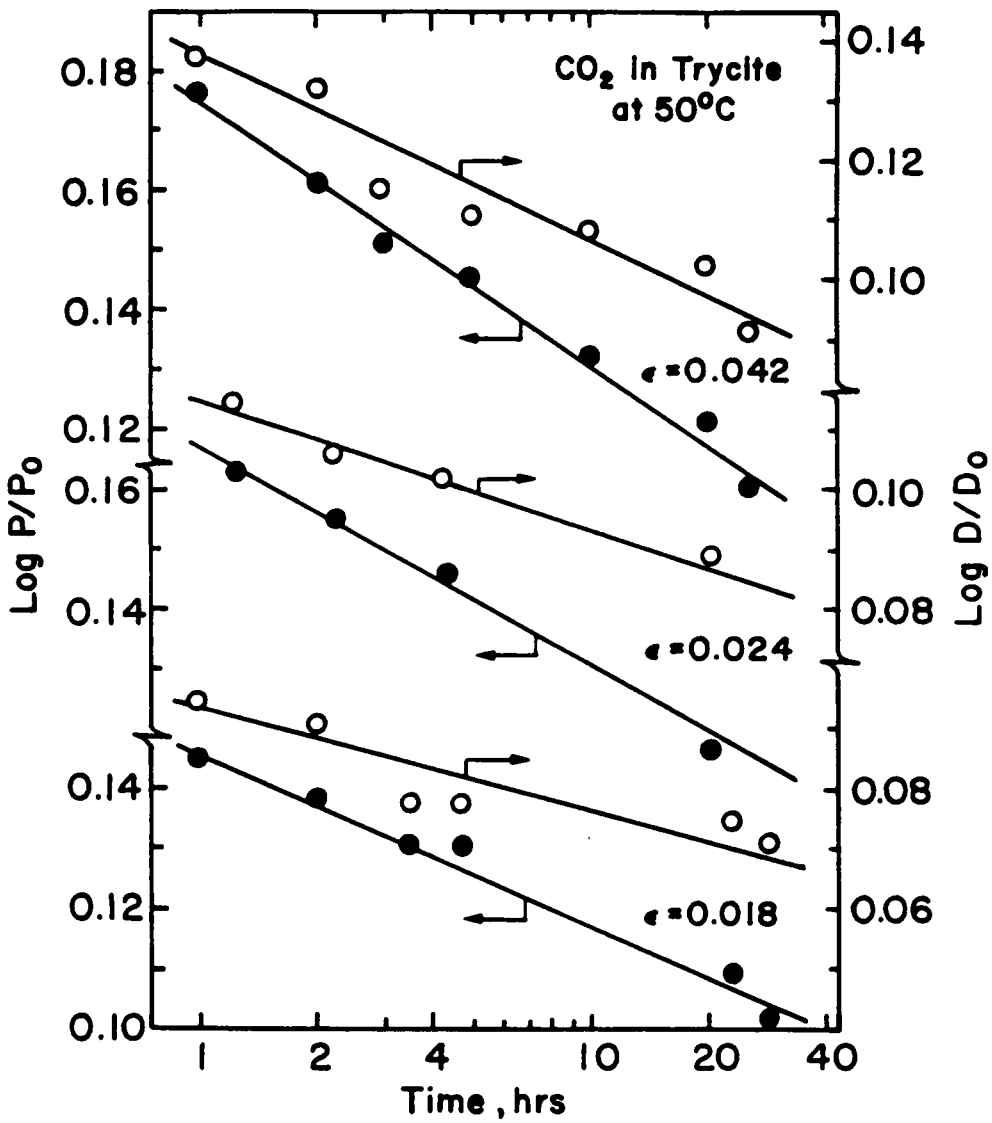

Figure 17. Time Dependence of P and D: Carbon Dioxide Diffusion Through a Trycite Film at 50 C Subjected to Different Strain Levels [37].

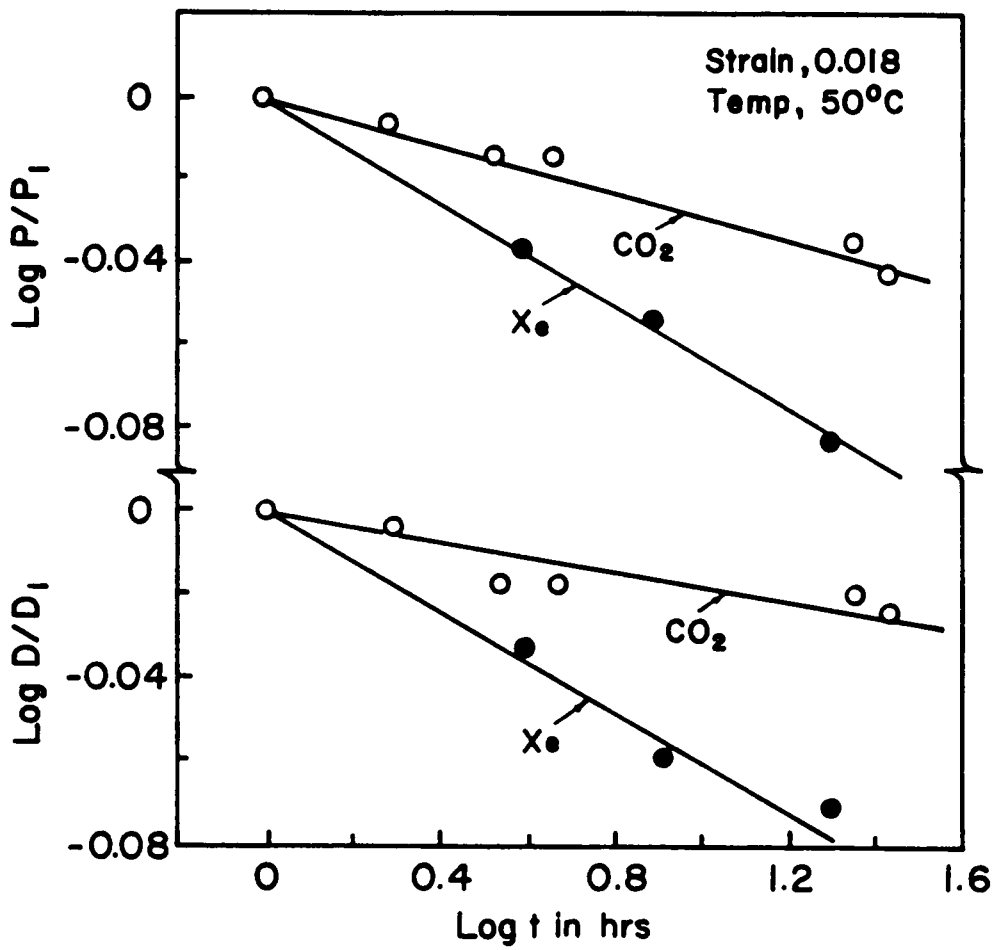

Figure 18. Effect of Penetrant Size on P and D: Trycite Film at 50 C, Subjected to a Strain of 0.018 [37]. (P and D were measured one hour after stretching)

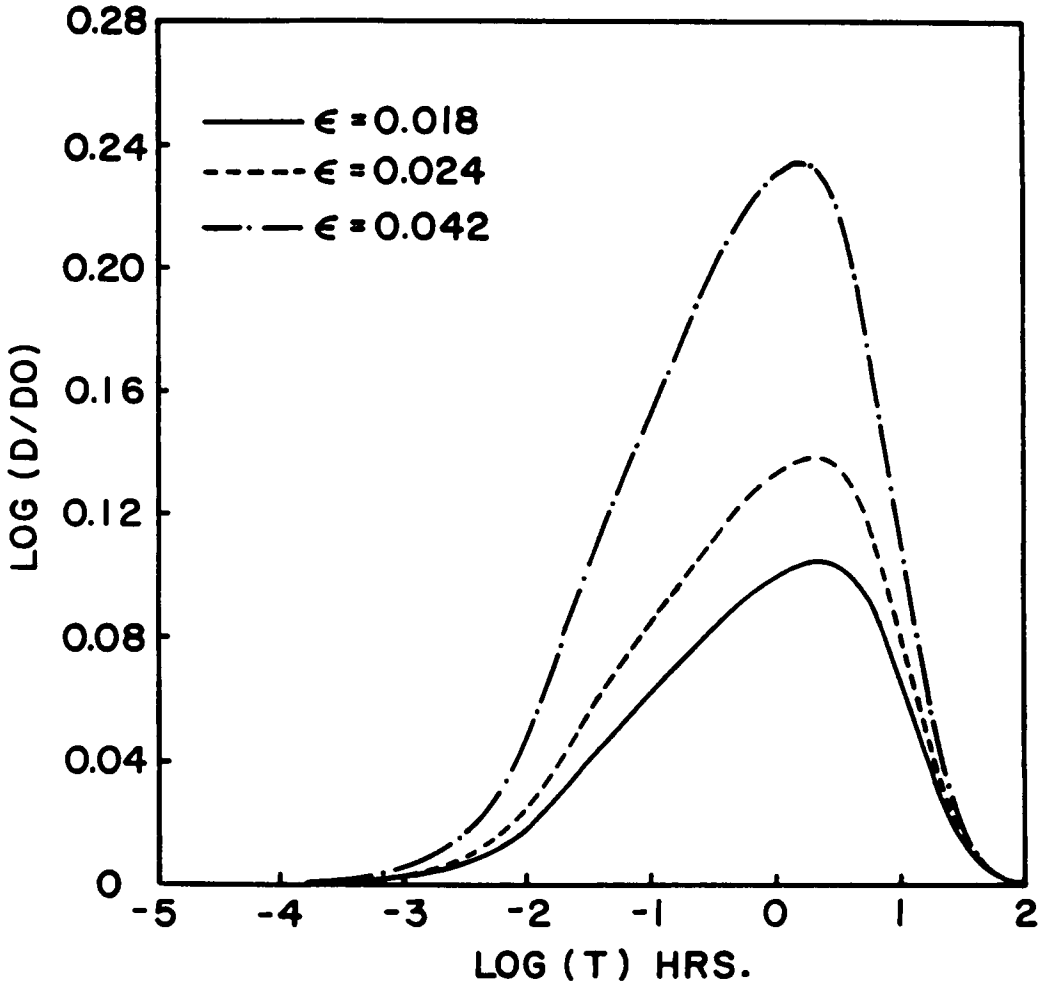

Figure 19. Time Dependence of D in a Polystyrene Film at 50 C and Influence of the Strain Level: Numerical Simulation with $B^D = .25$.

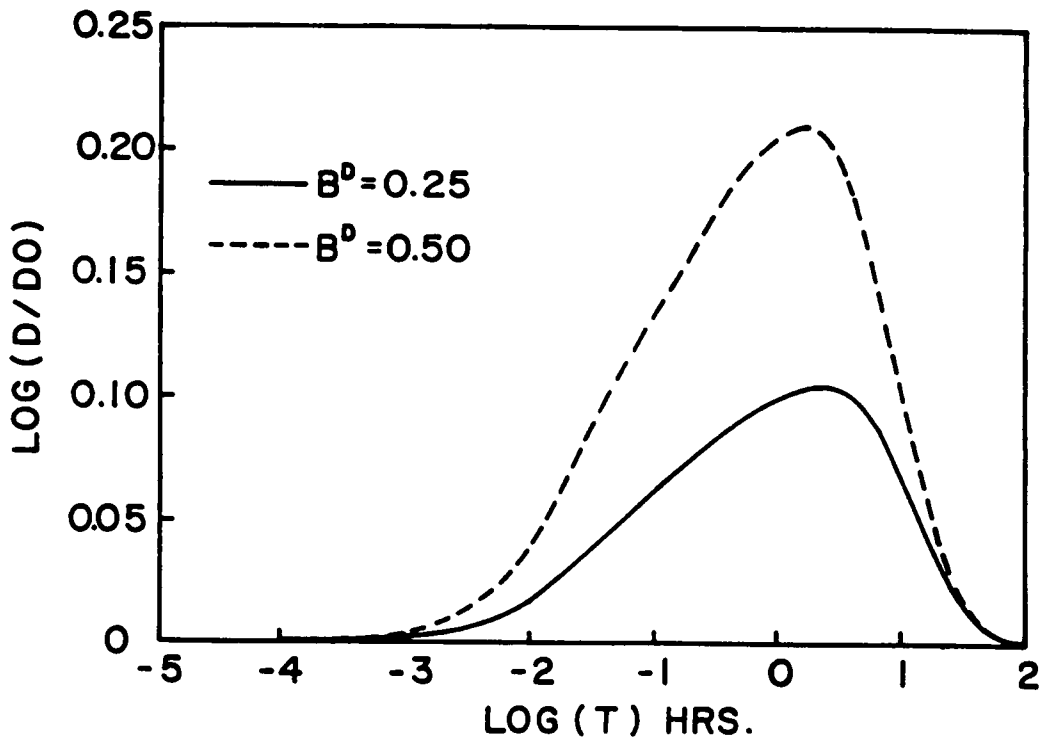

Figure 20. Time Dependence of D in a Polystyrene Film at 50 C and Influence of the Void Size Parameter: Numerical Simulation with $\varepsilon = .018$.

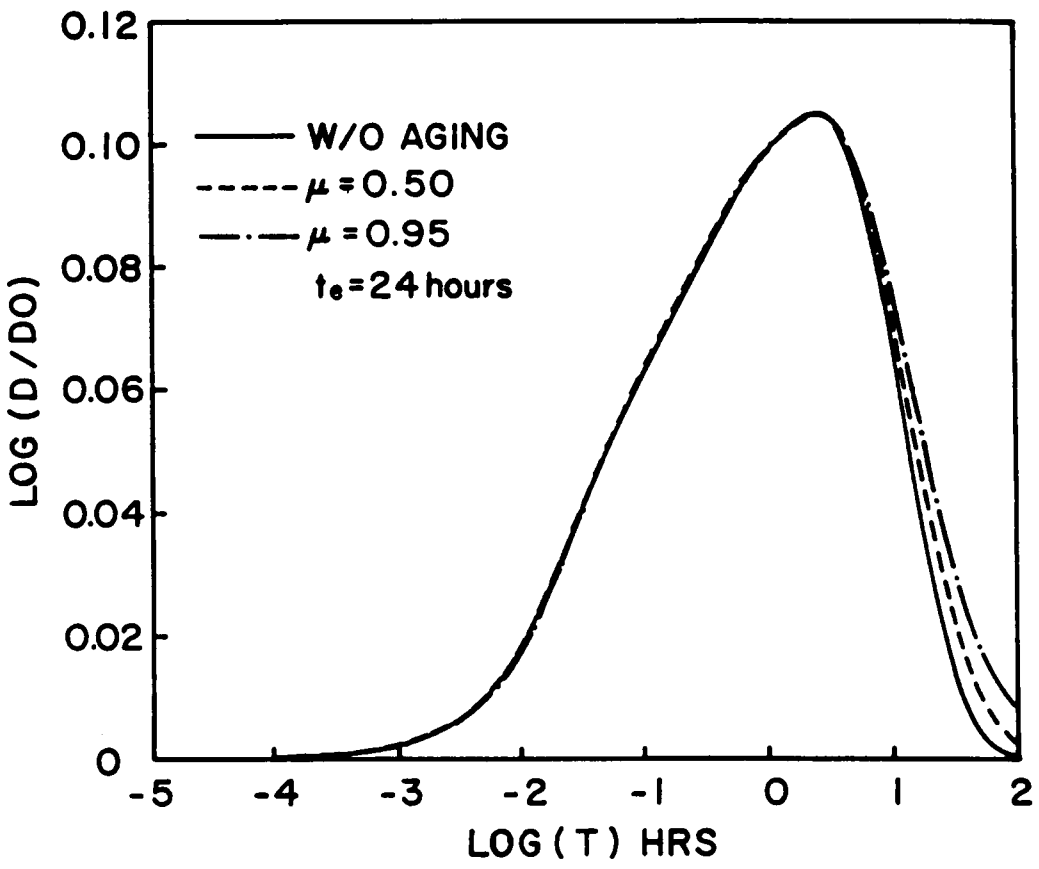

Figure 21. Time Dependence of D in a Polystyrene Film at 50 C and Influence of Physical Aging: Numerical Simulation with $B^D = 0.25$ and $\varepsilon = .018$.

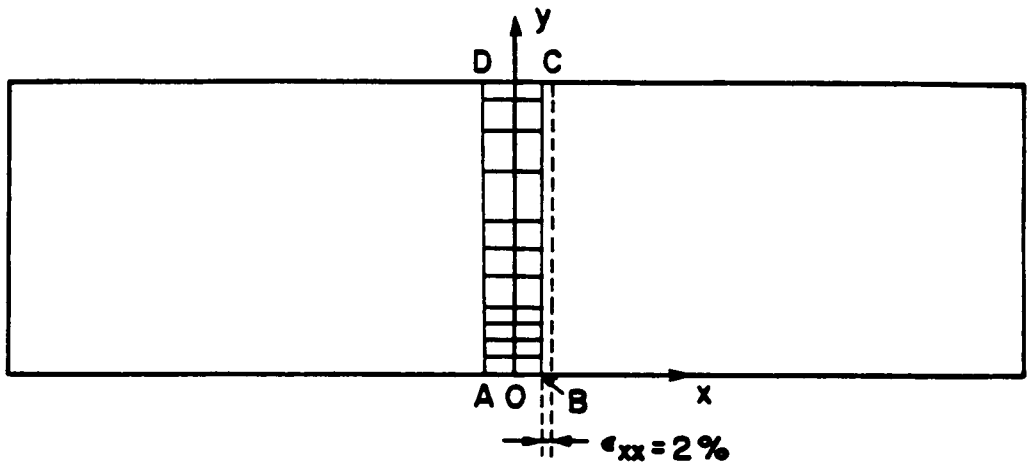

DIFFUSION BOUNDARY CONDITIONS:

AB : $\bar{C} = 1$

DC : $\bar{C} = 0$

BC : $J = 0$

AD : $J = 0$

Figure 22. Butt Joint Geometry and Bond Line Discretization.

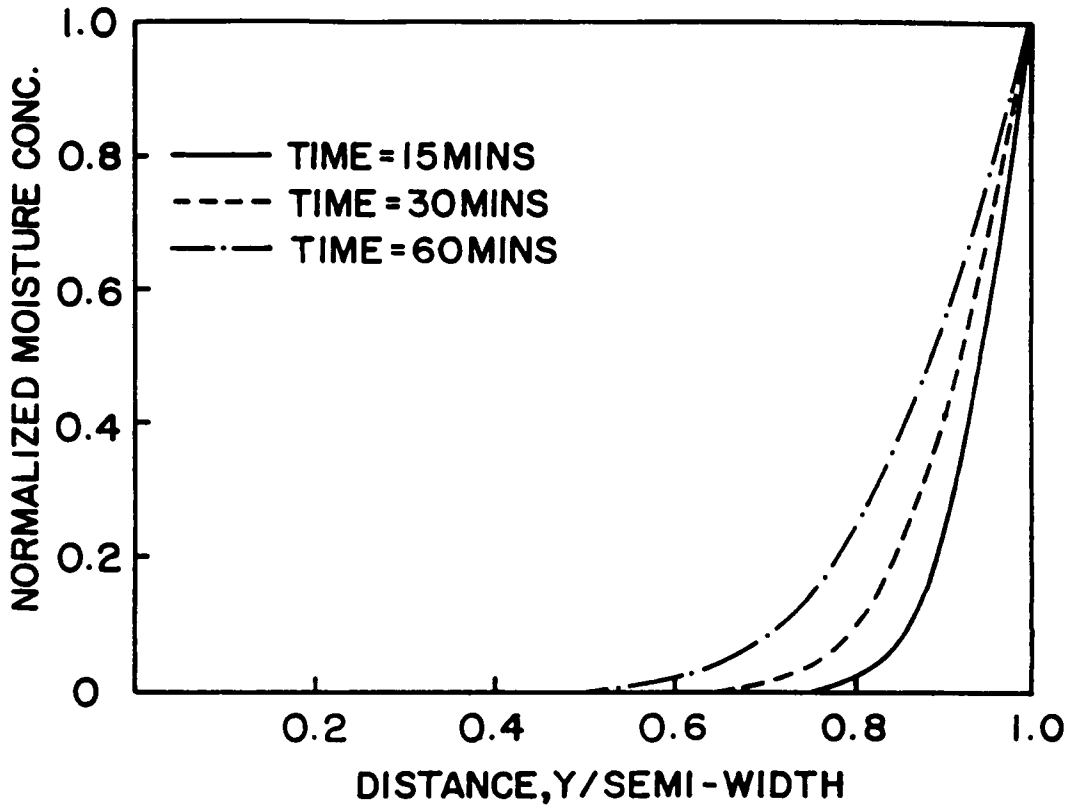

Figure 23. Simulation of diffusion in a Butt Joint (Case 1): Moisture Profiles Within the Adhesive in the Absence of Coupling.

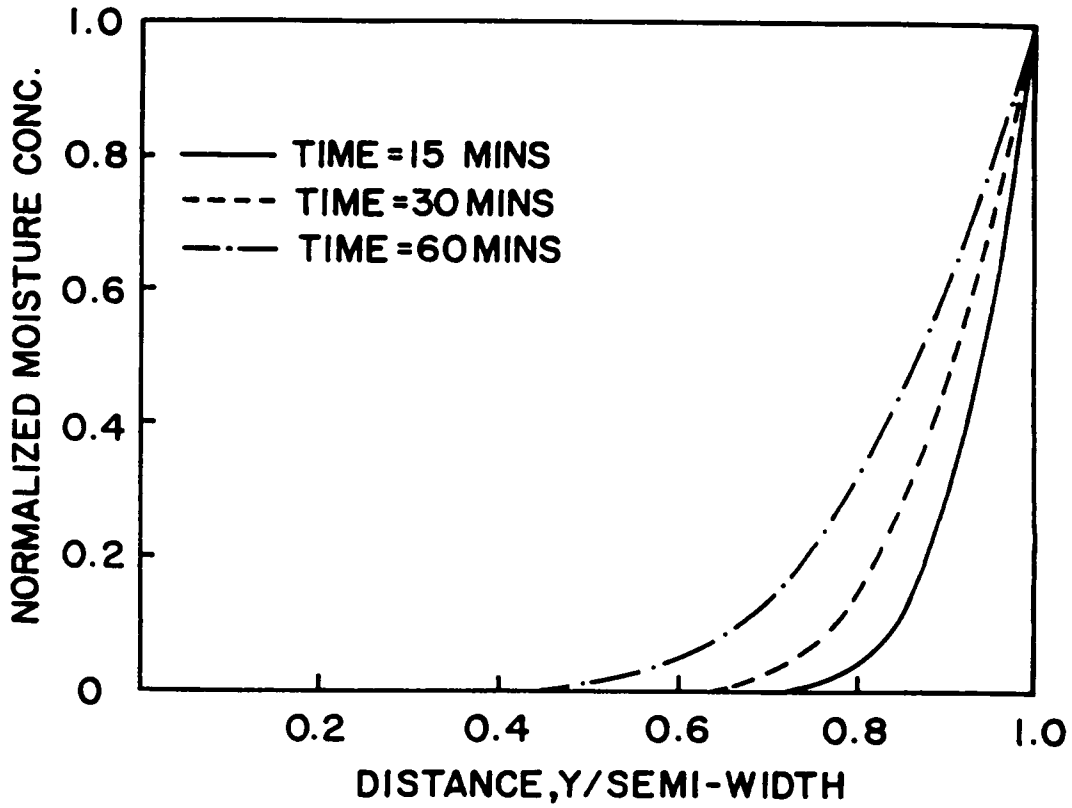

Figure 24. Simulation of Diffusion in a Butt Joint (Case 2): Moisture Profiles Within the Adhesive With a Strain Dependence in D.

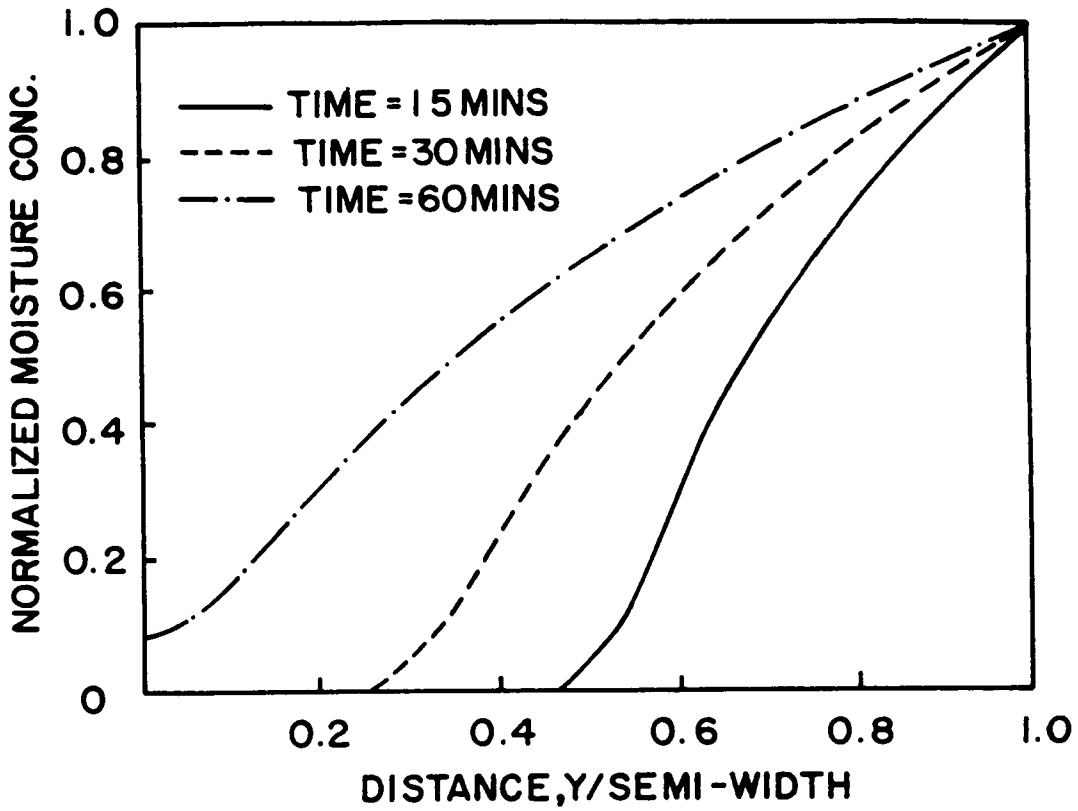

Figure 25. Simulation of Diffusion in a Butt Joint (Case 3): Moisture Profiles Within the Adhesive With a Strain and Concentration Dependence in D.

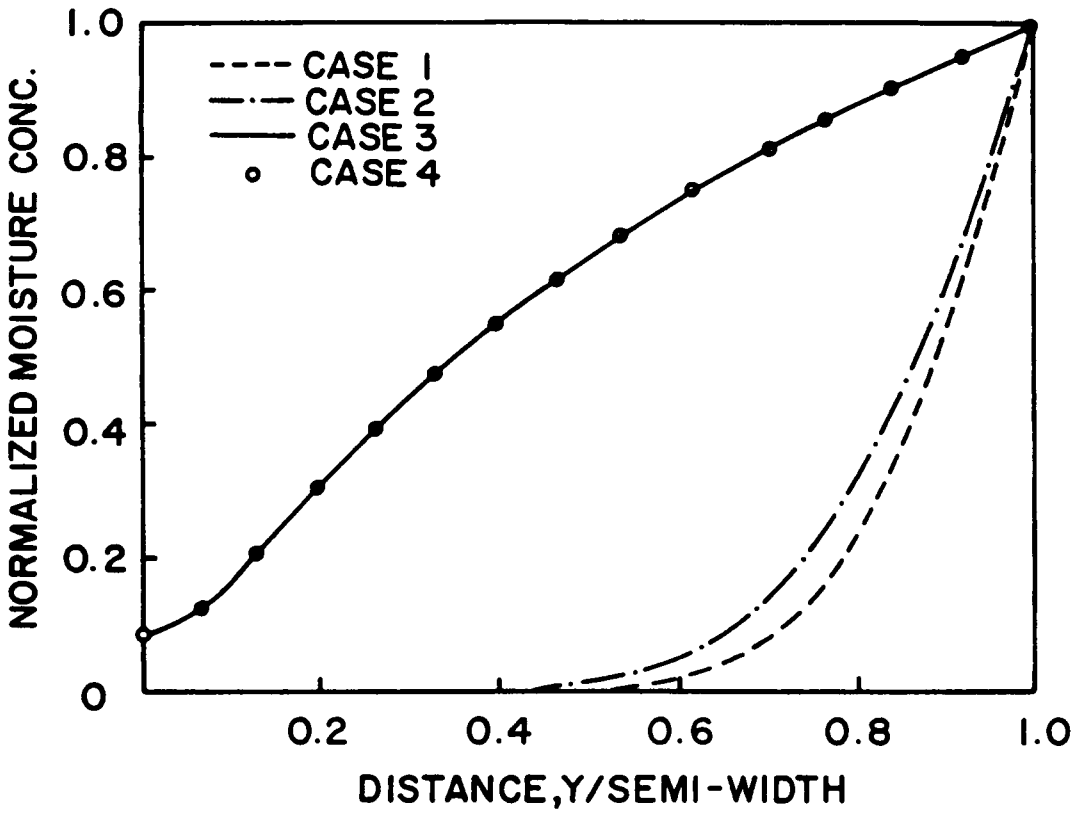

Figure 26. Comparison Between Cases 1, 2, 3 and 4: Moisture Profile Within the Adhesive at t = 60 min.

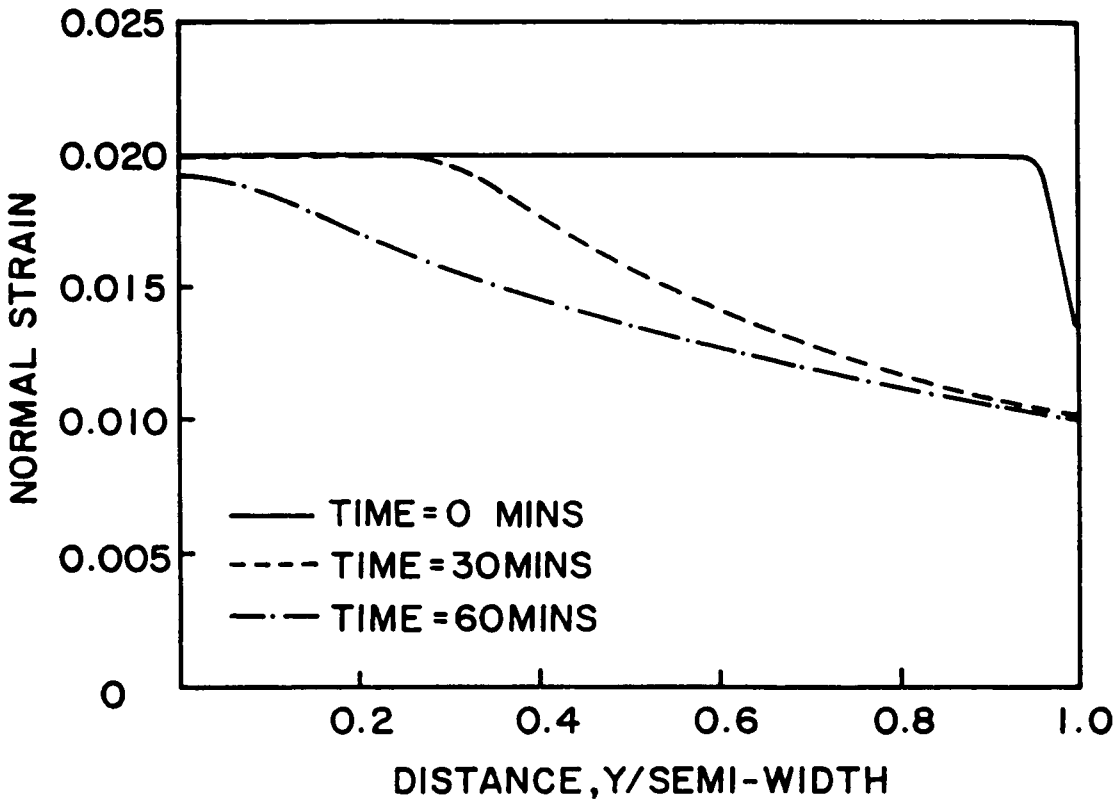

Figure 27. Simulation of the Strain Distribution in a Butt Joint (Case 3): Variation of the Normal Strain Distribution in the Adhesive, Accompanying Moisture Diffusion.

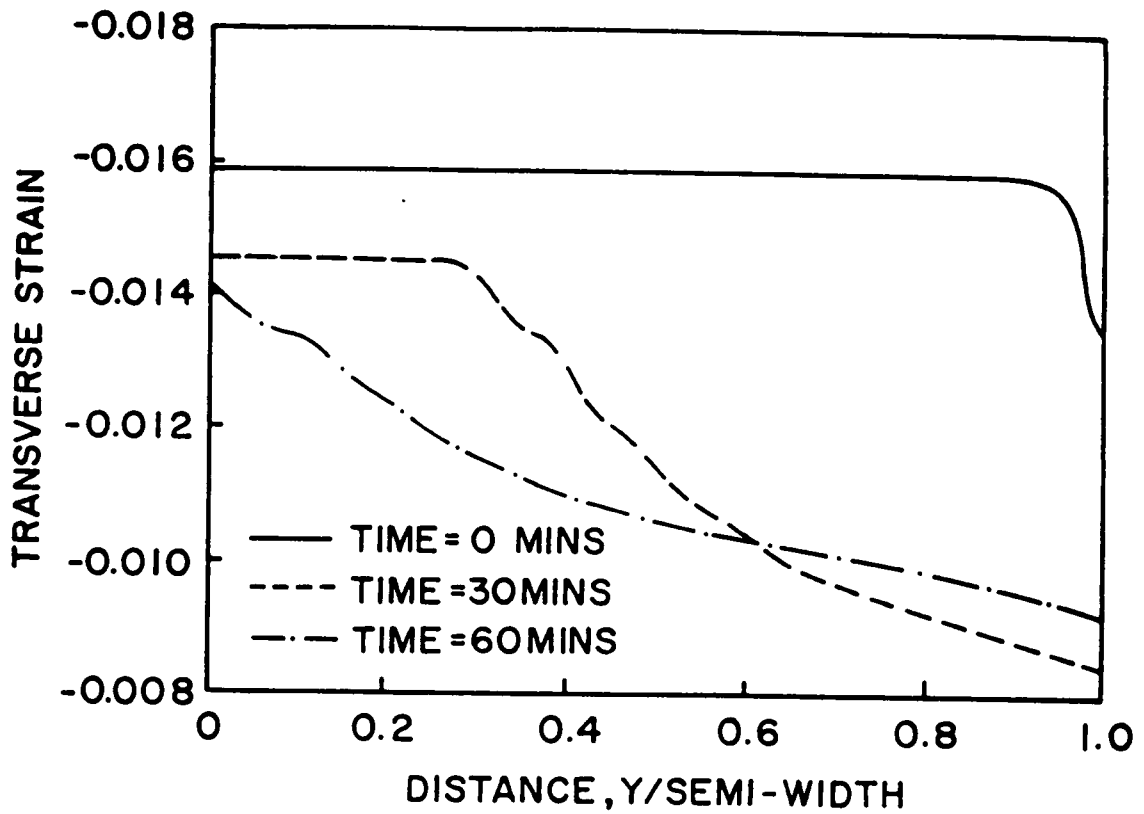

Figure 28. Simulation of the Strain Distribution in a Butt Joint (Case 3): Variation of the Transverse Strain Distribution in the Adhesive, Accompanying Moisture Diffusion.

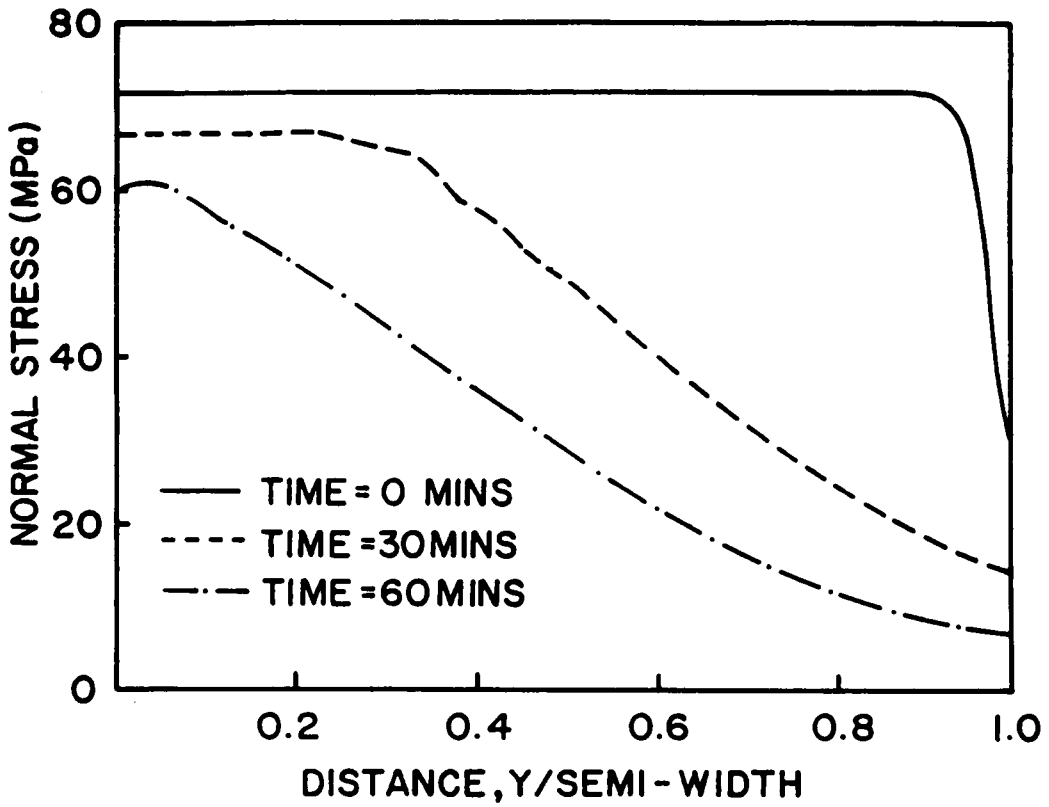

Figure 29. Simulation of the Stress Distribution in a Butt Joint (Case 3): Variation of the Normal Stress Distribution in the Adhesive, Accompanying Moisture Diffusion.

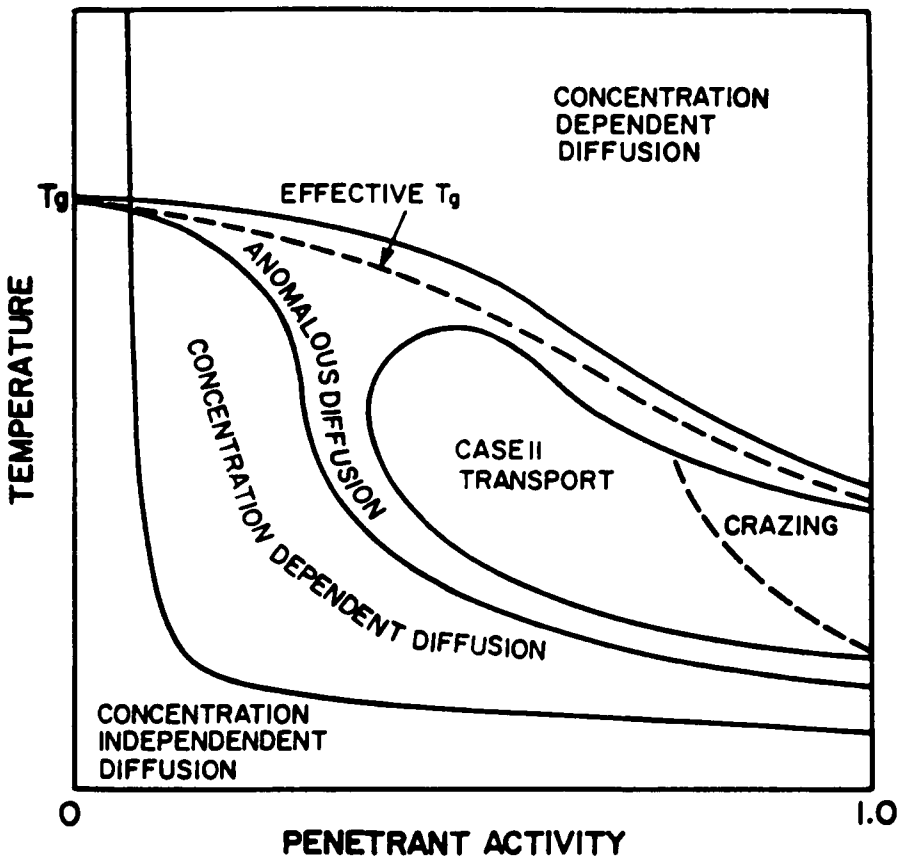

Figure 30. Hopfenberg-Frish Chart of Anomalous Diffusion: Effect of Penetrant Activity on Transport Kinetics [6].

4. BOUNDARY EFFECTS ON MOISTURE TRANSPORT IN ADHESIVES JOINTS:

Introduction:

The purpose of this section is to examine interfacial transport, namely diffusion through the boundary region bridging the adherend and the adhesive. It was postulated at the beginning of our discussion on diffusion, that a hydrophilic oxide could in principle alter the free energy of the water molecules locally. The resulting perturbation in the flux was initially included in component J^{ϕ} of the flux. Our goal is now to show that:

(1) Although a hydrophilic substrate gives rise to an interfacial pressure, component J^{ϕ} of the flux can be neglected.

(2) Recent experimental findings suggest that other types of boundary effects, which involve mobility changes, rather than a thermodynamic driving force, are more likely.

The Disjoining Pressure:

It will be assumed that no cavity or crack is present in the interphase region; that diffusion, not wicking, is the primary transport mode through the interphase. Further, it will be assumed that no contaminant is present in the interphase, excluding osmotic effects. Let us consider a transition region between a high energy oxide layer, which is impermeable to water, and a polymer containing diffusing water molecules. The high energy surface causes the water molecules to feel a stronger intermolecular field in the vicinity of the substrate than in the bulk polymer. The resulting drop in free energy is expected to provide a driving force for local perturbations in the diffusional flux. Penetrant molecules such as H_2O will tend to drift along the direction which reduces their potential energy, that is , perpendicular to the substrate surface. Once equilibrium is reached, this thermodynamic force normal to the surface gives rise to an interfacial pressure known in the literature as disjoining pressure[40–42] . Water molecules are still attracted to the surface but their mean free path is now much smaller. As a result, an excess concentration is present locally, causing an interfacial pressure. Thus the disjoining pressure is a measure of the hydrophylic character of the substrate. From a thermodynamical point of view, a parallel can be made between disjoining pressure and surface tension:

- Surface tension arises because molecules feel a weaker intermolecular field at the boundary of their diffusion domain. It is a measure of the work required to transport a molecule from the bulk region to the surface. Surface tension tends to reduce the dimension of the interface region.
- The disjoining pressure, then is just the opposite of surface tension: it arises because molecules feel a stronger intermolecular field at the boundary of their diffusive domain then they do in the bulk. It is a measure of the work required to transport a molecule from the boundary to the bulk region. Unlike surface tension, the disjoining pressure tends to expand the size of the boundary region.

In the following development, the disjoining pressure will be defined in the framework of equilibrium thermodynamics; the contribution of the surface potential to the diffusion flux will be assessed and a governing equation for interfacial diffusion will be derived. The interphase will be defined as the boundary region where the intermolecular field of water is different from that inside the bulk polymer. Since the oxide is assumed to act as a diffusion barrier, it follows that the interphase is confined to the polymer side of the interface. Note that this particular definition of the interphase is purely arbitrary. It has value, only in a context limited to the next few pages.

Let superscript σ denote a variable associated with the interphase. The interphase will be treated as a separate phase in the thermodynamics sense. For a small reversible change dU^{σ} in the internal energy of the interphase, one has:

$$dU^{\sigma} = TdS^{\sigma} + \Sigma \mu_i dn_i^{\sigma} - PdV^{\sigma} \tag{115}$$

where: T = Temperature, S = Entropy, μ = Chemical Potential, n = Number of moles, P = Pressure, and V = Volume. Since S, n, V are extensive variables, one can write:

$$U^{\sigma} = TS^{\sigma} + \Sigma \mu_i n_i^{\sigma} - PV^{\sigma} \tag{116}$$

Differentiating (116) and subtracting (115) yields:

$$S^{\sigma} dT - V^{\sigma} dP + \Sigma n_i^{\sigma} d\mu_i = 0 \tag{117}$$

Since the water is found in mixture with the polymer, the interphase can be treated as a two-component system. Thus, the free energy of this system may be written as:

$$\Sigma n_i^{\sigma} d\mu_i = n_{H_2O}^{\sigma} \; d\mu_{H_2O} + n_R^{\sigma} \; d\mu_R \tag{118}$$

where subscript R stands for polymer. Expression (117) is analogous to the expression derived by Gibbs for a surface[40] , except the terms involving surface tension and surface area are replaced by terms involving interphase pressure and interphase volume respectively.

At constant temperature, combining (117) and (118) will yield an isotherm:

$$dP = \frac{n^{\sigma}_{H_2O}}{V^{\sigma}} \; d\mu_{H_2O} + \frac{n^{\sigma}_{R}}{V^{\sigma}} \; d\mu_{R} \tag{119}$$

Or, if n^{σ}_{R} is close to unity, which is valid when the penetrant is at low concentrations:

$$dP = \left(n^{\sigma}_{H_2O} + \frac{\partial \mu_R}{\partial \mu_{H_2O}} \right) \frac{d\mu_{H_2O}}{V^{\sigma}} \tag{120}$$

Expression (120) indicates that a change in the chemical potential of water may cause a change in interphase pressure. Assuming that changes in μ_{H_2O} are mainly associated with the nature of the surface not with the polymer, it can be stated that : $\frac{\partial \mu_R}{\partial \mu_{H_2O}} = 0$. Expression (120) then becomes:

$$dP = \frac{n^{\sigma}_{H_2O}}{V^{\sigma}} \; d\mu_{H_2O} \tag{121}$$

Note that $V^{\sigma}/n^{\sigma}_{H_2O}$ is the partial molar volume of water, also denoted $\bar{9}_{H_2O}$. In the problem of interest, the absolute value of dP is the disjoining pressure. Consequently, the disjoining pressure is given by:

$$\Pi = -\Delta P^{\sigma} \tag{122}$$

The significance of expression (122) is that the interphase behaves as though its boundaries were repelled by a disjoining pressure Π. The phenomenon mainly results from three different types of interactions: electrical, dispersion and polar. The disjoining pressure may be written as the sum of three components[41]:

$$\Pi = \Pi_{\text{electric}} + \Pi_{\text{dispersion}} + \Pi_{\text{polar}} \tag{123}$$

Π is the pressure differential between the bulk and the interphase due to the presence of a stronger intermolecular field in the interphase:

$$\Pi = P_{\text{surface}} - P_{\text{bulk}} \tag{124}$$

At this point, another analogy can be made with osmotic pressure: In an osmotic device, the solvent is transferred to a solution through a semi-permeable membrane, due to the presence of a gradient in free energy between the two contiguous chambers; the net flow stops when equilibrium pressure $\Delta P = \frac{\Delta \mu_{H_2O}}{\bar{\vartheta}_{H_2O}}$ is established in the solution chamber. In a joint, the interphase region can be seen as the analog of the solution, and the bulk polymer region can be seen as the analog of the semi-permeable membrane.

The chemical potential μ_{H_2O} of water, is not constant across the thickness of the interphase, rather it is a function of the distance z to the surface. Noting that: $n_{H_2O}\,\mu^{\sigma}_{H_2O} = G^{\sigma}$, we find that[40]:

$$\Pi(z) = -\frac{1}{A}\left(\frac{\partial G^{\sigma}}{\partial z}\right)_{A,T,V} \tag{125}$$

where: A = surface area

It becomes clearer then, that the disjoining pressure is a measure of the work expanded to move a molecule of water from the surface to the bulk region:

$$\int_0^{\infty} A\ \Pi(z)\ dz = G^{\sigma}_B - G^{\sigma}_S \tag{126}$$

where G^{σ}_S and G^{σ}_B are the free energies at the surface and in the bulk respectively. $G^{\sigma}_B - G^{\sigma}_S$ then, is a boundary free energy, very much like a surface free energy at the surface of a liquid.

Potential Assisted Diffusion:

Consider a planar interface defined by three perpendicular axes O_x, O_y and O_z. Let O_z be the out-of-plane axis with the origin on the interface plane and the positive direction pointing toward

the polymer. According to the previous reasoning, a potential field will exist in the vicinity of any hydrophilic surface, in which water molecules will "fall". The potential energy W_P^{ϕ} of a water molecule will be a function of z only. The average drift velocity $\mathbf{V}$ of the water molecules in the presence of such an attraction can be written as:

$$\mathbf{V} = -B\nabla W_P^{\phi} \tag{127}$$

where: B = local molecular mobility

The molecular flux $\mathbf{J}_P^{\phi}$ resulting from the potential field is given by:

$$\mathbf{J}_P^{\phi} = -CB\nabla W_P^{\phi} \tag{128}$$

In the most general case, the diffusion coefficient is related to mobility by[43]:

$$D = BkT\Omega \tag{129}$$

The thermodynamic factor Ω becomes important only when the energy of mixing of the system is high. Again, this is unlikely in the context of the problem at hand. Ω will be treated simply as an unknown constant.

For the sake of clarity, the stress induced flux $\mathbf{J}^{\sigma}$ will be omitted in the flux equation. This simplification, will in no way affect the final conclusion. Using Cartesian coordinates and noting that $\frac{\partial W_P^{\phi}}{\partial x} = \frac{\partial W_P^{\phi}}{\partial y} = 0$, the total flux becomes:

$$\mathbf{J} = -D\frac{\partial C}{\partial x}\,\mathbf{i} - D\frac{\partial C}{\partial y}\,\mathbf{j} - D\left(\frac{\partial C}{\partial z} + \frac{\Omega C}{kT}\frac{\partial W_P^{\phi}}{\partial z}\right)\mathbf{k} \tag{130}$$

Expressing the conservation of mass and combining with the flux equation, yields the governing equation for interfacial diffusion:

$$\frac{\partial C}{\partial t} = \frac{\partial}{\partial x}\left(D\frac{\partial C}{\partial x}\right) + \frac{\partial}{\partial y}\left(D\frac{\partial C}{\partial y}\right) + \frac{\partial}{\partial z}\left\{D\left(\frac{\partial C}{\partial z} + \frac{\Omega C}{kT}\frac{\partial W_P^{\phi}}{\partial z}\right)\right\} \tag{131}$$

A Functional Form for the Potential Energies Associated with the Polar, Dispersion and Electric Interactions:

The following discussion will deal with the force field experienced by an **isolated** gas molecule placed in the immediate vicinity of a surface. This means that the gas behaves ideally, or stated another way, that an individual molecule does not feel the intermolecular field created by the species belonging to the same phase. Although this assumption does not adequately represent the conditions experienced by penetrant molecules mixed with a polymer matrix, useful information can be obtained on the range of the interfacial force field. The potential energy $W_p^{\phi}(z)$ represents the work required to move an isolated molecule from the surface of the oxide to a distance z from the surface:

$$\int_0^z \frac{\partial W_p^{\phi}}{\partial z}\, dz = W_p^{\phi}(z) - W_p^{\phi}(o) \tag{132}$$

(A random orientation is assumed for the water molecules)

It has been mentioned earlier that the disjoining pressure is the net of several components: dispersion, polar and electrical. As a first step, only the first two interactions, collectively known as Van der Waal forces, will be considered. A list of three intermolecular forces contributing to the Van der Waal component of the disjoining pressure is given in Table 4. Note that the power dependency is -6 in all three cases. When passing from a molecule-molecule interaction to a molecule-surface interaction, the total interaction energy becomes the sum of the individual interactions. Since oxide dipoles (eg: hydroxyl groups) are scattered on the surface of the oxide, dipole-dipole interactions are to be integrated over the entire surface S:

$$W_P^{\phi 1} = -\iint \frac{C_1}{z^6}\, dS \tag{133}$$

where: $C_1 = \text{constant}$

The dispersion force exists between any pair of molecules or atoms regardless of polarity. Consequently dispersion interactions are to be integrated over the entire volume V of the substrate:

$$W_P^{\phi 2} = -\iiint \frac{C_2}{z^6}\, dV \tag{134}$$

where: $C_2 = \text{constant}$

In performing the above integrations, the exponent on z drops by two units in the case of dipole-dipole interactions and by three units in the case of dispersion interactions:

$$W_P^{\phi l} = -\frac{\omega_l}{z^{n_l}} \tag{135}$$

where subscript 1 corresponds to dipole- dipole interactions; subscript 2 corresponds to dispersion interactions; ω_l is a constant, $n_1 = 4$, and $n_2 = 3$.

To avoid having an infinite potential at the surface, which would be meaningless physically, it is convenient to write the potential $W_P^{\phi l}$ as:

$$W_P^{\phi l} = -\frac{\omega_l}{(z+a)^{n_l}} \tag{136}$$

where a may be physically interpreted as the molecular radius of water.

Let us now evaluate ω_l from the disjoining pressure Π^0 at the surface, that is, at z = 0. According to expression (125) we have:

$$\Pi^0 = -\frac{1}{A} \quad \frac{\partial G^\sigma}{\partial z} \mid z = 0 \tag{137}$$

Since a variation in the potential energy of the molecules corresponds to an equal variation in the free energy of the system[15], we have:

$$dG^\sigma = n^\sigma_{H_2O} N_a \, dW^\phi_P \tag{138}$$

with: N_a = Avogadro's Number.

And combining expressions (136), (137) and (138) yields:

$$\omega_l = \frac{\Pi^0_l a^{n_l+1}}{4\Gamma N_a} \tag{139}$$

where Γ is the surface concentration of moisture at equilibrium.

Finally, the potential energy can be written as follows:

$$W^{\phi l}_P = -\Pi^0_l \frac{a^{n_l+1}}{4\Gamma N_a} \quad \frac{1}{(a+z)^{n_l}} + W_P{}^\circ \tag{140}$$

where: $W_p{}^\circ$ = An arbitrary integration constant

Π^p_1 = polar component of the disjoining pressure

Π^p_2 = dispersion component of the disjoining pressure

The z component of the interphase flux may then be written as:

$$J^\phi_z = \frac{D\Omega C}{kT} \quad \frac{1}{(a+z)^{n_l+1}} \tag{141}$$

From equation (141), it becomes apparent that J_z^{ϕ} drops by 97 %, two molecular radii away from the surface, in the case of polar forces; and drops by 94 %, two molecular radii away, in the case of the dispersion force. Note that the distance z at which J_z^{ϕ} vanishes is very close to the atomic scale. In fact, within the small boundary region where J_z^{ϕ} vanishes, an integration performed over a continuous domain as in equations (133) and (134) yields incorrect results. In a region so close to the surface, a **discrete summation** of all interactions would be necessary. In spite of this limitation of the continuum treatment, an important conclusion can be drawn: J_z^{ϕ} due to Van der Waals forces may be neglected for all practical purposes. Note that this does not mean that these interactions or the disjoining pressure are negligible in absolute terms within the domain size considered. What is inferred from our reasoning is simply that the **gradients** in the corresponding potential energies vanish at an extremely short distance, thereby causing negligible flux perturbations, at least as long as the penetrant is not found in a condensed phase.

Let us now examine the effect of the electrical component of the disjoining pressure. By performing an integration similar to that in expressions (133) and (134), it can be shown that the electric field Φ in the vicinity of a uniformly charged plate (same as a plate of infinite dimensions), is independent of distance z and is given by[44] :

$$\Phi = \frac{\sigma}{2\varepsilon_0} \tag{142}$$

where: σ = Surface charge density

ε_0 = Dielectric constant of the medium

Since water molecules behave as small dipoles, let us consider their potential energy in an electric field. The potential energy $W_p^{\phi 3}$ of randomly oriented dipoles placed in electric field Φ is given by[40]

$$W_p^{\phi 3} = - < \mu > \Phi \tag{143}$$

where $< \mu >$ is the average dipole moment of the molecule

It is reasonable to assume that a few monolayers away from the surface plane, the dipoles are undergoing random thermal agitation, or stated an other way, that $<\mu>$ is independent of z. If the variation in the dielectric constant is not too steep, this means that W_p is almost constant and its gradient in the z direction very small. Again, the conclusion is that the local flux perturbation is likely to be minimal.

A more rigorous treament of the physics of fluids near solid surfaces has been given by Teletzke and coworkers[45]. The equation of state of a non-polar fluid near a solid was obtained by summing all the potential energies of the fluid-solid interactions and fluid-fluid interactions, and by allowing fluid density to vary as a function of distance to the solid. For closed isothermal systems, the equilibrium density profiles and disjoining potential profiles were obtained by solving for the minima of the total free energy of the system and requiring conservation of mass. The effect of bulk density and fluid temperature on the boundary density profiles was discussed in detail on the basis of a parametric numerical analysis. The finding which is of interest to us is that, in all the cases considered, any excess density or any disjoining potential fluctuation was found to vanish at a distance from the solid corresponding to 10-20 (fluid) molecular radii. Thus, we have some additional indication that the surface energy of the substrate alone cannot account for flux perturbations beyond a distance corresponding to a few monolayers of penetrant.

Effect of Interphase Polymer Rheology:

It has been widely suggested that polymer conformation is likely to be altered in the boundary region near the interface. Recent results obtained from the study of thin polysulfone films on anodized Al 2090 substrates[46] seem to indicate that segmental mobility is reduced in a region extending as far as a few microns away from the substrate / adhesive interface. For example, a higher than normal T_g, as well as variations in dielectric loss factor, mechanical loss factor, and rheological activation energy have been reported in the boundary region[46,47]. In addition, these property

changes have been found to be sensitive to surface pretreatment. Note that a local drop in polymer viscosity, if it is related to lower free volume, is likely to decrease the mobility (or diffusion coefficient) of penetrant molecules near the interface plane. In another study, Knollman[48] has measured shear modulus variations in the interfacial region of a AF 453 (Epoxy) / Al 6061 bond, using an ultrasonic wave technique. He showed that the shear modulus of the epoxy starts to drop from its bulk value, as far as 0.3 mm away from the substrate. These various property changes strongly suggest that the diffusion coefficient in the interphase may deviate from its bulk value.

Changes in molecular mobility inside the interphase can be translated mathematically by using a diffusion enhancement factor D^{σ}. With such an approach, the interfacial diffusion coefficient D^{σ} will be related to the bulk diffusion coefficient D by:

$$D^{\sigma}(T, \sigma, C) = D^{\sigma}\ D(T, \sigma, C) \tag{144}$$

Note that the functional form of the diffusion coefficient is unchanged, only its magnitude differs. This simple approach has been used successfully in metallic diffusion studies, in order to incorporate the effect of high diffusivity paths such as dislocation pipes and grain boundaries[49]. It can be easily implemented in a finite element code by assigning different values of D^{σ} in various boundary regions. The intent of this parameter is not to give an arbitrary fitting parameter, but rather to be a method to account for molecular mobility differences in the polymer as a function of proximity to the boundary. Variations in diffusivity across the transition region can be represented, simply by refining the Finite Element mesh near the boundary and by varying the diffusion enhancement factor in a stepwise manner. The main challenge obviously, lies in developing techniques for measuring D on very thin films in contact to a substrate.

Conclusion:

Although the surface energy of the substrate can give rise to an interfacial pressure, it cannot alone account for flux perturbations, mainly because the range of the interfacial force field is extremely short. Whence, if interfacial diffusion effects exist, they must be related to changes in the molecular mobility. A number of recent findings indirectly suggest such an effect, and also indicate that the thickness of the polymer layer affected can be quite large. It is not clearly known at this time whether D^e is smaller or greater than one. However, if future studies show that D^e is greater than one (ie: lower diffusivity locally), this will mean that bulk diffusion is rate controlling, and that interface effects are not very important in the context of a durability study. It is instructive to remember that we have assumed we were dealing with a neatly fabricated joint, namely that no damage or contaminants were present in the boundary region. These restrictions exclude wicking or osmotic effects in interfacial moisture transport.

Table 4. Intermolecular Forces Contributing to The Disjoining Pressure [40].

Force between molecule A & molecule B	Potential Energy
APOLE-APOLE (London Dispersion)	$W_p = -\frac{3}{2} \frac{I_A I_B}{I_A + I_B} \frac{\alpha_A \alpha_B}{r^6}$
DIPOLE-DIPOLE (Keesom Orientation)	$W_p = -\frac{3}{2} \frac{N_A^2 N_B^2}{kT} \frac{1}{r_6}$
DIPOLE-INDUCED DIPOLE (Debye Induction)	$W_p = -(\mu_A^2 \alpha_B + \mu_B^2 \alpha_A) \frac{1}{r^6}$

Symbols: W_p = Potential Energy
r = Distance
α = Polarizability
μ = Dipole Moment
I = Ionization Potential

5. THE CRITICAL CONCENTRATION MODEL FOR JOINT DURABILITY PREDICTION

Introduction:

In Chapters 1, 2 and 3, a general treatment for the diffusion of small molecules through polymers has been proposed, with the objective of providing better predictions of environment penetration into adhesive joints. In our treatment of diffusion, no particular restriction, except molecular size, has been placed on the nature of the penetrant species. Thus, in principle, we are now in possession of a general predictive tool for calculating the rate of environment ingression.

The second stage, in the study of durability, involves the loss of integrity of the interfacial regions. Contrary to diffusion, the precise mechanisms of joint degradation are extremely dependent

upon a particular adhesive / substrate / environment combination. Environmental attack is known to cause loss of strength by four types of mechanisms, operating in an isolated manner or in conjunction[50,51]:

(1) By physically and / or chemically attacking the adhesive; e.g: swelling-induced loss of mechanical strength, polymer hydrolysis.
(2) By causing a sign change in the work of adhesion (bond line displacement by water).
(3) By breaking interfacial covalent bonds; e.g: hydrolysis.
(4) By physically and / or chemically degrading the substrate; e.g: corrosion or hydration of the oxide layer.

Therefore, a specific failure criterion for environmental failure, as well as specific test procedures, must be developed for each adhesive / substrate / environment combination of interest. This unfortunate state of affairs forces us to limit ourselves to particular cases and to favor an empirical approach over a general theoretical approach. Nonetheless, a simple failure criterion has been discovered by Gledhill et *al.*[52], which makes quantitative durability predictions possible for at least one important category of adhesive joints: epoxy-to-steel joints in humid environments. The purpose of this chapter is mainly to review this Gledhill's proposal and to show how it can be used in conjunction with diffusion data, to calculate residual strength as a function of exposure time.

The Failure of Epoxy-to-steel Joints in High Humidity Environments:

The failure criterion proposed by Gledhill et *al.*[52] is based on data collected earlier on the behavior of mild steel-epoxy joints in humid environments[53,54]. The main results from these previous studies may be summarized as follows:

* AES and XPS shows that dry failure is primarily cohesive[53] (close to the oxide but not interfacial).
* AES and XPS shows that, after exposure to water, the locus of failure is exactly between the metal oxide and the adhesive[53] (100 % adhesive).
* Substrate corrosion is not the cause of environmental failure but, rather a post failure phenomenon[54].
* As long as chemisorption and interdiffusion across the interface are absent, the mechanism for environmental failure is bond line displacement. Further, thermodynamic considerations based on surface free energy measurements can predict interface stability for a number of liquids[54].
* Below a certain relative humidity level, no degradation by moisture is observed, even after long times.

These results led Gledhill et *al.* to formulate a number of working hypotheses listed below:

(1) There exists a critical level of water concentration C_C in the adhesive, below which joint strength remains intact.
(2) At the point where concentration C exceeds C_C, there exists a sharp boundary between an outer weakened region where failure is interfacial, and an inner region where failure is cohesive in the adhesive.
(3) Below C_C, fracture strength is equal to dry fracture strength.

(4) The outer region, or region of incipient interfacial debonding, has negligible residual fracture strength and may be assimilated to an environmental crack.

According to this type of reasoning, durability appears to be entirely governed by transport kinetics. Three parameters play a crucial role: (1) the rate diffusion, (2) adhesive bulk fracture strength and (3) the critical moisture concentration. A simple characterization along these lines was undertaken by Gledhill et *al.* . The diffusion coefficient of water in the adhesive (unstressed) was measured at several temperatures by sorption. Bulk adhesive toughness was determined, using a compact tension specimen. The critical concentration was determined indirectly; namely, after measuring fracture strength on an exposed butt joint specimen, an environmental crack dimension was calculated from simple fracture mechanics. Then, by comparing crack size with the calculated moisture distribution at the time conditioning was interrupted, the critical concentration was deduced. The value of C_C for the steel/epoxy system studied was found to be 1.35 % in weight. At this point, it is useful to note that C_C was obtained from combined fracture and diffusion data at **one** temperature level only.

In order to verify the model in a conclusive manner, residual butt joint strength versus exposure time was calculated at a number of **other** temperature levels, and compared with experiment. As demonstrated by Figure 31, fairly good agreement was found. Note that when the saturation level exceeds the critical concentration, temperature affects the failure rate by changing the diffusion coefficient of water in the adhesive. When the saturation level is below the critical concentration (i.e., 20 C, 55% RH), no debond is seen.

Although Gledhill et *al.* ascertained C_C implicitely, a more direct method can be used. For example, residual strength can be measured after conditioning several specimens under varying relative humidities, until equilibrium sorption is achieved. After measuring solubility, it then becomes possible to extract C_C by locating the knee in the σ_f vs. C curve. This procedure was used by Comyn and coworkers[55] in a study of the durability of pretreated aluminum / FM 1000 bonds. In the next section, the direct method will be used to determine the residual fracture strength as a

function of moisture content in the case of a Ultem 1000-to-aluminum bond. The effect of surface pre-treatment will be studied.

The Case of Ultem-to-Aluminum Bonds:

Specimen Fabrication and Testing:

Double cantilever beam specimens with Aluminum 2024 adherends and with an Ultem 1000 bond line were used in this study. The specimens were fabricated by compressing Ultem sheets between pretreated aluminum beams, at a temperature of 240 C (460 F) and with a pressure of 7 kPa (1000 psi). Bond thickness was set to a value of .254 mm (.010") by using shims. The dimensions of the beams were 3.2 mm x 15 mm x 139 mm (1/8" x .59" x 5.5"). These dimensions were chosen to prevent plastic yield within the expected load range. Beam width was calculated from the diffusion coefficient obtained in chapter 2 in order for equilibrium sorption to be attained after one month of exposure to humidity. All the beams were carefully polished with 3M W2 AN4 sand paper prior to chemical treatment. Three types of surface preparations were used: (1) solvent degreasing only, (2) solvent degreasing and an FPL etch, and (3) solvent degreasing and a sodium hydroxide etch recommended in Reference 56 (3 to 10 min. in 568g/l DI water, rinse in DI water and air dry).

All the DCB specimens were conditioned at 50C and under a controlled relative humidity. The principle of the conditioning fixture was exactly identical to that described in Figure 7 of Chapter 2, with the obvious difference that no mass measurement was needed. A total of 8 conditioning compartments were used simultaneously, each with a different saturated salt solution and a different vapor activity. The list of the various salts used and the corresponding relative humidities

at 50 C is given in Table 5. Each compartment contained six specimens (two of each surface treatment were represented). In addition, six more specimens were placed in a vacuum oven at 50 C for the same length of time, so as to obtain fully dried control specimens. After 40 days of conditioning residual Mode I fracture toughness for a given relative humidity was determined by averaging ten measurements from two specimens (five measurements per specimen). These tests were performed on an MTS hydraulic machine, under a constant crosshead rate of .001 inch per second. For every measurement, crack length was obtained from the beam compliance prior to the onset of debonding and the fracture energy value was computed from the crack length and the critical debond load by using elementary beam theory (see chapter 6).

Results and Discussion:

Upon visual examination, all the failure loci, including those observed on dried specimens seemed to be interfacial between Ultem and the Aluminum oxide. All the data points from the fracture study are shown in Figure 32. Each data point is the average of ten measurements. The averaging scheme was quite useful in that it reduced the large scatter found in the toughness measurements. Against our expectations, Figure 32 does not show any evidence of a critical relative humidity for any of the surface treatments. (Note that the critical relative humidity is related to the critical concentration by solubility) According to Gledhill, the critical concentration corresponds to the transition between cohesive and interfacial failure. It follows that the absence of critical concentration in our results can probably be attributed to the fact that the bonds were not of sufficient quality to exhibit cohesive strength at low relative humidity. It also appears that the Sodium Hydroxide treatment proposed in Reference 56 did not lead to any improvement in bond strength as compared to a solvent degreased substrate.

Conclusion:

Gledhill and his coworkers have developed a simple procedure to predict the failure of epoxy-to-steel joints exposed to humidity. The method is based on the critical concentration concept. The good agreement between theoretical predictions and experiment indicates that the diffusion rate of moisture is the rate controlling parameter for durability in this class of adhesive bonds. The characterization required for the proposed analysis includes the diffusion coefficient of water in the adhesive, the solubility of water in the adhesive, the bulk fracture strength of the adhesive and the concentration of incipient failure C_c. Unfortunately, our experimental results on the Ultem to Aluminum system remain inconclusive.

Table 5. List of the Salt Solutions Used for Relative Humidity Control.

SOLUTION (SATURATED)		RELATIVE HUMIDITY AT 50°C (%)
MAGNESIUM CHLORIDE	$MgCl_2$	35
POTASSIUM CARBONATE	$(K_2CO_3)2H_2O$	47
CALCIUM CARBONATE	$Ca(NO_3)_2$	60
SODIUM NITRITE	$Na(NO_2)$	66
SODIUM CHLORIDE	NaCl	85
AMMONIUM SULFATE	$(NH_4)_2SO_4$	89
SODIUM SULFATE	$(Na_2SO_4)10H_2O$	98
PURE WATER	H_2O	100

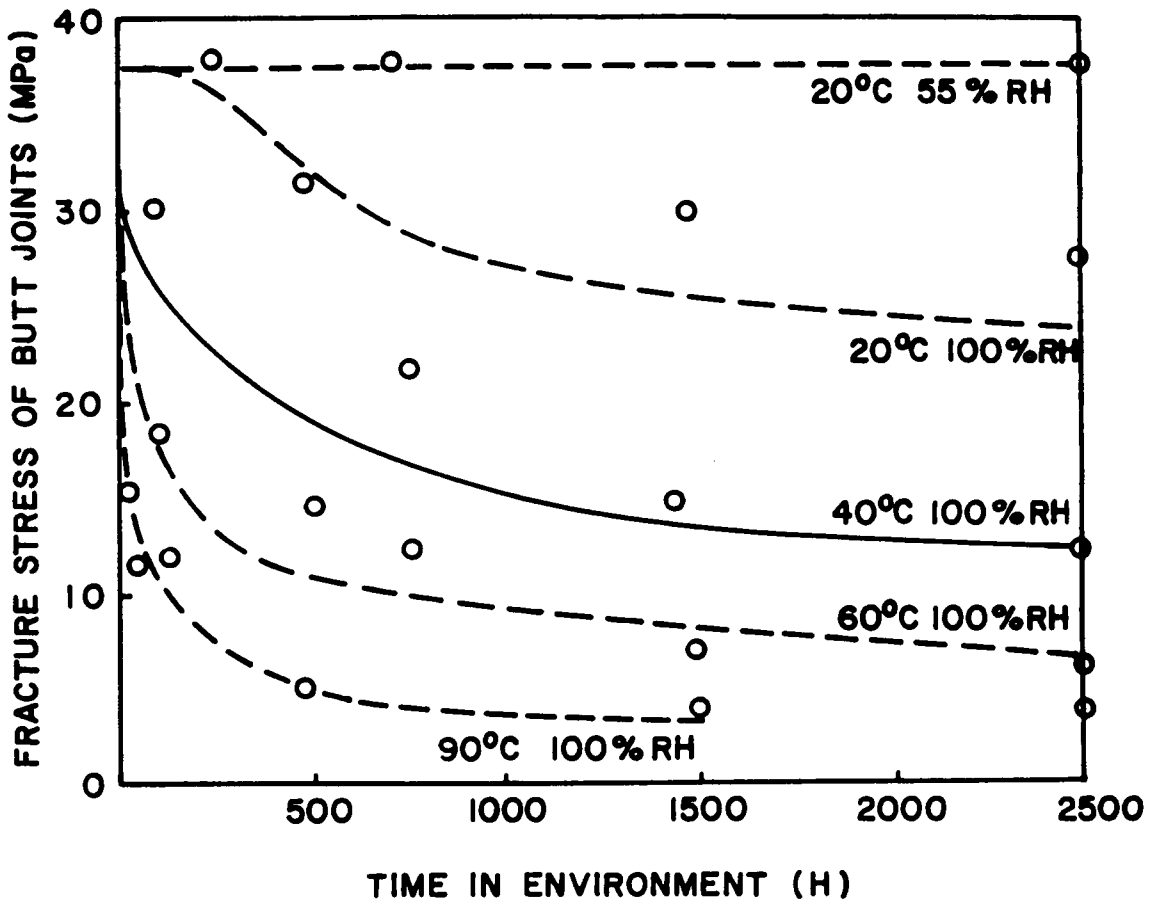

Figure 31. Butt Joint Fracture Stress Versus Time in Environment: Points are Experimental Measurements, the Solid Line is the Curve Fit from Which the Critical Concentration Was Determined, the Dashed Lines Are Theoretical Predictions [52].

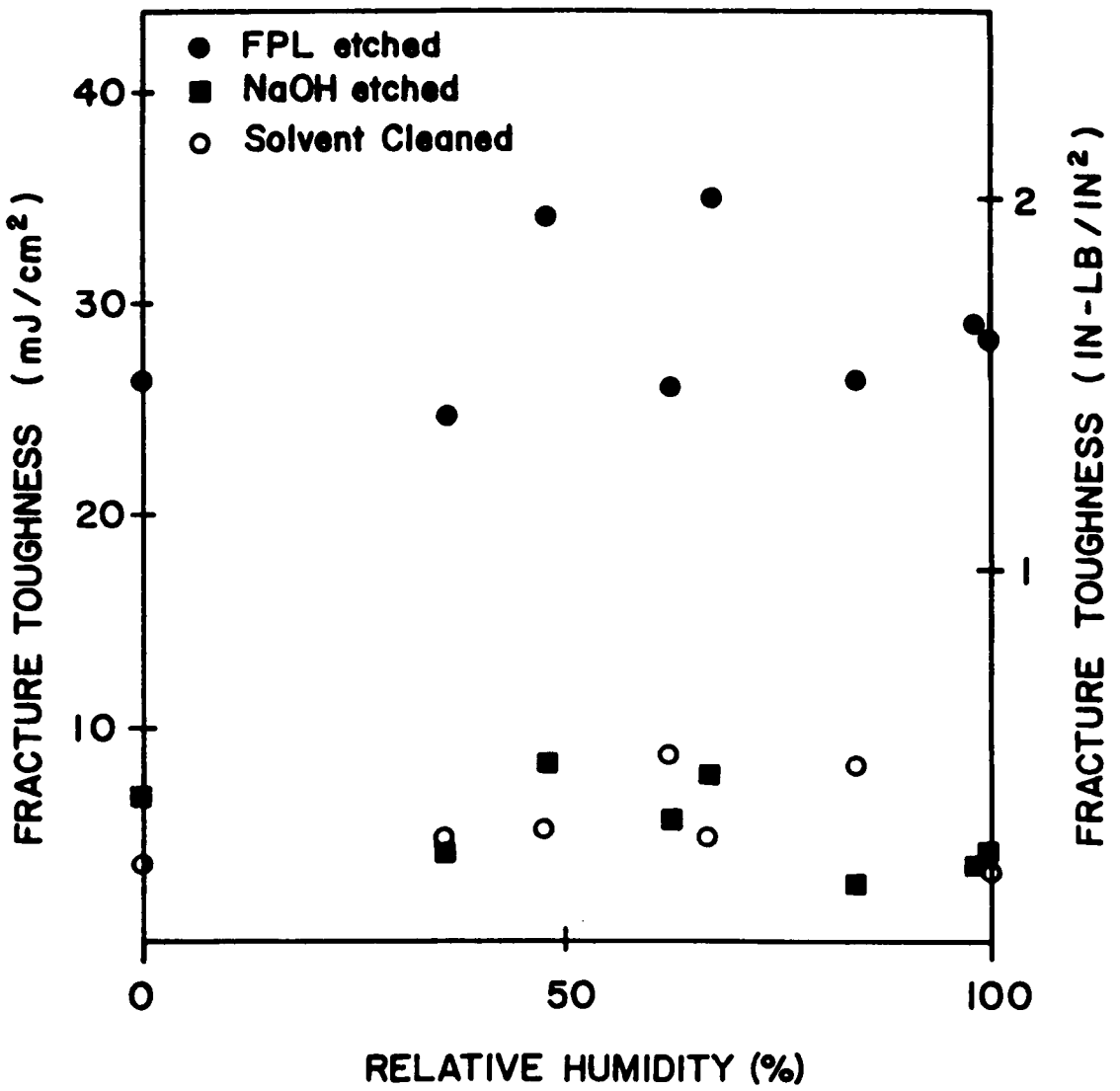

Figure 32. Residual Fracture Strength Vs. Relative Humidity: Aluminum 2024-to-Ultem DSCBs Were Conditioned Under Several Relative Humidities at 50 C and Zero Stress.

6. DEBOND PREDICTIONS IN THE PRESENCE OF AN AGRESSIVE ENVIRONMENT: THE CASE OF RUBBER-TO-STEEL JOINTS IN SEAWATER.

Introduction:

In Chapters 1 to 5, a general treatment of environment-assisted failure has been proposed. It was shown that there exists strong evidence that such an approach can yield good results for a large class of structural joints, when exposed to water as the primary degradation agent. Unfortunately, as we will see with the case of rubber-to-steel joints in marine environment, other penetrants than water can play an active part in bond degradation. These penetrants can greatly complicate the analysis of the problem by inducing chemical reactions with the adhesive, which in turn can dras-

tically alter the diffusive process. In such a case, novel approaches specifically tailored to the problem at hand must be devised.

This chapter will illustrate this point by addressing the special case of rubber-to-metal bonds subjected to a cathodic potential, in seawater. The failure mode will be explained, a fracture test will be described, and a scheme to predict debond rate will be suggested. The emphasis will be placed on the mechanical analysis of the fracture process in rubber-to-steel joints.

The Cathodic Debonding of Rubber-to-Steel Joints in Marine Environment:

Elastomer to metal bonding is an important adhesion problem for a variety of modern structures and components. Major applications include the automotive, tire, shipbuilding, and off shore drilling industries. In these applications, the rubber may serve to inhibit corrosion, to seal the component from intrusion of unwanted substances, or as a load bearing structure. Although acceptable bonds are routinely produced for many of these functions, bond durability can be a problem under certain environmental exposure. Of current concern are the rubber to metal bonds for marine applications. Although these bonds have been shown to be quite durable in seawater environments, the presence of small amounts of cathodic potential can rapidly deteriorate the adhesive bond[57]. Cathodic potential may be provided by the galvanic action of dissimilar metals. This situation is intentionally created on many marine structures by the use of sacrificial zinc anodes. Ironically, these anodes serve to protect the steel hull but degrade the performance of rubber bonds, paint, and other organic coatings. Even if the metal substrates are initially electrically

insulated from the anodes, corrosion products and sediment can build up on the components to permit the flow of electrons.

Cathodic debonding processes have been widely studied by researchers in the area of thin organic coatings[58-59]. When metallic substrates are exposed to aqueous salt solutions and supplied with free electrons, reduction of dissolved oxygen or water at the adhesive to metal oxide interface occurs and locally increases the pH. When these reaction products are sequestered inside a small debonded region or adhesive layer, an extremely high pH can result. Several mechanisms have been proposed to explain the relatively rapid debonding that results from the alkaline environment[58-61]. Although the mechanisms responsible for the bond deterioration are complex and not entirely understood, our observations have indicated that the high pH hydrolyzes the polymeric primer leaving a weakened bond. The weakened zone may remain intact unless a sufficient force is applied.

A variety of tests have been advocated for evaluating the adhesion of a flexible layer bonded to a rigid substrate. The cone test (ASTM D-429) has been widely used for measuring the adhesion of rubber to metal substrates. The design of this test causes debonding to initiate at the interior of the specimen, however, making it inappropriate for tests subjected to environmental exposure. A number of different specimens have been based around the peel concept. These include the climbing drum peel test (ASTM D-1781), the floating roller peel test (ASTM D-3167), and the simple peel test, using 180° peel (ASTM D-903) or other angles. Unfortunately, the fixtures associated with these tests are quite cumbersome to use in a harsh liquid environment.

The various peel tests have been utilized for measuring fracture energies of rubber to metal bonds, but they have a number of limitations. All of these tests tend to induce very large deformations at the debond tips. These extreme distortions produce significant material and geometric nonlinearities which make the specimens very difficult to analyze. If one wishes to measure time dependent fracture energies, the viscoelastic dissipation in the relatively large rubber bulk can alter the results. Although fabric can be embedded in the rubber to minimize the strain energy stored[62], localized large deformations can still induce substantial energy dissipation in a nonlinear viscoelastic material. To minimize these difficulties, a specimen is needed in which the deformations are smaller and in which the viscoelastic dissipation is reduced.

In an effort to avoid some of the problems associated with these specimens, several improved techniques have been developed and one of these will be reported herein. The objective of the current work has been to develop tests to measure the critical strain energy release rates for the rubber to metal bonds in various stages of deterioration. A test for determining G_c for elastomer to rigid adherend bonds subjected to aqueous environments will be described. Although the technique is equivalent to the widely used Double Cantilever Beam Specimen, special problems and attributes are important for the extension of this technique to evaluate elastomer to metal bonds.

The Double Cantilever Sandwich Beam:

The double cantilever sandwich beam (DCSB) illustrated in Figure 33 is a modification of the double cantilever beam (DCB) originally proposed by Ripling, et *al.*[63]. The specimen is shown with an extensometer mounted on the unit for measuring the displacements during the calibration study.

The DCSB specimen consists of a thin layer of elastomer bonded between two metal adherends. Although the elastomer appears much like a thick adhesive, the intent is to study the adhesive **between the steel and the rubber**. Thus, the elastomeric layer is to be seen as a soft adherend in a constrained state. This type of geometry greatly reduces viscoelastic dissipation in the rubber for three reasons: (1) the volume of the elastomer is minimal, (2) the strain levels are smaller than in other specimens, thereby minimizing the nonlinear effects, and (3) the elastomer is highly constrained, forcing it to deform in a bulk rather than shear mode. (The bulk behavior of polymers tends to be substantially less time dependent than the shear behavior.) In the following section, it will be shown that the specimen can be analyzed with a closed form beam-on-elastic-foundation solution.

Design and Analysis of the Double Cantilever Sandwich Beam:

The experimental phase of the work was conducted on two different specimen geometries with dimensions given in Table 6. Type 2 is a refined version of type 1, having thicker adherends and a thinner layer of rubber. The steel adherends were vapor degreased, grit blasted with steel grit, and vapor degreased again in tri-chloroethane 1,1,1 in preparation for bonding. Two coats of Chemlok 205 primer (blend of chlorinated rubber and phenol formaldehyde) and two coats of Chemlock 220 topcoat (proprietary) were brushed on the adherends, allowing each to dry prior to applying the next. After preheating the mold in a platen press, specimens along with uncured 5109-S neoprene rubber were inserted. The adhesive and rubber were vulcanized at 154°C (310°F) for 1.5 hr at a nominal pressure of 3.45 MPa (500 psi).

In order to characterize the toughness of adhesive bonds, the relationship between the strain energy release rate, load, and crack length must be known. This relationship has been predicted analytically and determined experimentally. Using an MTS servo-hydraulic load frame, load-deflection behavior was obtained for the two specimen configurations as a function of crack length. Deflections were measured with an extensometer and increments in crack length were made by using a fine-toothed saw to cut the rubber. Although tension specimens of the rubber had exhibited considerable creep, the DCSB specimens did not show measurable time dependence presumably because of the minimal amount of rubber loaded in a triaxial fashion.

Figure 34 illustrates the measured compliance of the type 1 specimen. The dashed line represents the predicted compliance based on neglecting the deformations in the rubber. It is the simple cantilever beam solution commonly used for the DCB specimen and assumes that the beam rests on a rigid foundation. The compliance is based on the relationship

$$C = 8a^3 / (Ebh^3) \tag{145}$$

in which a is the crack length, E is the Young's Modulus of the adherend, b is the specimen width, and h is the thickness of each metallic adherend. Since the measured compliance is consistently higher than the simple prediction, an improved approximation is required. To achieve this, the thin rubber layer was assumed to act as a classical elastic foundation and a closed form solution based on the finite length beam on an elastic foundation solution given by Hetenyi[64] was developed. Kanninen[65] has employed a similar beam on elastic foundation solution for the monolithic double cantilever beam specimen to account for transverse deformations.

Referring to Figure 35, one can calculate the total beam deflection at point B as:

$$y_B = y_A + \theta_A \cdot a + Pa^3/3EI \tag{146}$$

The slope and deflection at point A can be calculated by utilizing Hetenyi's solution for a finite beam on an elastic foundation. For the case of equal applied forces on the two beams, symmetry requires that there be no horizontal (frictional) forces and the fracture mode is pure mode I, since the nonsymmetry due to the rubber remaining on one adherend produces negligible error.

The applied force P at point B is translated to point A and an equivalent moment is also applied at point A. The characteristic root of the governing differential equation for a beam on an elastic foundation is:

$$\lambda = \sqrt[4]{\frac{k}{4EI}} \tag{147}$$

For beams of finite length, the solution depends on the nondimensional quantity $[\lambda(L-a)]$. For the current problem, this quantity exceeds π and according to Hetenyi, the beam may be classified as a long finite length beam. For an applied force P at point A, the slope and deflection at A are given by:

$$\theta_A = \frac{2P\lambda^2}{k} \frac{\sinh^2\lambda\rho + \sin^2\lambda\rho}{\sinh^2\lambda\rho - \sin^2\lambda\rho} \tag{148}$$

$$y_A = \frac{2P\lambda}{k} \frac{\sinh\lambda\rho\ \cosh\lambda\rho\ -\ \sin\lambda\rho\ \cos\lambda\rho}{\sinh^2\lambda\rho\ -\ \sin^2\lambda\rho} \tag{149}$$

with: $\rho = L - a$

and for an applied moment of (Pa) at point A, the slope and deflection are given by:

$$\theta_A = \frac{4Pa\lambda^3}{k} \frac{\sinh\lambda\rho\ \cosh\lambda\rho\ +\ \sin\lambda\rho\ \cos\lambda\rho}{\sinh^2\lambda\rho\ -\ \sin^2\lambda\rho} \tag{150}$$

$$y_A = \frac{2Pa\lambda^2}{k} \frac{\sinh^2\lambda\rho\ +\ \sin^2\lambda\rho}{\sinh^2\lambda\rho\ -\ \sin^2\lambda\rho} \tag{151}$$

By superimposing these results and substituting them into equation (146), one obtains a closed form solution for the deflection of the DCSB specimen.

The remaining task for completing the analysis is the determination of the foundation stiffness, k. This is a difficult parameter to determine analytically because of the complex triaxial stress state in the rubber. As a first step, k was determined from experimental compliance data. Although the calculated values of foundation stiffness show a slight decrease as the debond increases in length the values are relatively stable and good agreement with experimental data is achieved as illustrated in Figure 34. Again one should note, however, that the value of k is chosen to give the best agreement with the compliance data rather than being determined independently. At this stage the foundation stiffness may be viewed as a curve fitting parameter. If one takes the observed foundation stiffness and multiplies by the thickness of the rubber layer and divides by the width of the beam, and effective elastic modulus of the rubber layer is determined. Values obtained are presented in Table 7 and as would be expected, due to the triaxial constraint, the effective modulus of the rubber is strongly affected by the thickness of the rubber layer. The measured values of effective modulus lie between the tensile modulus of the rubber, 4.14 MPa (600 psi), and the bulk modulus, 876 MPa (127 ksi), and increase rapidly as the rubber thickness decreases.

As a second step in ascertaining the foundation characteristics, it was shown that the foundation stiffness can be predicted analytically using a procedure developed by A. N. Gent et *al.*[66,67]. The overall deformation of the block of rubber is assumed to result from the superposition of the deformation of the unconstrained block and a shear deformation necessary to restore displacement continuity along the bonded interfaces. The normal force may be written in the form:

$$F = f_c A E' \varepsilon \tag{152}$$

in which A is the cross-sectional area of the block, E' is Young's modulus of the rubber, ε is the normal strain in the rubber and f_c is a corrective factor accounting for the constraining effect of the adherends. In the case of a rectangular block of infinite length, $A = bt$, $\varepsilon = \frac{2y}{t}$ and $f_c = \frac{4}{3} + \frac{1}{3} b^2/t^2$, where b is block width, t is block thickness and y is deflection in each beam.

Whence, for a foundation of unit width the normal stress would be:

$$\sigma = f_c E' \varepsilon t \tag{153}$$

or

$$\sigma = 2 f_c E' y \tag{154}$$

Now in the theory of Beams on Elastic Foundations, the foundation stiffness k is defined by:

$$\sigma = k y / b \tag{155}$$

Taking $b = 1$ and comparing (154) and (155) yields:

$$k = 2 f_c E' \tag{156}$$

Table 7 shows that the foundation stiffness obtained from the above relationship and obtained previously by curve fitting the experimental data are in reasonable agreement. It should be noted that the solution to the deflection equation is quite insensitive to the value used for k . As

a result, excellent agreement with the experimental compliance data is obtained, even with variations of k as large as 30%.

It must be noted that the solution given by Gent for the infinitely long block of finite width is not completely appropriate for the solution to the beam on elastic foundation because it: (1) does not account for the end occurring at the debond tip and (2) does not account for the damped sinusoidal displacements. Both of these factors should result in an overprediction of the foundation stiffness. Nonetheless, the errors introduced do not seem to strongly affect the calculations of the strain energy release rate and these approximations seem adequate to estimate the foundation stiffness.

To further verify the model, a strain gage was mounted on the outer surface of one of the steel adherends and the strain was recorded for various debond lengths. The results from this are presented in Figure 36. The gage was positioned 127 mm (5 in) from the loading end. When the debond tip is near end B, the strains measured are very small. As the debond approaches the gage, the strains become positive where the beam oscillations induce a tensile mode in the rubber. As the oscillation passes on ahead of the gage, the compressive strains induced by bending in the adherends increase up to a maximum value equal to that predicted by simple beam theory for $M = P \bullet 127\,mm$. The predicted values of strain from the beam-on-elastic-foundation analysis are seen to agree very well with the experimental data.

To better understand how various parameters affect the performance of the DCSB, parametric deflection studies are presented in Figures 37 to 39. Figure 37 illustrates the effect of the debond length on the normalized deflections for the type 1 specimen. Figure 38 shows how changing the rubber thickness would change the deflections for a given adherend thickness. Decreasing the thickness reduces the amount of bending oscillation and shortens the characteristic oscillation distance, in addition to reducing the time dependence as mentioned before. Clearly the rubber sandwich should be made as thin as practical. Figure 39 shows that increasing the adherend thickness reduces dramatically the oscillations, in addition to increasing the maximum available strain energy for debond propagation.

In order to test loaded specimens in a harsh environment, it is highly desirable to use a simple, self-loading device. The Boeing wedge specimen is a form of the DCB which is loaded by driving a wedge between the adherends to produce a constant displacement test. Unfortunately, the available G for this type of load is highly dependent on the debond distance, obeying an inverse fourth power relationship with crack length. Although this type of loading can be used, the technique is very sensitive to small errors in debond measurement, and the available strain energy decreases so rapidly that the measurements must be taken at very small increments in debonding to obtain accurate information. In an effort to avoid these difficulties, a loading device which would impose a relatively constant value of G would be beneficial.

To investigate a constant G test, one can write a closed form solution for the required force necessary to produce a constant G rate:

$$P^2 = \frac{2Gb}{\partial C/\partial a} \tag{157}$$

The expression for $\partial C/\partial a$ is given in Appendix. Figure 40 represents parametric iso-G curves for specimen type 2. The indicated fracture energies are typical of G_c for the weakened bonds. The vertical portion of the limit of validity domain represents a detached length of 216 mm (8.5 in) after which the remaining support is too short for the analysis to be valid. The curved portion of the limiting domain represents rotations of the loaded end of the beam which exceed 8 degrees and may result in beam foreshortening errors.

Iso-G loading can be accomplished quite simply by using a spring to load the specimen. Figure 41 illustrates the loaded fixture in place in the testing environment. Simple helical compression springs were used to provide the energy to the system. Figure 42 illustrates the force available from a given spring for several different preload rates superimposed on a desired Iso-G curve. By properly selecting the spring stiffness and the preload, one can obtain an Iso-G test window with a width of 50 mm (2 in). Thus one is able to set up the loading device to provide a relatively constant debond driving force over a relatively long debond distance. With a small assortment of springs and with judicious choices of the preload, one can follow a required G curve

over most of the length of the specimen. A compact load cell and an extensometer can be used to monitor the actual applied G to correct for small deviations. By holding G relatively constant, however, the collection of debond growth data is greatly simplified.

Specimen Design Guidelines:

In designing DCSB specimens, the following guidelines may prove helpful:

- Make the soft layer as thin as practical to minimize the viscoelastic effects.
- Select a specimen width which is large compared to the elastomer thickness in order to increase the constraining action on the elastomer.
- Determine the appropriate G range for the adhesive system and select a beam thickness which can provide the desired G values while remaining in the small deflection envelope.
- The remaining bonded length should be large enough that the long finite length beam assumption is valid.
- For the Iso-G loading, superimpose the spring load decay curves on the Iso-G parametric curves and select an appropriate initial load and spring constant to give the desired result.

Difficulties with Interaction Between Diffusion and Fracture:

Because the specimen was designed to measure the fracture energy of debonding under conditions of cathodic delamination, the adherends were not thick enough to permit testing of the dry bond. Preliminary tests were conducted in seawater or NaOH solutions with cathodic potential applied. Slow debond rates were measured but difficulties were encountered because the results were not consistent. When specimens were broken open after testing, a significant chevron or reverse tunneling effect was noted. The reasons for this phenomena, which is opposite of that experienced in standard DCB specimens, is that the peel stresses are higher at the outside of the specimen because of the "poker chip" effect, and because diffusion occurs from these edges into the specimen. Because the chevron effect was so severe, meaningful debond distances could not be obtained.

As other tests on the neoprene to steel bond were conducted, it became apparent that moisture diffused into the specimen and left the bond intact but severely weakened. When choosing between adhesive systems for applications exposed to cathodic potential, the two most important parameters to measure appear to be the rate at which diffusion occurs and the retained strength of the weakened bond. Although the DCSB appeared to be limited for measuring fracture parameters while diffusion into the specimen was occurring, it was decided that the important fracture parameter to measure was the critical strain energy release rate of the **weakened bond**. Several specimens were conditioned in environment to produce a weakened, but intact, cathodically degraded bond. By imposing potential to only one adherend, this bond was preferentially weakened. Once the specimens were conditioned they were tested in a tension test machine. This weakened bond strength was found to be approximately .054 J/m^2. This fracture energy is four orders of magnitude smaller than the 60 J/m^2 value corresponding to the dry strength of the joint (cohesive in rubber). Estimates for the weakened bond strength were also obtained by an alternate approach[68] and were

found to be within 20%. This is considered to be quite good agreement because of the difficulty in uniform fabrication and conditioning of specimens, and the extremely small values of G_c.

A Technique for Predicting Debond in Mechanically Loaded joints:

The residual fracture strength data discussed in the previous section were obtained after conditioning specimens in the absence of an external mechanical load. Thus, this type of information is inherently insufficient for predicting debond rate in actual service conditions where stress is present. The reason is that depending on the applied stress level, the debond tip may coincide with the advancing weakened bond, or may lag behind. If the applied stress is high enough, debond can proceed faster than the diffusion process (with the Chemlok 205/220 system, failure is cohesive when the bond has not been weakened). In the absence of applied or residual stress, diffusion of the environment still occurs, although adherend separation may not occur. At intermediate stress levels, the debond tip coincides with the advancing weakened bond; stress opens the weakened region, allowing convection to transport species, rather than the slower diffusion process.

Whence it appears that the driving force for the opening mode of fracture (mode I), because it governs the relative position of the debond tip with respect to the diffusion front, must be the rate determining parameter. We conclude that a crucial piece of information in a durability study is the debond rate versus G_I curve (This kind of dynamic fracture data may be obtained with the DSCB specimen, or with a variety of other specimens based on the blister concept). A complete debond rate versus G_I curve offers the advantage of scanning the entire range of rate controlling situations in a purely empirical way. The rate of debond of a real life structure can then be calculated simply

by iteratively computing the current mode I component of the energy release rate and updating the debond tip position, using an experimental data base obtained by the techniques described herein.

Conclusion:

The DCSB offers distinct advantages over other specimens for measuring the critical strain energy release rate for elastomers bonded to a rigid adherend because it minimizes the viscoelastic dissipation. It is easily fabricated and can be analyzed with a closed form beam on elastic foundation solution. Foundation stiffness can be predicted with a rubber elasticity analysis. A simple spring loading device can be used to provide near constant G loading over a relatively wide test window. When using the specimen in an aqueous environment, diffusion at the sides can cause spurious results. For these cases however, specimens conditioned to equilibrium can be tested with good results. Finally, a simple procedure is available, for using experimental debond data to predict the service life of joint structures, even when the precise degradation mechanisms are not known.

Table 6. DCSB Specimen Dimensions

Specimen Type	Bond Thickness	Beam Length	Adherend Thickness	Beam Width
#1	1.27 mm (0.05 in)	273 mm (10.75 in)	3.18 mm (0.125 in)	25.4 mm (1.00 in)
#2	0.76 mm (0.0a in)	267 mm (10.5 in)	6.35 mm (0.250 in)	25.4 mm (1.00 in)

Table 7. Foundation Stiffness and Effective Modulus of the Rubber Layer

Specimen Type	Bond Thickness	Foundation Stiffness $k = 2f_cE$ (Predicted)	Foundation Stiffness k (Experimental)	Effective Modulus kh/b (Experimental)
#1	1.27 mm (0.05 in)	1.11 MPa (162 ksi)	0.68 MPa (98.9 ksi)	34.4 MPa (5.00 ksi)
#2	0.76 mm (0.03 in)	3.07 MPa (446 ksi)	3.45 MPa (500 ksi)	103.5 MPa (15.0 ksi)

Appendix:

The compliance of a DCSB specimen is given by: $C = 2y_B/P$

$$C = \frac{1}{EI\lambda^3}\,\frac{\sinh\lambda\rho\,\cosh\lambda\rho - \sinh\lambda\rho\,\cos\lambda\rho}{(\sinh^2\lambda\rho - \sin^2\lambda\rho)} + \frac{a}{EI\lambda^2}\,\frac{\sinh^2\lambda\rho + \sin^2\lambda\rho}{(\sinh^2\lambda\rho - \sin^2\lambda\rho)} + \frac{2a^2}{EI\lambda}\,\frac{\sinh\lambda\rho\,\cosh\lambda\rho + \sin\lambda\rho\,\cos\lambda\rho}{(\sinh^2\lambda\rho - \sin^2\lambda\rho)} + \frac{2a^3}{3EI}$$

where: $\rho = (L - a)$

The derivative of the compliance with respect to debond length is given by:

$$\frac{\partial C}{\partial a} = \lambda\,\frac{\partial C}{\partial D}, \qquad \text{with } D = \lambda(L - a)$$

$$\frac{\partial C}{\partial D} = -\frac{2}{EI\lambda}(L - D/\lambda)^2 + \frac{1}{EI\lambda^3}\{(\cosh^2 D + \sinh^2 D - \cos^2 D + \sin^2 D)(\sinh^2 D - \sin^2)$$

$$-2(SinhD\ CoshD - sinD\ cosD)^2\}/(\sinh^2 D - \sin^2 D)^2$$

$$+\frac{2}{EI\lambda^2}\{[2(SinhD\ CoshD + sinD\ cosD)(L - D/\lambda) - 1/\lambda(\sinh^2 D + \sin^2 D)](\sinh^2 D - \sin^2 D)$$

$$-2(\sinh^2 D + \sin^2 D)(L - D/\lambda)(SinhD\ CoshD - sinD\ cosD)\}\ /\ (\sinh^2 D - \sin^2 D)^2$$

$$+\frac{2}{EI\lambda}\{[(\cosh^2 D + \sinh^2 D + \cos^2 D - \sin^2 D)(L - D/\lambda)^2$$

$$- 2/\lambda(L - D/\lambda)(SinhD\ CoshD + sinD\ cosD)] (\sinh^2 D - \sin^2 D)$$

$$-2(L - D/\lambda)^2(\sinh^2 D\ \cosh^2 D - \sin^2 D\ \cos^2 D)\}/ (\sinh^2 D - \sin^2 D)^2$$

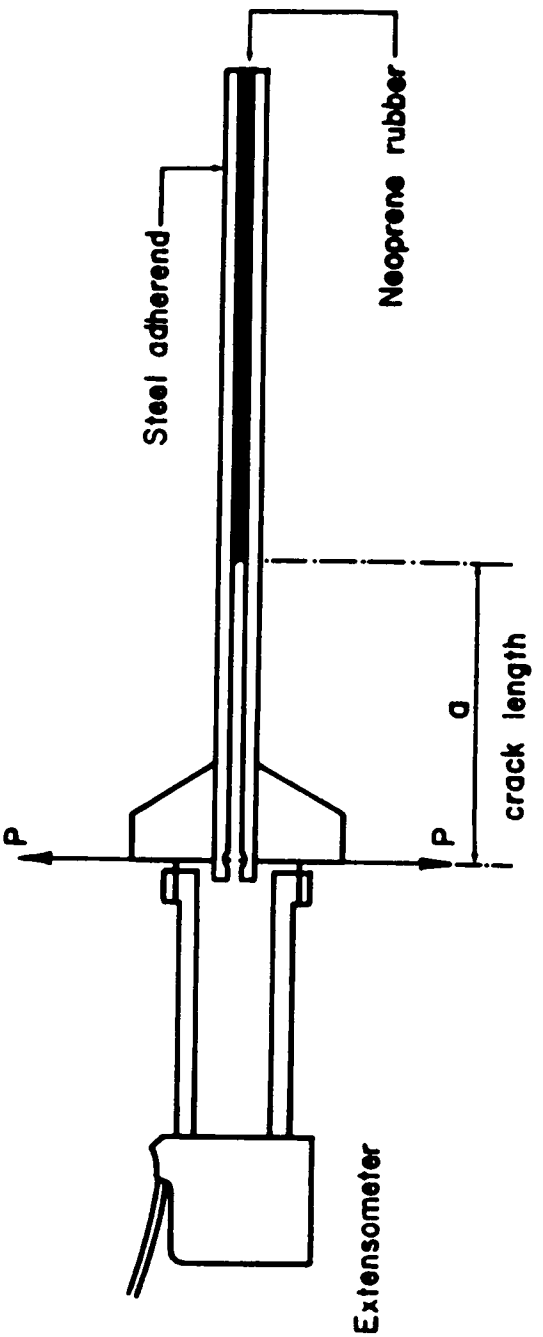

Figure 33. Double Cantilever Sandwich Beam Specimen: Extensometer Mounted for Compliance Measurements.

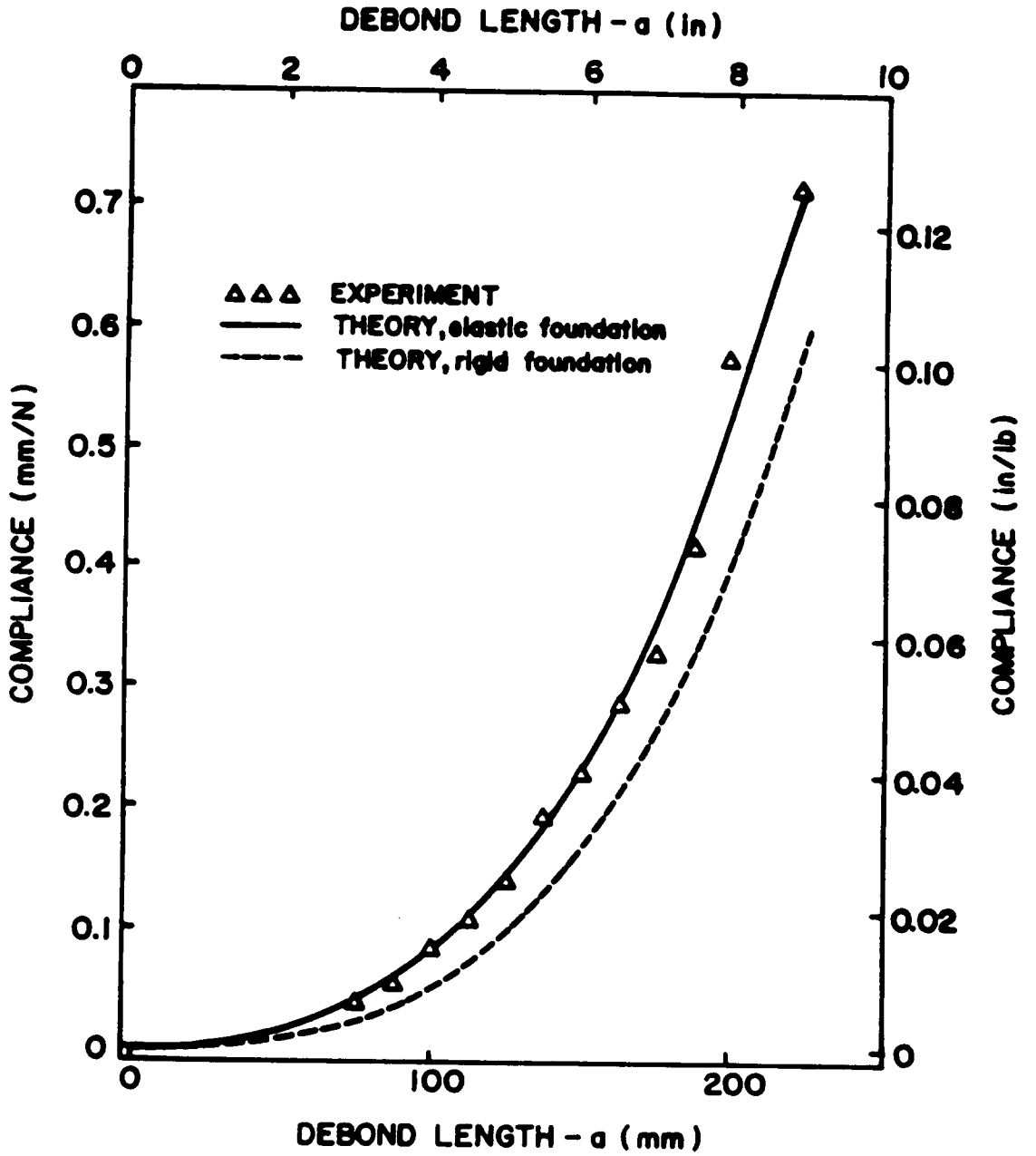

Figure 34. Experimental and Predicted Compliance vs. Debond Distance.

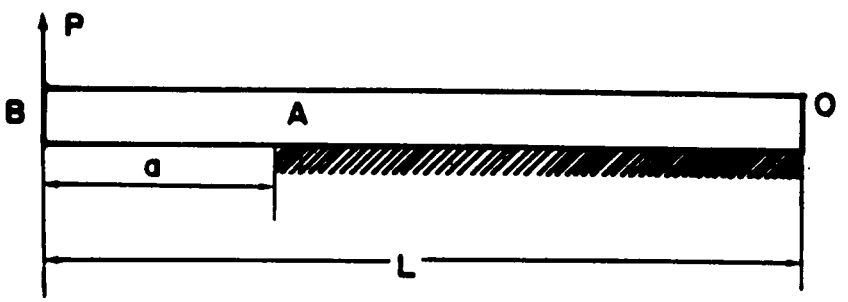

Figure 35. Upper Half of DSCB Modeled as a Beam on Elastic Foundation.

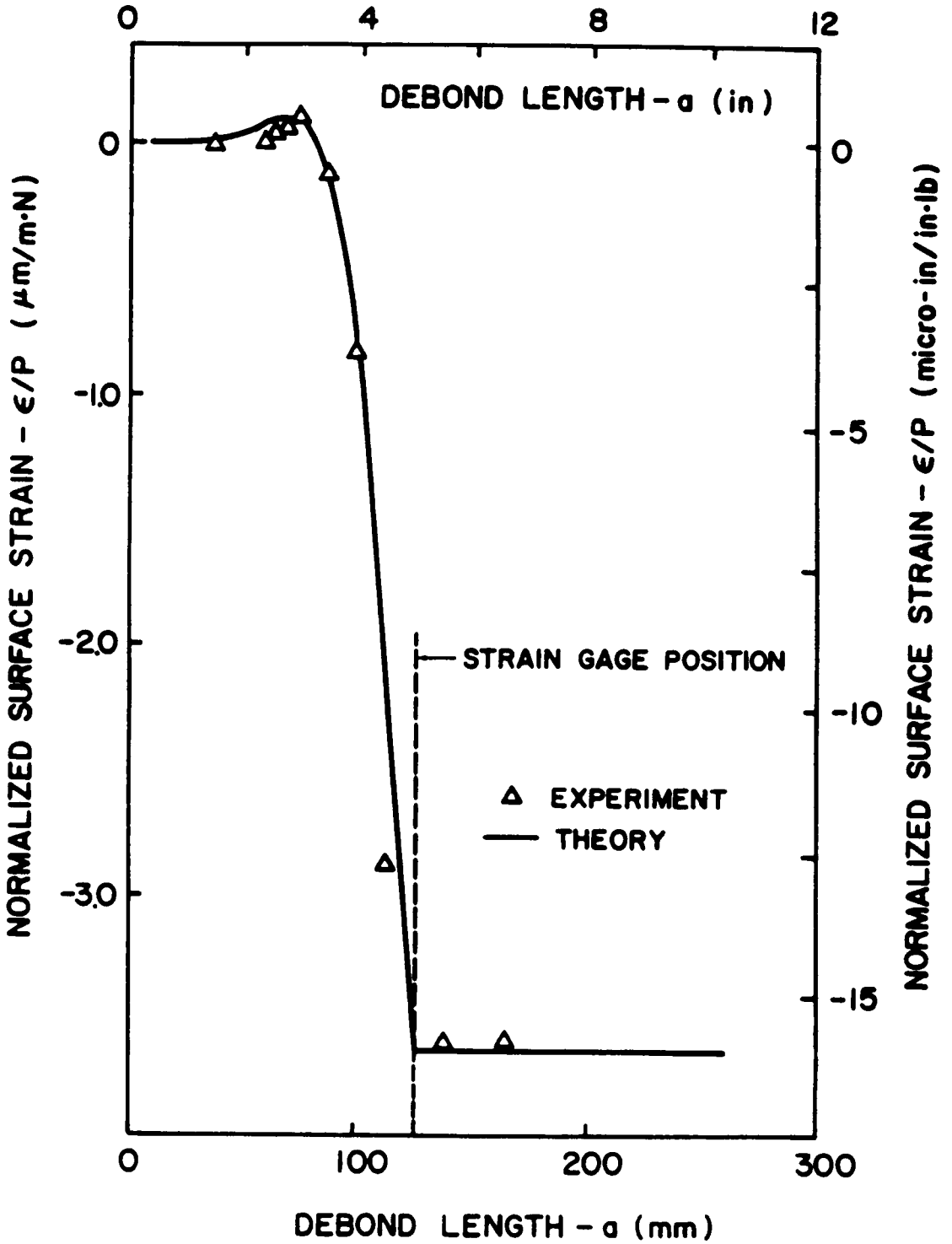

Figure 36. Comparison of Experimental and Predicted Surface Strain: Normalized Surface Strain at Position x = 127 mm (5 in) as a Function of Debond Length (Specimen 2).

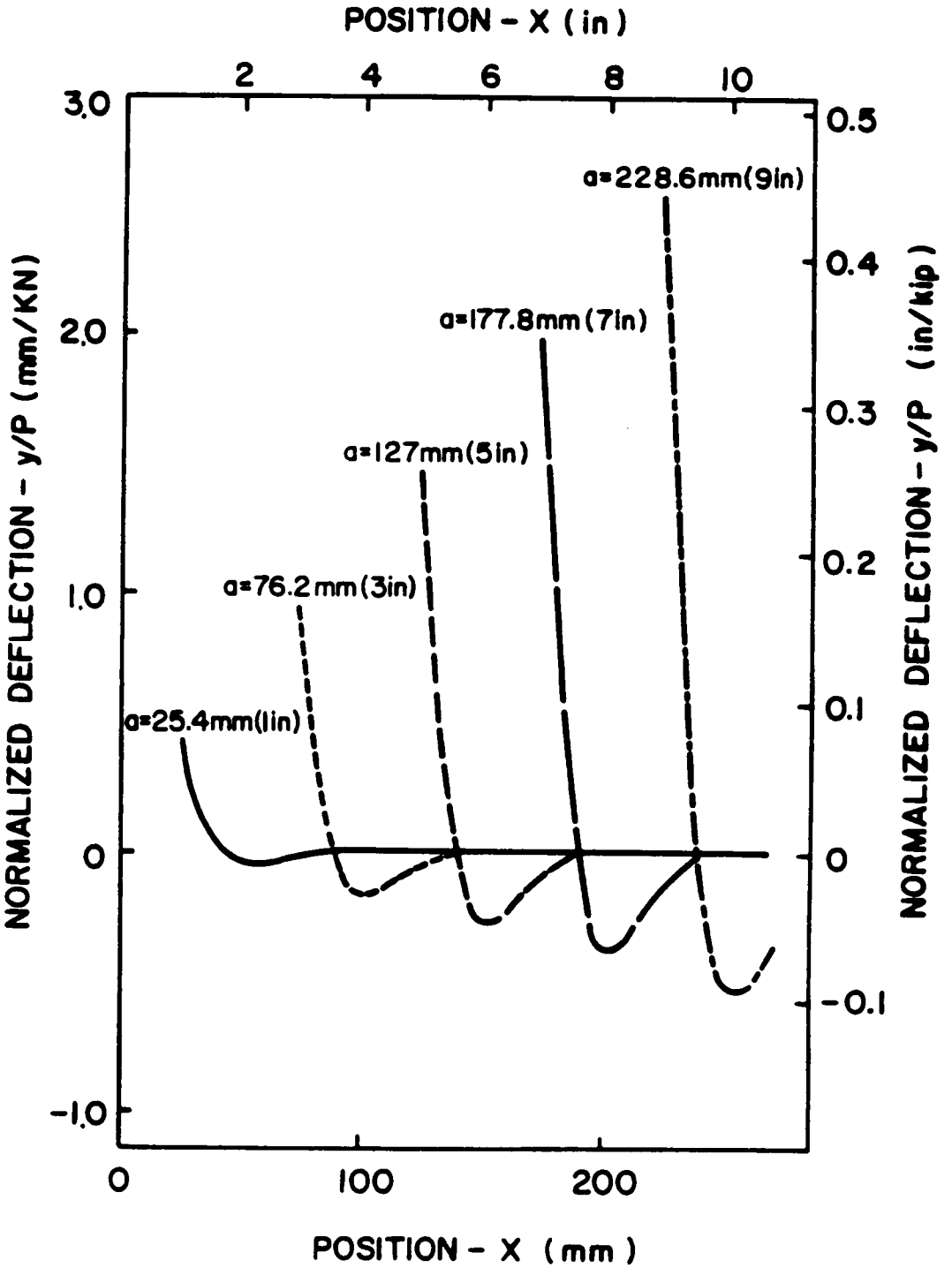

Figure 37. Predicted Normalized Deflections for Different Debond Lengths.

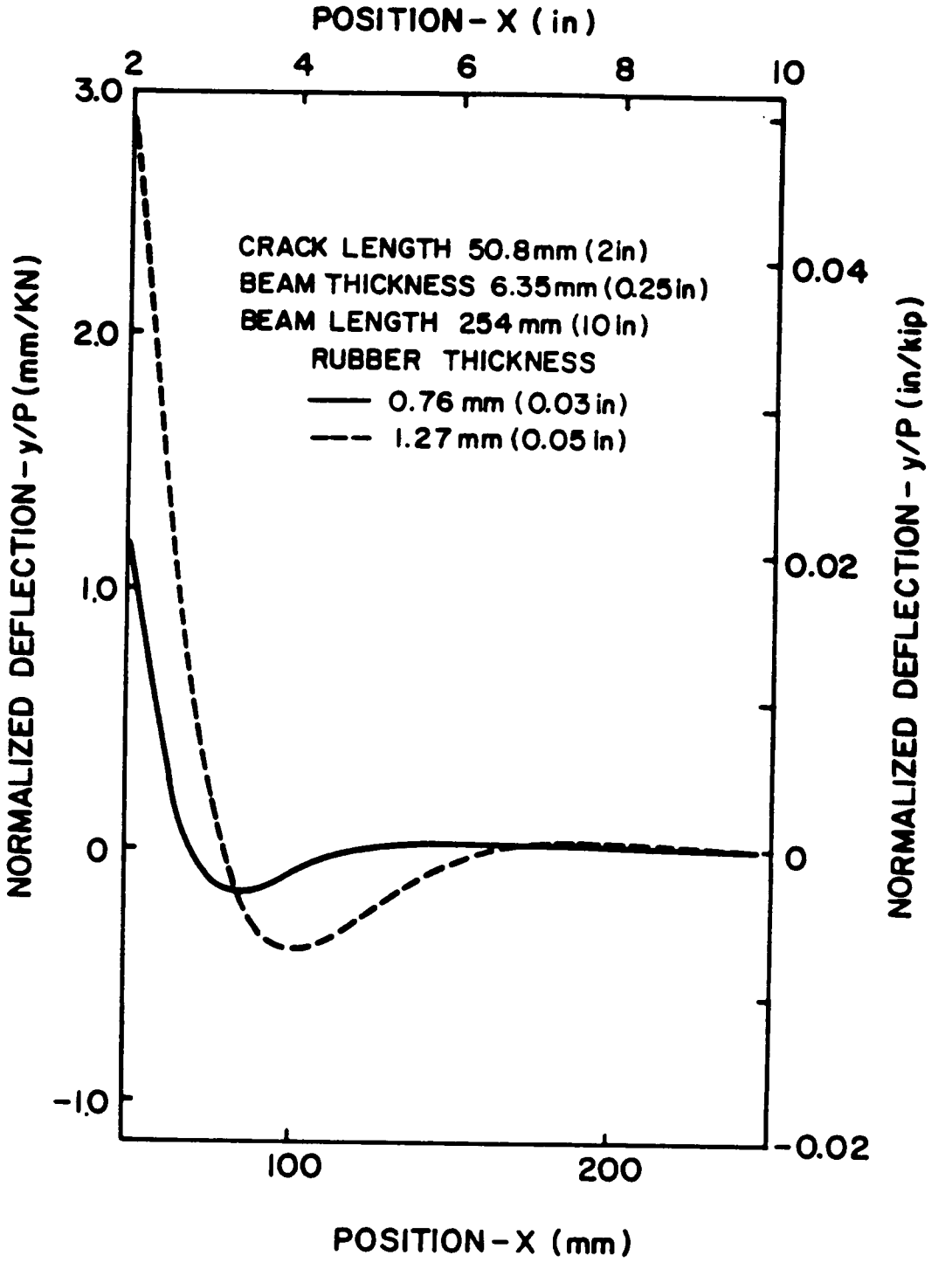

Figure 38. Predicted Normalized Deflections for Various Rubber Thicknesses.

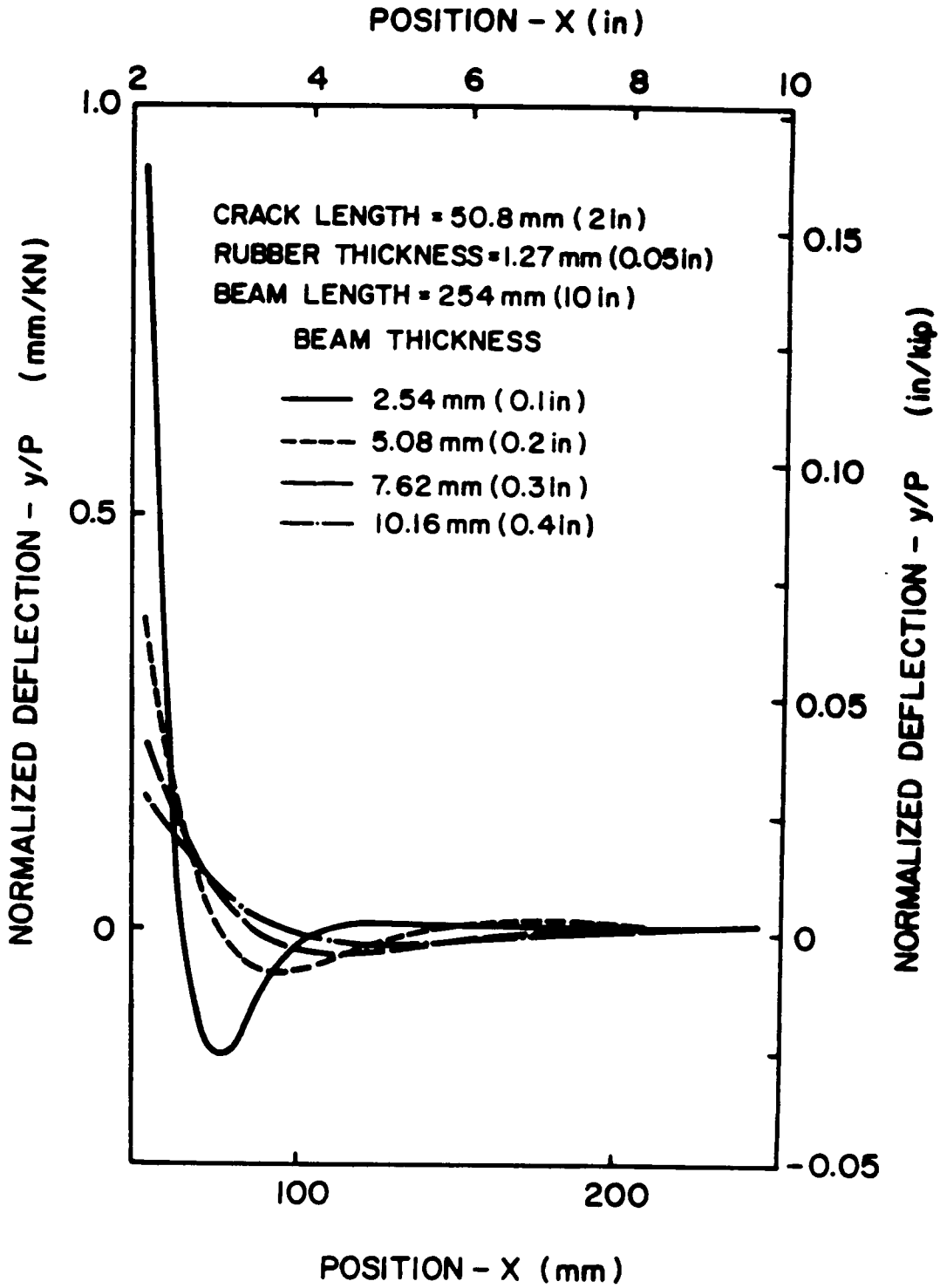

Figure 39. Predicted Normalized Deflections for Various Beam Thicknesses.

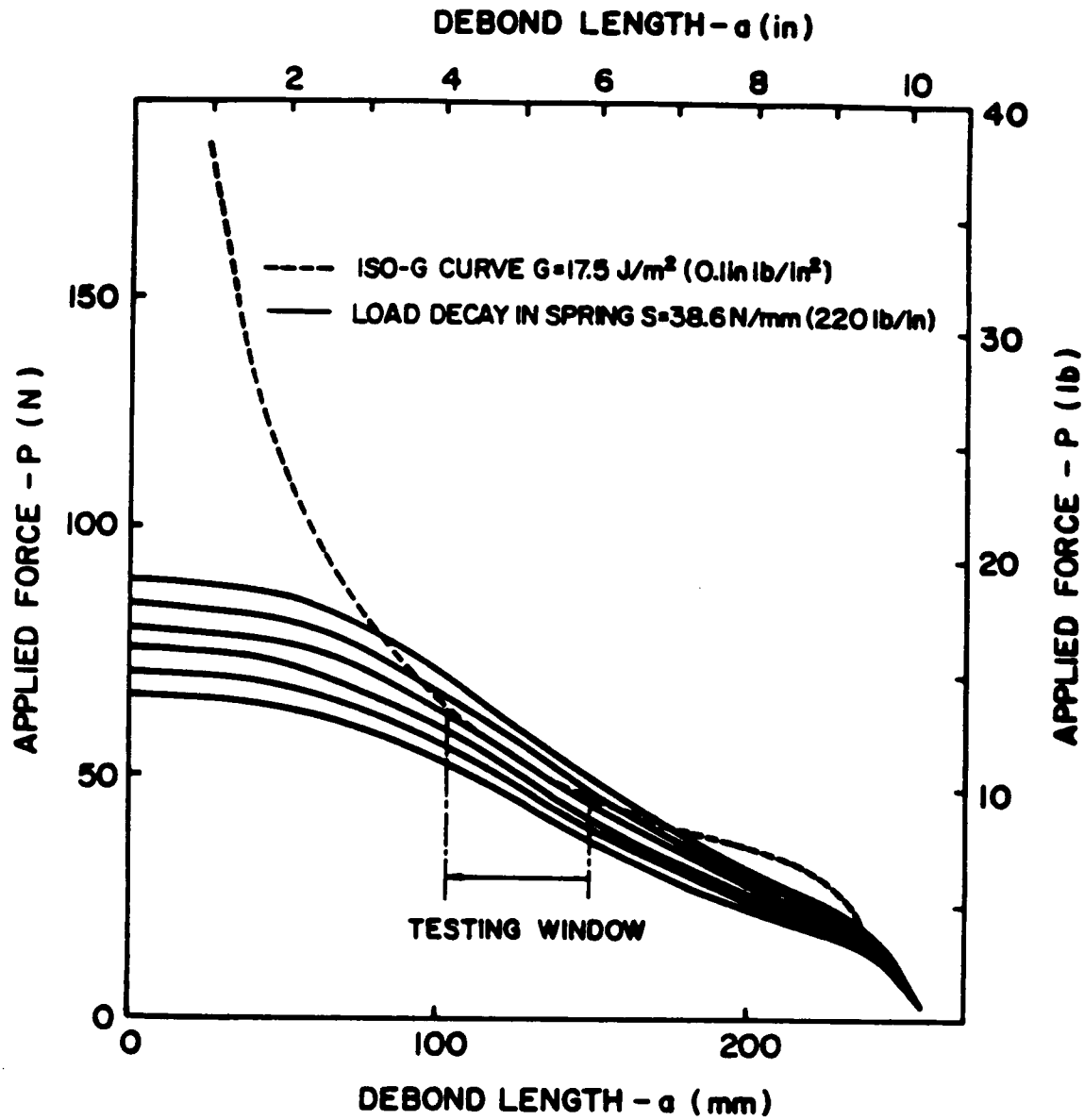

Figure 40. Load Decay vs. Debond Length: Each Curve Corresponds to a Constant Energy Release Rate Level in Specimen 2.

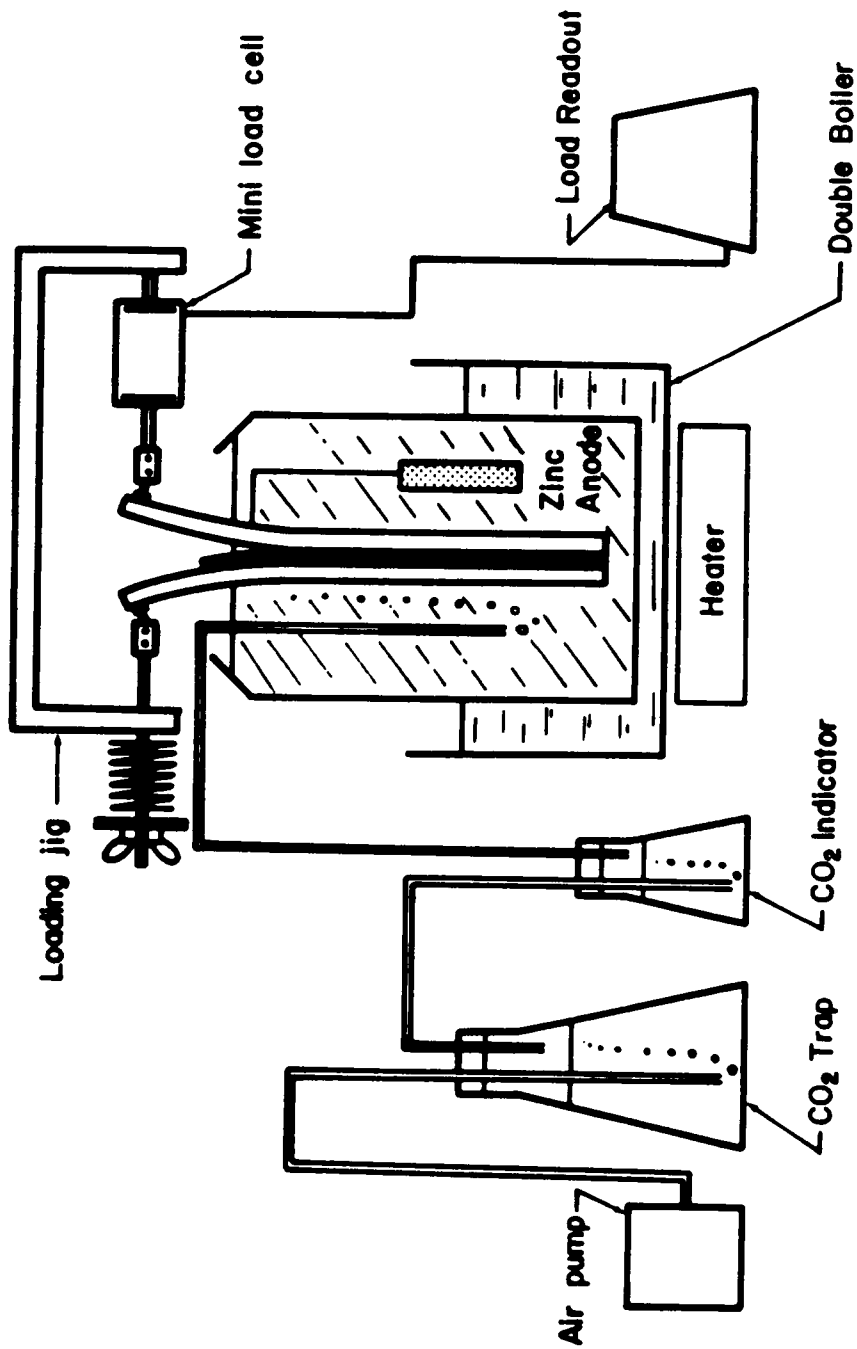

Figure 41. Setup for Accelerated Delamination Studies.

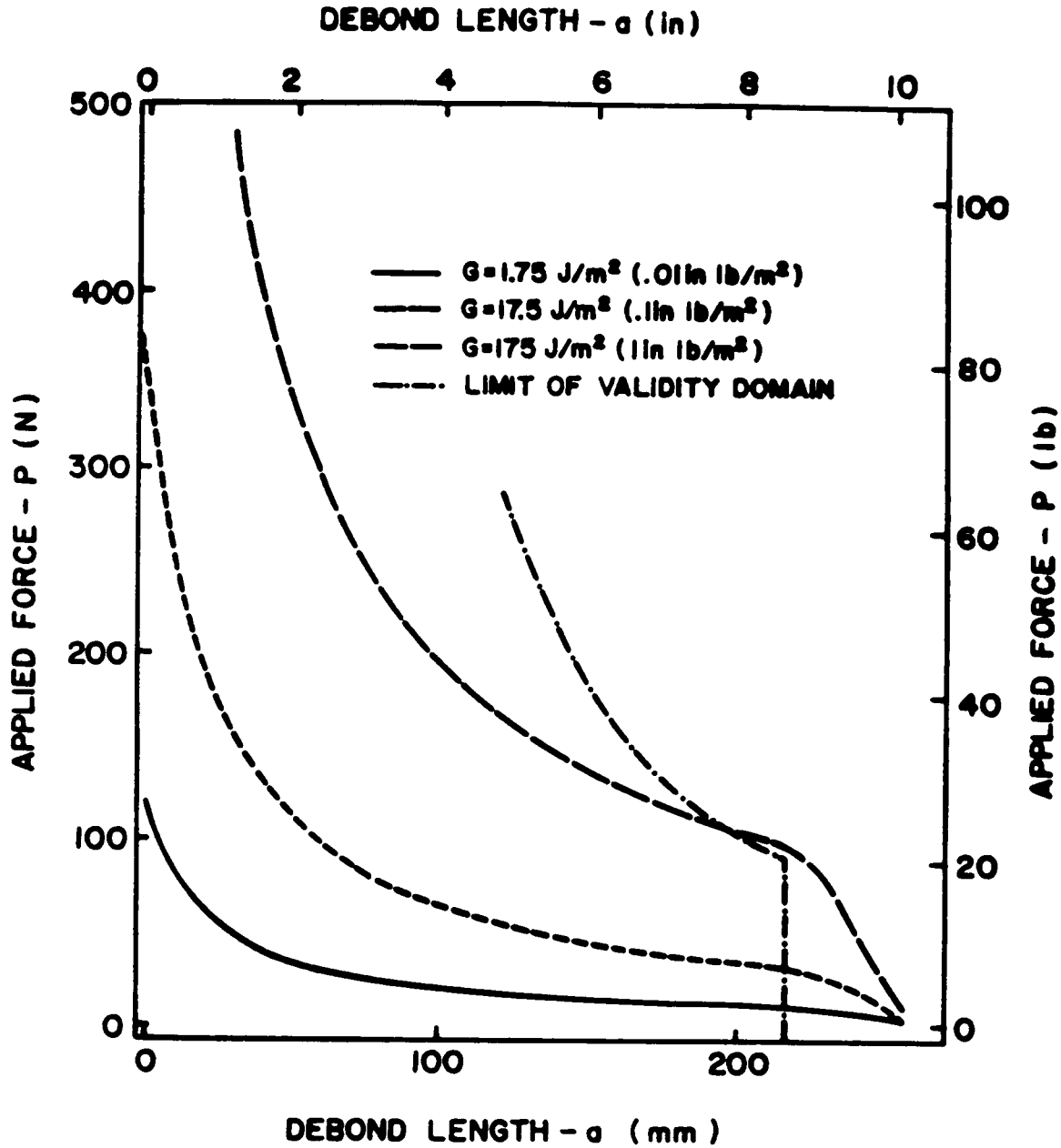

Figure 42. Available G for Several Preloads on an Iso-G Curve.

SUMMARY AND CONCLUSION:

In the case of polymer-to-metal bonds, water diffusion through the adhesive is a rate controlling factor for durability. The diffusion of small molecules such as water in a polymer can be understood at the molecular level by invoking the concept of free volume already used extensively in the field of polymer rheology. The free volume treatment of diffusion in polymers is very helpful in understanding the effect of temperature, mechanical deformation and physical aging on diffusivity and solubility. In addition, by recognizing that the free volume controls both the rate of segmental rearrangement and the transport rate of small foreign molecules, diffusion and viscoelasticity can be unified into one single theoretical treatment. This unified continuum approach greatly facilitates the modelling of coupling effects between diffusion and stress relaxation. Further, we found that the observed decrease in the durability of metal-to-polymer bonds in humid environments due to increased temperature and stress can be explained by the accelerated transport rate of water under these conditions. Boundary diffusion is also a possible path for water transport in adhesive joints. Theoretical considerations as well as recent experimental results show that flux perturbations near the boundaries of the adhesive layer are likely to be related to local fluctuations in polymer properties, not surface energetics.

Another key requirement for improved durability prediction is the development of failure criteria for interfacial failure in the presence of water and stress. Existing models are still very em-

pirical and limited to specific adherend-interphase-polymer systems. In the case of mild steel-to-epoxy bonds, the critical concentration concept seems to yield very promising results.

Finally, a convenient and well understood specimen geometry to study interfacial debonding experimentally is the Double Sandwich Cantilever Beam specimen. The mechanical analysis and test procedure for the DSCB specimen has been adapted to the study of the interfacial debonding of rubber-to-steel joints in harsh environments. The soft polymeric layer increases the overall compliance of the specimen and necessitates a beam-on-elastic-foundation-type of analysis.

The following recommendations for joint design can be made from our study:

(1) Select an adhesive with low water solubility to prevent water from reaching the interface in sufficient concentration. Another beneficial effect of low solubility is to minimize swelling stresses and their adverse effect on diffusion rate and interface fracture.

(2) If recommendation (1) cannot be met, select an adhesive with a low water diffusivity so as to slow down the sorption rate.

(3) Minimize peel stresses in order to lower the diffusion coefficient and slow down mode I crack growth, which is extremely detrimental to durability.

(4) Promote stable, receptive oxides capable of developing strong chemical bonds with the polymer. Such bonds are not easily displaced by the physical intermolecular forces acting around water molecules.

REFERENCES:

1. R. W. Fahien, *Fundamentals of Transport Phenomena* (McGraw Hill, New York, 1983). Chap.10, pp. 480-570.

2. M. Tirrell and M. F. Malone, *Journal of Polymer Science: Polymer Physics Edition*, **Vol. 15, No. 9**, 1569 (1977).

3. J. Crank, *The Mathematics of Diffusion* (Oxford at the Clarendon Press , London, 1956), 1st ed.

4. H. L. Frish, E. E. Wang and T. K. Kwei, *Journal of Polymer Science*, **A-2, F**, 879 (1969).

5. N. L. Thomas and A. H. Windle, *Polymer*, **23**, 529 (1982).

6. R. M. Felder and G. S. Huvard, *Methods of Experimental Physics* (Academic Press, New York, 1980), Edited by R. A. Fava, Vol. 16, Polymers, Part C, Chap 17, pp. 315-377.

7. J. Comyn, *Polymer Permeability* (Elsevier Applied Science Publishers, London and New York, 1985), Chap. 2-3, pp. 11-117.

8. F. A. Long and D. Richmond, *Journal of the American Chemical Society*, **82**, 513 (1960).

9. P. Neogi, M. Kim and Y. Yang, *AIChE Journal*, **Vol. 32, No. 7**, 1146 (1986).

10. D. Turnbull and M. H. Cohen, *The Journal of Chemical Physics* , **34**, 120 (1961).

11. M. H. Cohen and D. Turnbull, *The Journal of Chemical Physics* , **31**, 1164 (1953).

12. P. B. Macedo and T. A. Litovitz, *The Journal of Chemical Physics* , **48**, 845 (1965).

13. J. D. Ferry, *Viscoelastic Properties of Polymers* (John Wiley and Sons Inc., New York, 1980), 3rd ed.

14. J. S. Vrentas, J. L. Duda, H. C. Ling and A. C. Jau, *Journal of Polymer Science Polym. Phys. Ed.*, **23** 289 (1985).

15. J. H. Noggle, *Physical Chemistry* (Little, Brown and Company, Boston, 1985), Chap. 9, pp. 445-449.

16. W. G. Knaus and J. J. Emri, *Composites and Structures*, **13**, 123 (1981).

17. S. Matsuoka, G. H. Frederickson and G. E. Johnson, *Lecture Notes in Physics 277, Molecular Dynamics and Relaxation Phenomena in Glasses* (Springer-Verlag, Berlin, 1985), pp. 188-202. Edited by T. Dorfmuller and G. Williams.

18. L. C. E. Struik, *Physical Aging in Amorphous Polymers and Other Materials* (Elsevier, Amsterdam, 1978), Chap. 10, pp. 125-134.

19. M. J. Adamson, *Some Free Volume Concepts of the Effects of Absorbed Moisture on Graphite/Epoxy Composite Laminates*, In Adhesion Science Review, Vol. 1, pp. 87-101. Edited by H. F. Brinson, J. P. Wightman and T. C. Ward, Commonwealth Press, Inc., 1987.

20. A. Cochardt, G. Shoeck and H. Wiedersich, *Acta Metallogr.*, **3**, 533 (1955).

21. F. S. Ham, *Journal of Applied Physics*, **30**, 915 (1959).

22. G. Akay, *Polymer Engineering and Science*, **Vol. 22, No. 13**, 798 (1982).

23. P. J. Flory, *Principles of Polymer Chemistry* (Cornell University Press, Ithaca, 1983), pp. 495-440.

24. A. Peterlin, *Journal of Macromolecular Science- Physics*, **B11 (1)**, 57 (1975).

25. H. Yasuda and A. Peterlin, *Journal of Applied Polymer Science*, **18**, 531 (1976).

26. J. C. Phillips and A. Peterlin, *Polymer Engineering and Science* , **Vol. 23, No. 13**, 734 (1983)

27. J. S. Vrentas, J. L. Duda and Y. C. Ni, *Journal of Polymer Science, Polym. Phys. Ed.*, **15** 2039 (1977).

28. R. W. Seymour and S. Weinhold, *Proceedings of Ryder Conference '85, Ninth International Conference on Oriented Plastic Containers*, 281 (1985).

29. L. H. Wang and R. S. Porter, *Journal of Polymer Science, Polym. Phys. Ed.*, **22**, 1645 (1984).

30. P. Zoller and P. Balli, *Journal of Macromolecular Science - Physics*, **B18**, 555 (1980).

31. *Ultem Polyetherimide 1987 Property Guide*, GE Plastics, Ultem Products Operation, Pittsfield MA.

32. S. Putter and S. Shimabukuro, *SM Report 87-10*, Grad. Aer. Labs., Cal Tech, Pasadena CA, April 1987.

33. R. Brandes, *Personal communication*, GE Plastics Division, Pittsfield MA.

34. J. N. Reddy and S. Roy, *Report No. VPI-E-85.18*, Department of Engineering Science and Mechanics, VPI&SU, Blacksburg, VA. (1985).

35. S. Roy and J. N. Reddy, *Report No. VPI-E-86.28*, Department of Engineering Science and Mechanics, VPI&SU, Blacksburg, VA. (1986).

36. S. Roy, *Ph.D Dissertation*, VPI & SU, Blacksburg, VA. (1987).

37. G. Levita and T. L. Smith, *Polymer Engineering and Science* **Vol. 21, No. 14**, 936 (1981).

38. T. L. Smith, W. Opperman, A. H. Chan and G. Lenta, *Polymer Preprints*, **24 (1)**, 83 (1983).

39. G. S. Springer, *Environmental Effects on Composite Materials Vol. 2*, (Technomic Publishing Company, Inc., 1984), pp. 15, 302.

40. A. W. Adamson, *Physical Chemistry of Surfaces*, (John Wiley & Sons, New York, 1982), 4th Ed.

41. B. V. Deryagin, N.A. Krotova and V.P. Smilga, *Adhesion of Solids*, (Studies in Soviet Science: Physical Sciences, New York, 1978).

42. A. Sheludko, *Colloid Chemistry*, (Elsevier, Amsterdam, 1966).

43. O. F. Devereux, *Topics in Metallurgical Thermodynamics*, (John Wiley & Sons, Inc., New York, 1983).

44. D. Halliday and R. Resnick, *Fundamentals of Physics* (John Wiley & Sons, New York, 1974), Chap.24, p.456

45. G. F. Teletzske, L. E. Scriven and H. T. Davis, *Journal of Colloid and Interface Science*, **Vol. 87, No. 2**, 550 (1982).

46. C. Ko, *PhD Dissertation*, VPI & SU, Blacksburg VA (1988).

47. E. Balcelle, *Master's Thesis*, (in progress), VPI & SU, Blacksburg VA (1988).

48. G. C. Knollman, *International Journal of Adhesion and Adhesives*, **Vol.5, No.3**, 137 (1985).

49. C. R. Houska, F. Dietrich and G.Bubbaraman, *Thin Solid Films*, **44**, 217 (1977).

50. A. J. Kinloch, *Journal of Materials Science*, **17**, 617 (1982).

51. S. R. Hartshorn, *Structural Adhesives; Chemistry and Technology*, (Plenum Press, New York, 1986), Edited by S. R. Hartshorn, Chap. 8, pp. 347-405.

52. G. A. Gledhill, A. J. Kinloch and S. J. Shaw, *Journal of Adhesion*, **11**, 3 (1980).

53. M. Gettings, F. S. Baker and A. J. Kinloch, *Journal of Applied Polymer Science*, **21**, 2375 (1977).

54. G. A. Gledhill and A. J. Kinloch, *Journal of Adhesion*, **6**, 315 (1974).

55. J. Comyn, *Durability of Structural Adhesives*, (Applied Science Publishers, London, 1983, Edited by A. J. Kinloch), Chap. 3, pp. 85-131.

56. T. Smith, *Journal of Adhesion*, **14**, 145 (1982).

57. A. Stevenson, *International Journal of Adhesion and Adhesives*, **Vol. 5, No. 2**, 81 (1985).

58. H. Leidheiser, W. Wang and L. Igetoft, *Progress in Organic Coatings*, **11**, 19 (1983).

59. W. Wang and H. Leidheiser, *Pourbaix Symposium Volume of the Electrochemical Society*, (New Orleans, Oct. 1984).

60. E. L. Koehler, *Corrosion-NACE*, **Vol. 40, No. 1**, 5 (1984).

61. J. S. Hammond, J. W. Holubka and R. A. Dickie, *Journal of Coatings Technology*, **51**, 45 (1979).

62. A. N. Gent, *Journal of Applied Polymer Science*, **21**, 2817 (1977).

63. E. J. Ripling, S. Mostovoy and R. L. Patrick, *Material Res. Stud.*, **4**, 129 (1977).

64. M. Hetenyi, *Beam on Elastic Foundation* (Ann Arbor, The University of Michigan Press, 1971), 9th Pr.

65. M. F. Kanninen, *International Journal of Fracture*, **Vol. 9, No. 1**, 83, (1973).

66. A. N. Gent and E. A. Meinecke, *Polymer Engineering and Science*, **Vol. 10, No. 1**, 48 (1970).

67. A. N. Gent, R. L. Henry and M. L. Roxburg, *Journal of Applied Mechanics*, **Vol. 41, Ser. E, No. 4**, 855 (1974).

68. D. A. Dillard, K. Liechti, D. R. Lefebvre, C. Lin and J. S. Thornton, *ASTM STP 981* (1988).

69. S. S. Wang, J. F. Mandel and F. J. McGarry, *International Journal of Fracture*, **Vol. 14, No. 1**, 39 (1978).

70. W. D. Bascom and R. L. Cottington, *Journal of Adhesion*, 7, 333 (1976).

71. H. Chai, *ASTM STP 893*, 209 (1986).

72. S. Mostovoy, E. J. Ripling and C. F. Bersh, *Journal of Adhesion*, 3, 125 (1971).

The vita has been removed from the scanned document